Summer 7-28-2015

Simulation and Validation of Radio Frequency Heating of Shell Eggs

Soon Kiat Lau
University of Nebraska-Lincoln, lskiat@huskers.unl.edu

Simulation and Validation of Radio Frequency Heating of Shell Eggs

by

Soon Kiat Lau

A THESIS

Presented to the Faculty of

The Graduate College at the University of Nebraska

In Partial Fulfillment of Requirements

For the Degree of Master of Science

Major: Food Science and Technology

Under the Supervision of Professor Jeyamkondan Subbiah

Lincoln, Nebraska

August, 2015

Simulation and Validation of Radio Frequency Heating of Shell Eggs

Soon Kiat Lau, M.S.

University of Nebraska, 2015

Advisor: Jeyamkondan Subbiah

Finite element models were developed with the purpose of finding an optimal radio frequency (RF) heating setup for pasteurizing shell eggs. Material properties of the yolk, albumen, and shell were measured and fitted into equations that were used as inputs for the model. When the egg was heated by itself, heating tend to be focused at the air cell to result in a "coagulation ring." The focused heating near the air cell of the egg prevented satisfactory pasteurization of the egg, but deeper analysis of the simulation results offered a new perspective on how non-uniform RF heating could occur in heterogeneous food products, especially those that contain air bubbles. By immersing the egg in deionized water, the "coagulation ring" disappeared and heating was concentrated in the yolk after RF heating. Extrapolation of the model suggested that 3 log reductions of *Salmonella* can be achieved within 37 min of RF heating followed by hot water immersion. In addition, the contamination of the water surrounding the egg was shown to have a positive impact on the heating rate up to a threshold, at which point further contamination decreased the effectiveness of the process. The knowledge gained in this study could be used to design pasteurization equipment for shell eggs that are faster than conventional equipment.

For the late D.F. and R, the grand magus

Acknowledgements

It goes without saying that a graduate student is nothing without his or her advisor. Dr. Jeyamkondan Subbiah is one of the most prominent figure in my life, and will remain as one whom I will always look up to. I used to be holed up in the world of microbiology and chemistry up until I met Dr. Subbiah who, along with his colleagues, introduced me to a whole new world of food science: engineering and simulations. There is no doubt that at least half of my scientific curiosity was seeded the moment I joined his program as a Master's student. Dr. Subbiah always provides encouraging advice for me to investigate things that I miss out in my research and perhaps most importantly, life advice that cannot be found anywhere else.

Dr. Harshavardhan Thippareddi provided a lot of advice at the beginning of my research, particularly in the area of eggs. Although eggs are so common, I found my knowledge in eggs rather lackluster; Dr. Thippareddi was the one who jumpstarted me in this area. He was also instrumental in the development of the *Salmonella* thermal death time model used in this research. Dr. Jones gave me some vital advice during the middle of my research and pointed out various areas for improvements. My models would never be the way they are now had I not taken classes under Dr. Florin Bobaru. Considering that a major part of this thesis is about simulations using the finite element model, the teachings of Dr. Bobaru helped propel me into this new research field and even prompted me to apply for a minor under his supervision.

Science is not always about racking one's brains; it also involves a lot of communication and cooperation. Therefore, my gratitude goes to Dr. Subbiah's secretary, Amber Patterson who tolerated my many last-minute orders for new equipment and supplies. Without her, my research may have been delayed for months due to lack of supplies! Scott Minchow produces some of the best custom-made equipment with extremely good craftsmanship. The aluminum egg used in the convective heat transfer experiments was possible thanks to information given by Scott. He also helped to build the custom test cells used in property measurements from scratch. This wouldn't be a project with eggs if there were no eggs to begin with! Therefore, I would like to thank Dr. Sheila Purdum from the Animal Science Department for providing me permission to obtain eggs straight from their department's coop. Leo Sweet is primarily responsible for helping me with the collection and also provided me with a lot of life advice and useful nuggets of knowledge. Thank you Leo!

My labmates, Jiajia Chen, Krishnamoorthy Pitchai and Sreenivasula Boreddy were extremely helpful at the beginning of my project. They helped me when I was still a newbie in experiments in general. They also explained their equipment usage procedures when I was trying to measure the properties of the eggs. The guidance and tips they gave me would have taken me weeks to figure out by myself.

Of course, I won't forget my beloved parents who cared for me since young until I left the nest and without whom, this thesis would have never existed!

Table of Contents

List of Tables

List of Figures

Chapter I: Introduction

1.1 The Good, The Bad, and the Tiny Killers

The world around us is teeming with bacteria. Good or bad, they are everywhere: on trees, on animals, in your hair, on your fingers that just brushed your hair, and just about anywhere else. Fortunately for us, not every bacterium is harmful to us. However, if harmful bacteria are present in the right place at the right time, they could cause a serious amount of damage. A group of these bacteria comes from the genus *Salmonella*. Named after Daniel Elmer Salmon (who, surprisingly, was not the discoverer!), the genus *Salmonella* hails from the Enterobacteriaceae family which includes any bacteria that lives in intestines (Norton, 1986). If we go deeper, the *Salmonella* genus consists of the species *S. bongori* and *S. enterica*. The latter has a few subspecies such as *S. enterica* subsp. *enterica* and *S. enterica* subsp. *arizonae*. The *Salmonella* genus has such a huge reputation for causing horrendous infections that we came up with a rather uncreative yet relevant term for such infections: Salmonellosis. Inflammation of the digestive tract, nausea, diarrhea, and damage to the intestinal lining are among some of the discomforts one could expect from having salmonellosis (Norton, 1986). In immunocompromised individuals, the infection could worsen and result in more diseases that could lead to death. In addition, the much dreaded Typhoid fever is caused by the *Typhi* serovar of *S. enterica* subsp. *enterica* (or more simply known as *Salmonella Typhi*). Certainly, the danger of Salmonella needs to be recognized and prevented. Thus, we arrive at an important question: How does *Salmonella* enter our intestines?

There are many answers to that question, but one of the more common entrance routes is through what we eat. *S. enterica* subsp. *enterica* serovar Enteritidis (shortened to *S.* Enteritidis) is usually found in poultry such as chickens and ducks which are unaffected by the bacteria (Centers for Disease Control and Prevention, 2015a). However, upon entering a human's intestines, *S.* Enteritidis will cause a series of infections leading to a case of salmonellosis. Considering that chickens and eggs are common foods, it is not a surprise that *S.* Enteritidis can easily cause problems when these foods are not cooked properly and thoroughly. Unfortunately, the presence of *Salmonella* is not just limited to poultry products; it actually has a huge presence in the food industry.

Just to give a big picture of how common *Salmonella* contamination occurs in foods, the Centers for Disease Controls and Prevention has a list of selected *Salmonella* outbreak investigations that include foods such as chicken, ground beef, cucumber, tomato, mango, cantaloupe, sprouts, Turkish pine nut, pot pie, sesame paste, peanut butter, and cereal (Centers for Disease Control and Prevention, 2015b). Needless to say, even though it normally lives in the intestines, *Salmonella* somehow finds its way into various food products, raw or cooked. This is a major concern because consumers do not expect pathogenic microorganisms to be in ready-to-eat foods such as peanut butter, thus they do not take actions to kill the microorganisms. Sometimes, consumers purposely undercook their food to achieve a desired result such as sunny side up eggs that still have a runny yolk. Therefore, a major part of the responsibility to control the presence of *Salmonella* in food products needs to be fulfilled by the food industry.

1.2 Radio Frequency Heating

There are a plethora of methods available for controlling microorganisms in food, be it mechanical (remove feathers, remove skin), chemical (chlorinated water), or thermal methods. The latter is one of the more commonly used methods since it is very straightforward: apply enough heat and all microorganisms will die. In addition, it is not possible to use mechanical and chemical methods in certain situations, such as when the microorganism is inside the food instead of the surface. Conventional thermal treatments normally use some form of medium such as steam or hot air to transfer heat to the food product. Most of the heat transfer only occurs on the surface of the food and the effectiveness of the process is limited by the rate of heat diffusion within the food. Therefore, the outer surface of the food is always hotter than the inside. For some food products, this is not desired.

Radio frequency (RF) heating is a form of dielectric heating, whereby a sample (food) is placed between two electrodes. Current is applied onto one of the electrodes while the other is grounded, thus causing propagation of electromagnetic waves between the electrodes. The food here acts as a "resistor" (more accurately, dielectric): it disrupts the normal propagation of the waves because the food has a set of unique properties called dielectric properties which are different from that of air. Dielectric properties consist of the dielectric constant and loss factor; the former determines how much of incoming electromagnetic energy can be stored by the food while the latter describes the amount of energy lost as heat during the storage. Since the electromagnetic waves are generated by an oscillator that operates at a certain frequency, dielectric heating can

actually be performed across a wide range of frequencies. A familiar form of dielectric heating is seen in microwave ovens, where the frequency of the waves is around 2.45 GHz. As for RF heating, the frequencies allocated by the National Telecommunications and Information Administration are 13.56 MHz, 27.12 MHz, and 40.68 MHz (Schroeder and Murray, 2003). At this frequencies, the proposed major mechanisms for which energy is lost as heat are orientation polarization whereby polar molecules (usually water) attempt to orient themselves with the electric field, and ion conductivity whereby hydrated ions move inside the sample according to the electric field (de Loor, 1968; Nyfors and Vainikainen, 1989). Considering that electromagnetic waves will travel through the food (just like how light travels through air and glass), both of these heat-generating phenomena will occur throughout the travel path of the waves thus generating heat in various quantities everywhere within the food.

The ability of RF heating to heat a food volumetrically as opposed to just the surface creates an exciting possibility: it is possible to either heat a food uniformly everywhere or even heat the insides while the surface remains cold. The former is commonly investigated. Back in the year 1962, Jason and Sanders used RF heating to thaw frozen fishes. Sanders (1966) continued his investigation on thawing meat and meat products a few years later. The effectiveness of RF heating for pasteurizing cured hams was later tested by Bengtsson et al. (1970). Research on RF heating for foods was rather quiet for a few decades after that, until the dawn of the second millennium when a slew of research suddenly began. The effectiveness of this novel heating method was investigated for sausage emulsions (Houben et al., 1991), meat doughs (van Roon et al.,

1994), starch solutions (Awuah et al., 2002), cherries (Ikediala et al., 2002), ground meat (Laycock et al., 2003), spherical fruits (Birla et al., 2004), milk (Awuah et al., 2005), tray foods (Luechapattanaporn et al., 2005), walnuts (Wang et al., 2007a, 2007b, 2005), meat emulsions (Lyng et al., 2007), and many more. These applications concentrated on various aspects such as pasteurization, sterilization, killing insects, or cooking. Research on RF heating has also started to move away from the traditional trial-and-error into computer simulations using the finite element method. Its capability was first investigated by Konrad (1982) and again later by Choi and Konrad (1991). Later on, RF heating for various foods was simulated, such as spherical fruits (Birla et al., 2008a, 2008b), dry foods (Tiwari et al., 2011a, 2011b), lasagna (Wang et al., 2012), dates (Ben-lalli et al., 2013), raisins (Alfaifi et al., 2014), and peanut butter (Jiao et al., 2014). Overall, the consensus is that RF heating is only able to heat certain food products uniformly, and sometimes processing aids (Jiao et al., 2014) or modifications to the RF applicator (Tiwari et al., 2011a) are needed to achieve that.

1.3 Objectives

The presence of *Salmonella* in a variety of foods beckons an investigation into RF heating as an alternative pasteurization method. Most notably, the multistate outbreaks of *Salmonella* in shell eggs gives reason to test the feasibility of RF heating on it (Centers for Disease Control and Prevention, 2012, 2009, 2007). Therefore, the next two chapters were written with the following objectives in mind:

- Chapter II: A literature review on how RF heating has been applied to food

- Chapter III: Develop a finite element model to understand the effects of RF heating on shell eggs
- Chapter IV: Optimize RF heating on shell eggs immersed in deionized water

1.4 Thesis Organization

Chapter II is a literature review on RF heating and its applications in the world of food. The theory of RF heating is explained in detail. The quality of food products processed using RF heating is also discussed. Details are also given on the mathematical model of the process which is commonly used in simulations.

Chapter III is an initial dive into RF heating of shell eggs with the purpose of pasteurizing it. The heating setup was a single shell egg placed between the RF electrodes. Its vertical position was adjusted using plastic cups. Before performing the simulations, the dielectric properties, thermal conductivity, and specific heat capacity of egg components were measured to be used as input into the finite element model. A total of 50 different RF heating configurations were simulated. One of the simulated setup was chosen for experimental validation.

Results from Chapter III indicate that a simple RF heating setup is not feasible for pasteurizing eggs. Therefore, in Chapter IV, the egg was immersed in deionized water during RF heating. Considering that the fluid surrounding the egg is now more capable of redirecting heat away from the egg, the convective heat transfer coefficient of the egg was measured when it is placed in deionized water. In addition, the significance of liquid movement within the egg was investigated. Following that, 90 different RF heating

configurations were simulated to find the optimal setup. One of these setups were validated experimentally.

The results from Chapter III and IV provide the reason and a way to overcome nonuniform RF heating caused by heterogeneous dielectric properties. The outcomes can serve as guidance for food manufacturers seeking to develop food products that will be processed using RF heating. As a whole, this thesis can be used as a reference for a food product developer who is considering RF heating as a pasteurization method.

1.5 References

Alfaifi, B., Tang, J., Jiao, Y., Wang, S., Rasco, B., Jiao, S., Sablani, S., 2014. Radio frequency disinfestation treatments for dried fruit: Model development and validation. J. Food Eng. 120, 268–276. doi:10.1016/j.jfoodeng.2013.07.015

Awuah, G.B., Ramaswamy, H.S., Economides, A., Mallikarjunan, K., 2005. Inactivation of Escherichia coli K-12 and Listeria innocua in milk using radio frequency (RF) heating. Innov. Food Sci. Emerg. Technol. 6, 396–402. doi:10.1016/j.ifset.2005.06.002

Awuah, G. b., Ramaswamy, H. s., Piyasena, P., 2002. Radio Frequency (rf) Heating of Starch Solutions Under Continuous Flow Conditions: Effect of System and Product Parameters on Temperature Change Across the Applicator Tube. J. Food Process Eng. 25, 201–223. doi:10.1111/j.1745-4530.2002.tb00563.x

Bengtsson, N.E., Green, W., Valle, F.R.D., 1970. Radio-Frequency Pasteurization of Cured Hams. J. Food Sci. 35, 682–687. doi:10.1111/j.1365-2621.1970.tb04844.x

Ben-lalli Ameziane, Bohuon, P., Collignan, A., Méot, J.-M., 2013. Modeling heat transfer for disinfestation and control of insects (larvae and eggs) in date fruits. J. Food Eng. 116, 505–514. doi:10.1016/j.jfoodeng.2012.11.031

Birla, S.L., Wang, S., Tang, J., 2008a. Computer simulation of radio frequency heating of model fruit immersed in water. J. Food Eng. 84, 270–280. doi:10.1016/j.jfoodeng.2007.05.020

Birla, S.L., Wang, S., Tang, J., Tiwari, G., 2008b. Characterization of radio frequency heating of fresh fruits influenced by dielectric properties. J. Food Eng. 89, 390–398. doi:10.1016/j.jfoodeng.2008.05.021

Birla, S.., Wang, S., Tang, J., Hallman, G., 2004. Improving heating uniformity of fresh fruit in radio frequency treatments for pest control. Postharvest Biol. Technol. 33, 205–217. doi:10.1016/j.postharvbio.2004.02.010

Centers for Disease Control and Prevention, 2015a. CDC Features - Keeping Backyard Poultry [WWW Document]. URL http://www.cdc.gov/features/salmonellapoultry/ (accessed 5.18.15).

Centers for Disease Control and Prevention, 2015b. Reports of Selected Salmonella Outbreak Investigations [WWW Document]. URL http://www.cdc.gov/salmonella/outbreaks.html (accessed 5.18.15).

Centers for Disease Control and Prevention, 2012. Multistate Outbreak of Human Salmonella Enteritidis Infections Associated with Shell Eggs (Final Update) [WWW Document]. URL http://www.cdc.gov/salmonella/enteritidis/index.html (accessed 10.16.13).

Centers for Disease Control and Prevention, 2009. Multistate Outbreak of Salmonella Infections Associated with Peanut Butter and Peanut Butter--Containing Products --- United States, 2008--2009. Morb. Mortal. Wkly. Rep. 58, 1–6.

Centers for Disease Control and Prevention, 2007. Multistate Outbreak of Salmonella Serotype Tennessee Infections Associated with Peanut Butter. Morb. Mortal. Wkly. Rep. 56, 521–524.

Choi, C.T.M., Konrad, A., 1991. Finite element modeling of the RF heating process. IEEE Trans. Magn. 27, 4227–4230. doi:10.1109/20.105034

De Loor, G.P., 1968. Dielectric properties of heterogeneous mixtures containing water. J. Microw. Power 3, 67–73.

Houben, J., Schoenmakers, L., Van Putten, E., Van Roon, P., Krol, B., 1991. Radio-frequency pasteurization of sausage emulsions as a continuous process. J. Microw. Power Electromagn. Energy 26, 202–205.

Ikediala, J.N., Hansen, J.D., Tang, J., Drake, S.R., Wang, S., 2002. Development of a saline water immersion technique with RF energy as a postharvest treatment against codling moth in cherries. Postharvest Biol. Technol. 24, 209–221. doi:10.1016/S0925-5214(02)00018-2

Jason, A.C., Sanders, H.R., 1962. Dielectric Thawing of Fish. 1. Experiments with Frozen Herrings. Food Technol. 16, 101.

Jiao, Y., Tang, J., Wang, S., 2014. A new strategy to improve heating uniformity of low moisture foods in radio frequency treatment for pathogen control. J. Food Eng. 141, 128–138. doi:10.1016/j.jfoodeng.2014.05.022

Konrad, A., 1982. Three-dimensional finite element solution of anisotropic complex potential problems. J. Appl. Phys. 53, 8408–8410. doi:10.1063/1.330375

Laycock, L., Piyasena, P., Mittal, G.S., 2003. Radio frequency cooking of ground, comminuted and muscle meat products. Meat Sci. 65, 959–965. doi:10.1016/S0309-1740(02)00311-X

Luechapattanaporn, K., Wang, Y., Wang, J., Tang, J., Hallberg, L.M., Dunne, C.P., 2005. Sterilization of Scrambled Eggs in Military Polymeric Trays by Radio Frequency Energy. J. Food Sci. 70, E288–E294. doi:10.1111/j.1365-2621.2005.tb07185.x

Lyng, J.G., Cronin, D.A., Brunton, N.P., Li, W., Gu, X., 2007. An examination of factors affecting radio frequency heating of an encased meat emulsion. Meat Sci. 75, 470–479. doi:10.1016/j.meatsci.2006.07.022

Norton, C.F., 1986. Microbiology, 2nd ed. Addison-Wesley, Reading, Mass.

Nyfors, E., Vainikainen, P., 1989. Industrial microwave sensors. Artech House.

Sanders, H.R., 1966. Dielectric thawing of meat and meat products. Int. J. Food Sci. Technol. 1, 183–192. doi:10.1111/j.1365-2621.1966.tb01805.x

Schroeder, N., Murray, M., 2003. United States Frequency Allocations.

Tiwari, G., Wang, S., Tang, J., Birla, S.L., 2011a. Analysis of radio frequency (RF) power distribution in dry food materials. J. Food Eng. 104, 548–556. doi:10.1016/j.jfoodeng.2011.01.015

Tiwari, G., Wang, S., Tang, J., Birla, S.L., 2011b. Computer simulation model development and validation for radio frequency (RF) heating of dry food materials. J. Food Eng. 105, 48–55. doi:10.1016/j.jfoodeng.2011.01.016

Van Roon, P.S., Houben, J.H., Koolmees, P.A., van Vliet, T., Krol, B., 1994. Mechanical and microstructural characteristics of meat doughs, either heated by a continuous process in a radio-frequency field or conventionally in a waterbath. Meat Sci. 38, 103–116. doi:10.1016/0309-1740(94)90099-X

Wang, J., Luechapattanaporn, K., Wang, Y., Tang, J., 2012. Radio-frequency heating of heterogeneous food – Meat lasagna. J. Food Eng. 108, 183–193. doi:10.1016/j.jfoodeng.2011.05.031

Wang, S., Monzon, M., Johnson, J.A., Mitcham, E.J., Tang, J., 2007a. Industrial-scale radio frequency treatments for insect control in walnuts: I: Heating uniformity and energy efficiency. Postharvest Biol. Technol. 45, 240–246. doi:10.1016/j.postharvbio.2006.12.023

Wang, S., Monzon, M., Johnson, J.A., Mitcham, E.J., Tang, J., 2007b. Industrial-scale radio frequency treatments for insect control in walnuts: II: Insect mortality and product quality. Postharvest Biol. Technol. 45, 247–253. doi:10.1016/j.postharvbio.2006.12.020

Wang, S., Yue, J., Tang, J., Chen, B., 2005. Mathematical modelling of heating uniformity for in-shell walnuts subjected to radio frequency treatments with intermittent stirrings. Postharvest Biol. Technol. 35, 97–107. doi:10.1016/j.postharvbio.2004.05.024

Chapter II: Literature Review

2.1 Radio Frequency Heating

Legend has it that, Percy Spencer, a self-educated Maine farm boy who grew to own a company in the electronics sector, decided to visit a laboratory in the 1940s that was testing magnetrons (Murray, 1958; Osepchuk, 1984). As he leaned near an open waveguide, he noticed that a peanut candy bar in his pocket began to melt. Curious, he got some popcorn, placed it near the wave guide, and soon the kernels began to pop. He came back the next day with a makeshift cavity made of a kettle with a hole punched into it and directed a waveguide to the hole. He plopped a shell egg into the kettle and in a few moments, the egg exploded! Electromagnetic heating was thus discovered, along with the help of his colleagues such as W. C. Brown, P. Derby, N. Alstad and others.

Radio frequency (RF) heating is a form of electromagnetic heating whereby a sample is heated by electromagnetic waves passing through it. Specifically for RF heating, the typical setup consists of a pair of parallel electrodes connected to an alternating voltage supply with the sample to be heated placed between the electrodes (Zhao et al., 2000). In this setup, whatever that lies between the electrodes function as a capacitor. The notion of a “good” capacitor in this context is inversed: a good capacitor in the field of electronics would be one that could store a lot of energy without losing it as heat. In RF heating, the opposite is preferred to maximize transfer of energy!

2.2 Theory

The waves generated for RF heating have frequencies of either 13.56 MHz, 27.12 MHz, and 40.68 MHz, as designated by the National Telecommunications and Information Administration (Schroeder and Murray, 2003). At these frequencies, it is theorized that the major mechanisms that convert electromagnetic energy into heat are orientation polarization whereby polar molecules (e.g. water) attempt to orient themselves with the electric field, and ion conductivity whereby hydrated ions inside the sample move according to the electric field (de Loor, 1968; Nyfors and Vainikainen, 1989). Considering that electromagnetic waves will travel through the sample just like how light travels through air and glass, both of these heat-generating phenomena will occur throughout the travel path of the waves thus generating heat in various quantities everywhere within the sample.

The amount of electromagnetic energy converted into heat is dependent on the dielectric properties of the sample. Dielectric properties consist of the dielectric constant, ε_r' and loss factor, ε_r''; the former determines how much of incoming electromagnetic energy can be stored by the sample while the latter describes the amount of energy lost as heat during the storage of energy. These properties usually change according to temperature and the frequency of the electromagnetic waves. One explanation for how the frequency dependence occurs is described by the "Debye resonance": polar molecules rotate faster as frequency is increased, but there will be a limit at which lattice limitations prevent the molecules from rotating too fast (Zhao et al., 2000). Besides that, a food that is too prone to RF heating will absorb so much electromagnetic energy at its surface that

a negligible amount will be absorbed in its center, thus decreasing the penetration depth of the waves (Zhao et al., 2000).

2.3 Food Applications

One attractive benefit of RF heating is that it could theoretically heat the entire sample and not just the surface because the waves can penetrate deep into the sample. In contrast, conventional thermal treatments that rely on air, steam, or water can only heat the surface of the sample. Therefore, RF heating has been tested and utilized for various food products.

The application of RF heating in food reported in the literature dates back to 1945 when Moyer and Stotz used it to blanch vegetables. A whole plethora of applications soon followed within the next seven decades: from meat to vegetables, for cooking to insect control, and even for freezing. **Table 2.1** provides a list of these various applications. The increase in research on RF heating at the dawn of the 20th century may have been caused by the push for food safety requirements (Zhao et al., 2000). More recently though, the introduction of the Food Safety Modernization Act has created a drive to find more novel processing methods to reduce contamination in food and RF heating happens to be a rather attractive solution.

Aside from real food applications, RF heating also has been investigated in various model foods to understand what parameters affect it. Examples of model foods include starch solutions (Awuah et al., 2002), fruit-shaped gellan gels (Birla et al., 2008), polyurethane foam (Wang et al., 2014), and meat blends (Nagaraj et al., 2015).

2.4 Nonuniformity

As mentioned earlier, RF heating has the potential to heat a food in a volumetric fashion instead of just the surface. However, this is the ideal situation; in reality, this is rarely seen. Foods are naturally diverse in terms of their properties and some such as fruits and lasagna have various components in them (Birla et al., 2004; Wang et al., 2012). Besides that, the shape of the food contributes to this problem too: sharp edges and corners always absorb more electromagnetic energy compared to other regions in the food (Tiwari et al., 2011). In light of these problems, there have been various methods developed, accidental or on purpose, for various food products to improve the uniformity of RF heating. These methods are listed in **Table 2.2**. One particular method that has been theorized but not tested in real-life applications is the modification of the electrodes.

2.5 Quality of Food

As seen in **Table 2.1**, a lot of RF heating applications on food has to do with controlling insect and microbial populations. To be frank, reducing or eliminating these pests could be as simple as applying some form of extreme heat or chemical treatment on the food product. For example, tossing chickens into a bonfire or bathing them in a concentrated sulfuric acid solution. Of course, these methods won't work because the final product still has to be edible (chicken ashes or corrosive chicken, anyone?). Therefore, the act of pasteurizing or sterilizing food has to be done in such a way that the quality of the end product is not severely degraded.

The usage of RF heating for foods can have three possible outcomes in terms of quality: better, insignificant differences, or worse. When Bengtsson et al. (1970) performed RF heating on cured hams, they found that not only was RF heating a shorter process compared to conventional hot water processing, RF-processed hams also had better juice retention, thus resulting in juicier hams and higher sensory scores. Similar trends were observed in the experiments performed by Laycock et al. (2003), but they also found that RF heating is not feasible for ground beef because the end product was too chewy and elastic. Meat doughs processed with RF heating were more firm and had larger irregularly shaped fat particles than their waterbath processed counterparts (van Roon et al., 1994). Liu et al. (2013) noted that while there were some changes in the firmness of RF-heated bread, these changes were deemed to be insignificant. Mangoes processed with RF heating and stored for 12 days were firmer than their control counterparts (Sosa-Morales et al., 2009).

Aside from texture, visual quality is an important parameter that determines the acceptance of a food product by consumers. Red and black pepper pasteurized with RF heating had no significant difference in terms of color when compared to untreated ones. Wang et al. (2007b) reported that the lightness, peroxide value, and oleic acid content of walnuts processed with RF heating and stored for 20 days were not significantly different than their control counterparts. RF-heated cherries has no significant changes in terms of color, although there was a slight effect on browning of the berry (Monzon et al., 2006). The calyx in ‘Fuyu’ persimmons browned during RF heating; this effect was more pronounced as treatment time was increased (Tiwari et al., 2008). The pulp of apples

heated with RF energy was found to be darker than their control counterparts (Wang et al., 2006).

From all these investigations, it is clear that the quality of the end product of RF heating can be anything from good to bad. Therefore, it will always be necessary to evaluate the quality of RF heated foods to confirm the feasibility of the method.

2.6 Simulations

Due to the natural variations present in food, it can be difficult to determine an optimal RF heating setup for a particular food. In fact, most of the applications listed in **Table 2.1** tended to focus on just one setup for an initial evaluation of the feasibility of RF heating. The difficulty in optimizing RF heating comes from the fact that there could be an infinite amount of ways to configure the RF oven, and even if an equation was developed for a particular food, it may not be useable for another kind of food. Since this problem is insurmountable by trial-and-error, simulations have been explored as a way to solve it.

Typically, problems that have to do with electromagnetic waves are described by the Maxwell's equation. However, the typical setup for RF heating has a particular feature that simplifies the equations to a quasistatic form. Normally, the gap between the electrodes is less than 1 m; in comparison, the wavelength at the frequency 27.12 MHz is approximately 11 cm. Therefore, within the gap, the wave is assumed to propagate at an infinite speed (Larsson, 2007). As a result, the Maxwell's equations can be simplified and the electric field, $\boldsymbol{E}$ is simply given as the negative gradient of voltage ($\boldsymbol{E} = -\nabla V$) if

everywhere is free space. For other materials such as food, $\boldsymbol{E}$ can be determined when given some properties of the food (Konrad, 1982):

$$-(\sigma + j\omega\varepsilon_o\varepsilon_r)(\nabla \cdot \nabla V) = 0$$

where σ is the electrical conductivity (S/m) of the domain, $j = \sqrt{-1}$ is the imaginary number, $\omega = 2\pi f$ is the angular frequency (s^{-1}), f is the frequency (Hz) of the RF waves, ε_0 is the permittivity of free space ($10^{-9}/(36\pi)$ F m^{-1}), and ε_r is the complex relative permittivity (dimensionless) which is normally expressed as the sum $\varepsilon_r = \varepsilon_r' - i\varepsilon_r''$, where ε_r' is the dielectric constant and ε_r'' is the loss factor, both of which are the dielectric properties of the food.

The common objective in modelling RF heating is to obtain the temperature profile of the food. Therefore, a link has to be created between the electromagnetic equations and heat transfer equations. Once $\boldsymbol{E}$ has been determined, power density, Q (W m^{-3}) within the material can be calculated as:

$$Q = 2\pi f \varepsilon_0 \varepsilon'' |\boldsymbol{E}|^2$$

where $|\boldsymbol{E}|$ is the amplitude of the electric field (V m^{-1}).

Q turns out to be a parameter in the Fourier's heat transfer equation, therefore it is now possible to calculate temperature, T (K) in the material:

$$\frac{\partial T}{\partial t} = \frac{k}{\rho C_p}\nabla^2 T + \frac{Q}{\rho C_p}$$

These set of equations are normally solved in a finite element model.

2.7. Summary

The sheer number of research on using RF heating in food applications gives a wealth of information for understanding the process better. Its ability to heat food volumetrically is a tremendous benefit to the food industry as it opens up a new world of possibilities. However, understanding of the process is not entirely mature because there still the problem of nonuniform heating still exists. With the help of simulations, it may be possible to find new ways to overcome nonuniform RF heating and speed up the incorporation of RF heating in the food industry.

1.6 References

Alfaifi, B., Tang, J., Jiao, Y., Wang, S., Rasco, B., Jiao, S., Sablani, S., 2014. Radio frequency disinfestation treatments for dried fruit: Model development and validation. J. Food Eng. 120, 268–276. doi:10.1016/j.jfoodeng.2013.07.015

Anese, M., Manzocco, L., Panozzo, A., Beraldo, P., Foschia, M., Nicoli, M.C., 2012. Effect of radiofrequency assisted freezing on meat microstructure and quality. Food Res. Int. 46, 50–54. doi:10.1016/j.foodres.2011.11.025

Awuah, G.B., Ramaswamy, H.S., Economides, A., Mallikarjunan, K., 2005. Inactivation of Escherichia coli K-12 and Listeria innocua in milk using radio frequency (RF) heating. Innov. Food Sci. Emerg. Technol. 6, 396–402. doi:10.1016/j.ifset.2005.06.002

Awuah, G. b., Ramaswamy, H. s., Piyasena, P., 2002. Radio Frequency (rf) Heating of Starch Solutions Under Continuous Flow Conditions: Effect of System and Product Parameters on Temperature Change Across the Applicator Tube. J. Food Process Eng. 25, 201–223. doi:10.1111/j.1745-4530.2002.tb00563.x

Bengtsson, N.E., Green, W., Valle, F.R.D., 1970. Radio-Frequency Pasteurization of Cured Hams. J. Food Sci. 35, 682–687. doi:10.1111/j.1365-2621.1970.tb04844.x

Ben-lalli Ameziane, Bohuon, P., Collignan, A., Méot, J.-M., 2013. Modeling heat transfer for disinfestation and control of insects (larvae and eggs) in date fruits. J. Food Eng. 116, 505–514. doi:10.1016/j.jfoodeng.2012.11.031

Birla, S.L., Wang, S., Tang, J., 2008. Computer simulation of radio frequency heating of model fruit immersed in water. J. Food Eng. 84, 270–280. doi:10.1016/j.jfoodeng.2007.05.020

Birla, S.., Wang, S., Tang, J., Hallman, G., 2004. Improving heating uniformity of fresh fruit in radio frequency treatments for pest control. Postharvest Biol. Technol. 33, 205–217. doi:10.1016/j.postharvbio.2004.02.010

Byrne, B., Lyng, J.G., Dunne, G., Bolton, D.J., 2010. Radio frequency heating of comminuted meats - considerations in relation to microbial challenge studies. Food Control 21, 125–131. doi:10.1016/j.foodcont.2009.03.003

Cathcart, W.H., Parker, J.J., Beattie, H.G., 1947. The treatment of packaged bread with high frequency heat. Food Technol. 1, 174–177.

De Loor, G.P., 1968. Dielectric properties of heterogeneous mixtures containing water. J. Microw. Power 3, 67–73.

Farag, K.W., Duggan, E., Morgan, D.J., Cronin, D.A., Lyng, J.G., 2009. A comparison of conventional and radio frequency defrosting of lean beef meats: Effects on water binding characteristics. Meat Sci. 83, 278–284. doi:10.1016/j.meatsci.2009.05.010

Gao, M., Tang, J., Villa-Rojas, R., Wang, Y., Wang, S., 2011. Pasteurization process development for controlling Salmonella in in-shell almonds using radio frequency energy. J. Food Eng. 104, 299–306. doi:10.1016/j.jfoodeng.2010.12.021

Ha, J.-W., Kim, S.-Y., Ryu, S.-R., Kang, D.-H., 2013. Inactivation of Salmonella enterica serovar Typhimurium and Escherichia coli O157:H7 in peanut butter cracker

sandwiches by radio-frequency heating. Food Microbiol. 34, 145–150. doi:10.1016/j.fm.2012.11.018

Houben, J.H., Van Roon, P.S., Krol, B., Jansen, W.J.L., 1990. Radio frequency pasteurization of moving sausage emulsions. Process. Qual. Foods 1.171–1.177.

Houben, J., Schoenmakers, L., Van Putten, E., Van Roon, P., Krol, B., 1991. Radio-frequency pasteurization of sausage emulsions as a continuous process. J. Microw. Power Electromagn. Energy 26, 202–205.

Huang, Z., Zhu, H., Yan, R., Wang, S., 2015. Simulation and prediction of radio frequency heating in dry soybeans. Biosyst. Eng. 129, 34–47. doi:10.1016/j.biosystemseng.2014.09.014

Ikediala, J.N., Hansen, J.D., Tang, J., Drake, S.R., Wang, S., 2002. Development of a saline water immersion technique with RF energy as a postharvest treatment against codling moth in cherries. Postharvest Biol. Technol. 24, 209–221. doi:10.1016/S0925-5214(02)00018-2

Jason, A.C., Sanders, H.R., 1962a. Dielectric Thawing of Fish. 1. Experiments with Frozen Herrings. Food Technol. 16, 101.

Jason, A.C., Sanders, H.R., 1962b. Dielectric Thawing of Fish. 2. Experiments with Frozen White Fish. Food Technol. 16, 107.

Jiao, S., Johnson, J.A., Tang, J., Wang, S., 2012. Industrial-scale radio frequency treatments for insect control in lentils. J. Stored Prod. Res. 48, 143–148. doi:10.1016/j.jspr.2011.12.001

Jiao, Y., Tang, J., Wang, S., 2014. A new strategy to improve heating uniformity of low moisture foods in radio frequency treatment for pathogen control. J. Food Eng. 141, 128–138. doi:10.1016/j.jfoodeng.2014.05.022

Kim, S.-Y., Sagong, H.-G., Choi, S.H., Ryu, S., Kang, D.-H., 2012. Radio-frequency heating to inactivate Salmonella Typhimurium and Escherichia coli O157:H7 on black and red pepper spice. Int. J. Food Microbiol. 153, 171–175. doi:10.1016/j.ijfoodmicro.2011.11.004

Konrad, A., 1982. Three-dimensional finite element solution of anisotropic complex potential problems. J. Appl. Phys. 53, 8408–8410. doi:10.1063/1.330375

Larsson, J., 2007. Electromagnetics from a quasistatic perspective. Am. J. Phys. 75, 230–239. doi:10.1119/1.2397095

Laycock, L., Piyasena, P., Mittal, G.S., 2003. Radio frequency cooking of ground, comminuted and muscle meat products. Meat Sci. 65, 959–965. doi:10.1016/S0309-1740(02)00311-X

Liu, Y., Tang, J., Mao, Z., Mah, J.-H., Jiao, S., Wang, S., 2011. Quality and mold control of enriched white bread by combined radio frequency and hot air treatment. J. Food Eng. 104, 492–498. doi:10.1016/j.jfoodeng.2010.11.019

Liu, Y., Wang, S., Mao, Z., Tang, J., Tiwari, G., 2013. Heating patterns of white bread loaf in combined radio frequency and hot air treatment. J. Food Eng. 116, 472–477. doi:10.1016/j.jfoodeng.2012.11.029

Llave, Y., Terada, Y., Fukuoka, M., Sakai, N., 2014. Dielectric properties of frozen tuna and analysis of defrosting using a radio-frequency system at low frequencies. J. Food Eng. 139, 1–9. doi:10.1016/j.jfoodeng.2014.04.012

Luechapattanaporn, K., Wang, Y., Wang, J., Tang, J., Hallberg, L.M., Dunne, C.P., 2005. Sterilization of Scrambled Eggs in Military Polymeric Trays by Radio Frequency Energy. J. Food Sci. 70, E288–E294. doi:10.1111/j.1365-2621.2005.tb07185.x

Mermelstein, N.H., 1998. Microwave and radiofrequency drying. Food Technol. 52, 84–86.

Mitcham, E.J., Veltman, R.H., Feng, X., de Castro, E., Johnson, J.A., Simpson, T.L., Biasi, W.V., Wang, S., Tang, J., 2004. Application of radio frequency treatments to control insects in in-shell walnuts. Postharvest Biol. Technol. 33, 93–100. doi:10.1016/j.postharvbio.2004.01.004

Monzon, M.E., Biasi, B., Simpson, T.L., Johnson, J., Feng, X., Slaughter, D.C., Mitcham, E.J., 2006. Effect of radio frequency heating as a potential quarantine treatment on the quality of "Bing" sweet cherry fruit and mortality of codling moth larvae. Postharvest Biol. Technol. 40, 197–203. doi:10.1016/j.postharvbio.2005.12.011

Moyer, J.C., Stotz, E., 1945. The Electronic Blanching of Vegetables. Science 102, 68–69. doi:10.1126/science.102.2638.68-a

Murray, D., 1958. Percy Spencer and his itch to know. Read. Dig.

Nagaraj, G., Singh, R., Hung, Y.-C., Mohan, A., 2015. Effect of radio-frequency on heating characteristics of beef homogenate blends. LWT - Food Sci. Technol. 60, 372–376. doi:10.1016/j.lwt.2014.08.039

Nyfors, E., Vainikainen, P., 1989. Industrial microwave sensors. Artech House.

Osepchuk, J.M., 1984. A History of Microwave Heating Applications. IEEE Trans. Microw. Theory Tech. 32, 1200–1224. doi:10.1109/TMTT.1984.1132831

Pircon, L.J., 1954. Diathermal processing of meat, in: Proceedings of the Sixth Research Conference. American Meat Institute.

Rice, J., 1993. RF technology sharpens bakery's competitive edge. Food Process. 6, 18–24.

Sanders, H.R., 1966. Dielectric thawing of meat and meat products. Int. J. Food Sci. Technol. 1, 183–192. doi:10.1111/j.1365-2621.1966.tb01805.x

Schlisselberg, D.B., Kler, E., Kalily, E., Kisluk, G., Karniel, O., Yaron, S., 2013. Inactivation of foodborne pathogens in ground beef by cooking with highly controlled radio frequency energy. Int. J. Food Microbiol. 160, 219–226. doi:10.1016/j.ijfoodmicro.2012.10.017

Schroeder, N., Murray, M., 2003. United States Frequency Allocations.

Shinde, A., Das, S., Datta, A.K., 2013. Quality improvement of orthodox and CTC tea and performance enhancement by hybrid hot air–radio frequency (RF) dryer. J. Food Eng. 116, 444–449. doi:10.1016/j.jfoodeng.2012.12.001

Sisquella, M., Casals, C., Picouet, P., Viñas, I., Torres, R., Usall, J., 2013. Immersion of fruit in water to improve radio frequency treatment to control brown rot in stone fruit. Postharvest Biol. Technol. 80, 31–36. doi:10.1016/j.postharvbio.2013.01.010

Sisquella, M., Viñas, I., Picouet, P., Torres, R., Usall, J., 2014. Effect of host and Monilinia spp. variables on the efficacy of radio frequency treatment on peaches. Postharvest Biol. Technol. 87, 6–12. doi:10.1016/j.postharvbio.2013.07.042

Sosa-Morales, M.E., Tiwari, G., Wang, S., Tang, J., Garcia, H.S., Lopez-Malo, A., 2009. Dielectric heating as a potential post-harvest treatment of disinfesting mangoes,

Part II: Development of RF-based protocols and quality evaluation of treated fruits. Biosyst. Eng. 103, 287–296. doi:10.1016/j.biosystemseng.2009.02.014

Tiwari, G., Wang, S., Birla, S.L., Tang, J., 2008. Effect of water-assisted radio frequency heat treatment on the quality of "Fuyu" persimmons. Biosyst. Eng. 100, 227–234. doi:10.1016/j.biosystemseng.2008.03.005

Tiwari, G., Wang, S., Tang, J., Birla, S.L., 2011. Analysis of radio frequency (RF) power distribution in dry food materials. J. Food Eng. 104, 548–556. doi:10.1016/j.jfoodeng.2011.01.015

Uemura, K., Takahashi, C., Kobayashi, I., 2010. Inactivation of Bacillus subtilis spores in soybean milk by radio-frequency flash heating. J. Food Eng. 100, 622–626. doi:10.1016/j.jfoodeng.2010.05.010

Van Roon, P.S., Houben, J.H., Koolmees, P.A., van Vliet, T., Krol, B., 1994. Mechanical and microstructural characteristics of meat doughs, either heated by a continuous process in a radio-frequency field or conventionally in a waterbath. Meat Sci. 38, 103–116. doi:10.1016/0309-1740(94)90099-X

Wang, J., Luechapattanaporn, K., Wang, Y., Tang, J., 2012. Radio-frequency heating of heterogeneous food – Meat lasagna. J. Food Eng. 108, 183–193. doi:10.1016/j.jfoodeng.2011.05.031

Wang, S., Birla, S.L., Tang, J., Hansen, J.D., 2006. Postharvest treatment to control codling moth in fresh apples using water assisted radio frequency heating. Postharvest Biol. Technol. 40, 89–96. doi:10.1016/j.postharvbio.2005.12.005

Wang, S., Ikediala, J.N., Tang, J., Hansen, J.D., Mitcham, E., Mao, R., Swanson, B., 2001. Radio frequency treatments to control codling moth in in-shell walnuts. Postharvest Biol. Technol. 22, 29–38. doi:10.1016/S0925-5214(00)00187-3

Wang, S., Monzon, M., Johnson, J.A., Mitcham, E.J., Tang, J., 2007a. Industrial-scale radio frequency treatments for insect control in walnuts: II: Insect mortality and product quality. Postharvest Biol. Technol. 45, 247–253. doi:10.1016/j.postharvbio.2006.12.020

Wang, S., Monzon, M., Johnson, J.A., Mitcham, E.J., Tang, J., 2007b. Industrial-scale radio frequency treatments for insect control in walnuts: I: Heating uniformity and energy efficiency. Postharvest Biol. Technol. 45, 240–246. doi:10.1016/j.postharvbio.2006.12.023

Wang, S., Tang, J., Johnson, J.A., Mitcham, E., Hansen, J.D., Cavalieri, R.P., Bower, J., Biasi, B., 2002. Process protocols based on radio frequency energy to control field and storage pests in in-shell walnuts. Postharvest Biol. Technol. 26, 265–273. doi:10.1016/S0925-5214(02)00048-0

Wang, S., Yue, J., Chen, B., Tang, J., 2008. Treatment design of radio frequency heating based on insect control and product quality. Postharvest Biol. Technol. 49, 417–423. doi:10.1016/j.postharvbio.2008.02.004

Wang, S., Yue, J., Tang, J., Chen, B., 2005. Mathematical modelling of heating uniformity for in-shell walnuts subjected to radio frequency treatments with intermittent stirrings. Postharvest Biol. Technol. 35, 97–107. doi:10.1016/j.postharvbio.2004.05.024

Wang, Y., Zhang, L., Gao, M., Tang, J., Wang, S., 2014. Evaluating radio frequency heating uniformity using polyurethane foams. J. Food Eng. 136, 28–33. doi:10.1016/j.jfoodeng.2014.03.018

Zhao, Y., Flugstad, B., Kolbe, E., Park, J.W., Wells, J.H., 2000. Using Capacitive (radio Frequency) Dielectric Heating in Food Processing and Preservation – a Review. J. Food Process Eng. 23, 25–55. doi:10.1111/j.1745-4530.2000.tb00502.x

Table 2.1. RF heating in various food applications.

Purpose	Food	Reference
Blanch	Vegetable	(Moyer and Stotz, 1945)
Drying	Cookie and snack food	(Mermelstein, 1998; Rice, 1993)
	Tea	(Shinde et al., 2013)
Freezing	Meat	(Anese et al., 2012)
Insect control	Apple	(Birla et al., 2004; Wang et al., 2006)
	Cherry	(Ikediala et al., 2002; Monzon et al., 2006)
	Date	(Ben-lalli et al., 2013)
	Lentil	(Jiao et al., 2012; Wang et al., 2008)
	Mango	(Sosa-Morales et al., 2009)
	Orange	(Birla et al., 2004)
	Persimmon	(Tiwari et al., 2008)
	Raisin	(Alfaifi et al., 2014)
	Soybean	(Huang et al., 2015; Wang et al., 2008)
	Walnut	(Mitcham et al., 2004; Wang et al., 2008, 2007a, 2007b, 2005, 2002, 2001)
	Wheat	(Wang et al., 2008)
Pasteurization or sterilization	Almond	(Gao et al., 2011)
	Bread	(Cathcart et al., 1947; Liu et al., 2013, 2011)
	Cured Ham	(Bengtsson et al., 1970)
	Egg	Chapter III and IV of this thesis
	Milk	(Awuah et al., 2005)
	Meat	(Byrne et al., 2010; Pircon, 1954; Schlisselberg et al., 2013; van Roon et al., 1994)
	Peach	(Sisquella et al., 2014)
	Peanut butter cracker	(Ha et al., 2013)
	Sausage emulsion	(Houben et al., 1991, 1990)
	Scrambled eggs	(Luechapattanaporn et al., 2005)
	Soybean milk	(Uemura et al., 2010)
	Spice	(Kim et al., 2012)
	Stone fruit	(Sisquella et al., 2013)
Thawing	Fish	(Jason and Sanders, 1962a, 1962b; Llave et al., 2014)
	Meat	(Farag et al., 2009; Sanders, 1966)

Table 2.2. Methods for overcoming nonuniform RF heating.

Method	Rationale	Food product	Reference
Enclose in another medium	- Reduces the disparity in dielectric properties between the food and the surrounding air, thus evening out the electric field distribution - Specifically for liquid media, convective heating or cooling can be induced on the surface of the food, if necessary	Apple	Birla et al., 2004
		Cherry	Ikediala et al., 2002
		Cured ham	Bengtsson et al., 1970
		Egg	Chapter III and IV of this thesis
		Mango	Sosa-Morales et al., 2009
		Orange	Birla et al., 2004
		Peanut butter	Jiao et al., 2014
		Scrambled egg	Luechapattanaporn et al., 2005
		Stone fruit	Sisquella et al., 2013
Modify electrodes	- Reduce the fringe effect from the edges of the electrode	Wheat flour	Tiwari et al., 2011
Mix or rotate food	- Redistribute electric field and heat within the food product	Apple	Birla et al., 2004
		Mango	Sosa-Morales et al., 2009
		Orange	Birla et al., 2004
		Walnut	Wang et al., 2007, 2005
Combine with an external heating or cooling device	- Reduces temperature variation in the food - Allows holding at a desired temperature	Apple	Birla et al., 2004
		Bread	(Liu et al., 2013, 2011)
		Lentil	Jiao et al., 2012
		Orange	Birla et al., 2004
		Walnut	Wang et al., 2007

Chapter III: Rings in Eggs: Improving Microbiological Safety of Shell Eggs Using Radio Frequency Heating

Abstract

A total of 50 different configurations of a radio frequency (RF) oven were simulated for heating of a shell egg using a finite element model with the purpose of pasteurizing the egg. Material properties of the yolk, albumen, and shell were measured and fitted into equations that were used as inputs for the model. A regression equation that relates the top electrode voltage to the gap between the electrodes and vertical position of the egg was also developed. Simulation and experimental results had good agreement in terms of temperature deviation (RMSE ranged from 0.35°C to 0.48°C) and both results also produced an eccentric product of focused heating (fondly) referred to as a 'coagulation ring.' The focused heating near the air cell of the egg prevented satisfactory pasteurization of the egg, but deeper analysis of the simulation results offered a new perspective on how non-uniform RF heating could occur in heterogeneous food products, especially those that contain air bubbles. The results can be used as a base for further development of RF heating on eggs and as guidance for developing heterogeneous food products that will be treated with RF heating.

3.1 Introduction

Approximately 42,000 cases of *Salmonella* infections are reported on an annual basis in the United States (Centers for Disease Control and Prevention, 2012a). *Salmonella* can contaminate a variety of foods, with shell eggs (eggs with intact shells) being one of the most common one. A multistate outbreak in the year 2010 that was associated with *S.* Enteritidis in shell eggs resulted in approximately 1,939 reported illnesses (Centers for Disease Control and Prevention, 2012b). Isolated outbreaks in gatherings or conventions were also linked to shell eggs (Centers for Disease Control and Prevention, 1988). In the international scene, the United Kingdom, Germany and Austria have also experienced *S.* Enteritidis outbreaks due to contaminated shell eggs (Hrivniaková et al., 2011; Janmohamed et al., 2011; Mossong et al., 2012). Considering that it is such a widespread problem, it is important to reduce the risk of *S.* Enteritidis in eggs.

The problem of pasteurizing shell eggs lies within finding a balance between the heat sensitivity of the albumen and the thermal resistance of *Salmonella*. *Salmonella* (excluding serotype Senftenberg) is more heat resistant in plain egg yolk, with higher D-values (60°C) from 0.28 to 1.1 min, than in plain egg white, with lower D-values (60°C) from 0.2 to 0.3 min (Doyle and Mazzotta, 2000; Jordan et al., 2011). However, the albumen begins to coagulate at 56.7°C while the egg yolk starts to coagulate at 65°C (Nakamura et al., 1982; Stadelman et al., 1995). These conditions create a difficult situation for traditional thermal processing where the egg yolk has to be heated longer or to a higher temperature than the albumen, even though it is located at the center of a shell

egg. One solution is to pasteurize the egg below the coagulation temperature of albumen for a long time, an approach that has been shown to take from 25 min up to 3 h to achieve 3 to 7 log reductions of *S.* Enteritidis (Hou et al., 1996; Schuman et al., 1997). Due to the long process time, alternative methods have been investigated. Irradiation at 1.5 kGy results in approximately 4 log reduction of *S.* Enteritidis in shell eggs, with minor changes in the color of the albumen and yolk (Serrano et al., 1997). However, there is consumer resistance against buying irradiated eggs. Dev and others (2008) investigated microwave heating of single shell eggs at the center of a domestic microwave oven and reported that the albumen and yolk heat at almost the same rate. However, domestic microwave ovens are unsuitable for an industrial processing line.

Another alternative method to consider is radio frequency (RF) heating. RF heating applies an alternating electric field to an object to generate internal heat mainly through two mechanisms: orientation polarization whereby polar molecules (usually water) attempt to orient themselves with the electric field, and ion conductivity whereby hydrated ions migrate according to the electric field (de Loor, 1968; Nyfors and Vainikainen, 1989). The latter is very dependent on the presence of solvents such as water, a major component in food products. Since RF heating operates at relatively low frequencies (13.56, 27.12 or 40.68 MHz) compared to microwave heating (915, 2450 MHz) and the penetration depth of a wave is inversely related to its frequency (Buffler, 1993), RF heating is able to penetrate deeper and heat food products more uniformly than microwave heating.

RF heating has been investigated for many food-related uses such as postharvest disinfestation (Jiao et al., 2012; Wang et al., 2010), cooking (Zhang et al., 2004), baking (Liu et al., 2013), drying (Shinde et al., 2013), and pasteurization (Gao et al., 2011). Unfortunately, RF heating can be hard to predict analytically if the food is heterogeneous, therefore some researchers have used numerical analysis to optimize the process (Alfaifi et al., 2014; Ben-lalli et al., 2013; Birla et al., 2008b; Marra et al., 2007; Tiwari et al., 2011a, 2011b; Wang et al., 2012, 2010). Some of these analyses have been shown to closely agree with experimental results (Birla et al., 2008b; Marra et al., 2007; Tiwari et al., 2011b; Wang et al., 2012). Therefore, computer simulations combined with validation studies is a powerful and indispensable approach to understand and optimize RF heating on non-homogenous food products.

The health risks caused by *S.* Enteritidis in shell eggs beg for an efficient yet consumer-friendly pasteurization process. The objective of this study is to determine the feasibility of RF heating on shell eggs. The specific objectives were to: (1) measure the dielectric properties, thermal conductivity, and specific heat capacity of shell eggs as a function of temperature; (2) develop a coupled electromagnetic and heat transfer model for RF heating on shell eggs using the measured properties; and (3) validate the simulation results with experimental results.

3.2 Materials and Methods

3.2.1 Measurement of Properties

3.2.1.1 Preparation of samples

Three major components of the eggs were measured: albumen, yolk, and shell. The albumen is considered to be a homogenized mixture of chalazae, thick albumen, and thin albumen; the yolk as a mixture of vitelline membrane and yolk; the shell as a combination of shell and shell membrane.

Eggs laid by White Leghorn chickens were obtained from the University of Nebraska-Lincoln Animal Science Department poultry farm. Guo and others (2007) observed that the dielectric properties of egg yolk and albumen change during storage. Therefore, the eggs were collected within 4 hours post-lay and processed for measurements within the same day to reduce such drifts in measurements. Collected eggs were candled and washed. Eggs with deformities such as blood spots were discarded.

The yolks of the eggs were separated from albumen using a spoon. The collected albumens were homogenized with a magnetic stirrer (11-100-49SH, Fisher Scientific, Waltham, MA) set at 240 rpm for 10 min while homogenization of yolks was done at 95 rpm for 10 min.

Since the property measurements require solids to be in powder form (Agilent Technologies, 2012; Carson and Kemp, 2014), it was necessary to prepare the egg shells accordingly. The interior of the shells were first scraped with a spoon to remove albumen and Kimwipes™ (Kimberly-Clark Corporation, Neenah, WI) were used to wipe off any

remaining albumen. The shells were weighed to obtain their wet mass. Preliminary trials showed that the moisture content of the shells do not change after 1 h at 105 °C, therefore the shells were dried in a convection oven (Model 6925, Fisher Scientific, Waltham, MA) subjected to the aforementioned conditions. Dried shells were cooled in a desiccator before they were weighed to determine their dry mass. The wet and dry mass values were used to determine the moisture content of the shells (dry basis), which ranges from 9% to 14%. The dried shells were then ground using a grain mill (Mill-Rite™ Grain Mill, Retsel Manufacturing Co., Inc., McCammon, ID) and sieved to an average particle size of 250 µm (USA standard sieve No. 60, Dual Manufacturing Co., Inc., Chicago, IL). The sieved shells were then dried in the same oven and temperature for 30 min to remove any moisture that may have been added during grinding and sieving. After drying, the powdered shells were cooled in a desiccator before adding double deionized water to obtain the original moisture content. The mixture was stirred thoroughly with a metal spatula to ensure the moisture is distributed evenly.

3.2.1.2Dielectric properties measurement

Dielectric properties measurements were performed using an Impedance/Material Analyzer (E4991A, Agilent Technologies, Inc., Santa Clara, CA) coupled with a temperature controlled chamber (MCBH-1.2-.33-.33-H/AC, Cincinnati Sub-Zero Products, Inc., Cincinnati, OH). The instrument setup and calibration procedure was performed at 20°C and is described in detail by Chen et al. (2013a, 2013b). While the liquid yolk and white can be measured using the same test cell used by the aforementioned authors, the egg shells required a different test cell because it has been

shown that dielectric properties of powders are affected by density (Nelson, 1984). Therefore, the same test cell (**Fig. 3.1**) was modified by adding an adjustable plunger. This add-on allows control of the volume (and thus, density) of the sample inside the test cell.

Calibrations were validated by measuring double deionized water. The dielectric properties of the samples were then measured over the frequency range of 10 – 3000 MHz, starting at 20 °C and at every 10 °C increment until 70 °C. All measurements were taken within ±0.5 °C of the target temperature and performed in triplicates.

3.2.1.3 Thermal conductivity measurement

The transient line heat source method (KD-2 Pro, Decagon Devices, Inc., Pullman, WA) was used to perform thermal conductivity measurements. Following manufacturer's recommendation, a shorter needle probe (KS-1) was used for albumen and yolk in the low power mode with a read time of 1 min while a longer needle probe (TR-1) used for egg shell in the high power mode with a read time of 5 min. The temperatures of the test cell and sample were controlled by a circulating water bath (9012A11B, PolyScience, Niles, IL).

A custom-built test cell and probe holder (**Fig. 3.2**) that satisfies the manufacturer's recommendation of at least 1.5 cm clearance from the probe to the test cell wall was built for the KS-1 probe. The test cell for the TR-1 probe follows the same design, but was slightly longer to accommodate its length. Just like the dielectric property measurements, the egg shell was compressed in the test cell to a certain volume

depending on the sample mass in order to achieve the original density of intact shells (**Table 3.1**). The TR-1 probe was coated with thermal paste (Arctic Silver® 5, Arctic Silver Incorporated, Visalia, CA) to improve thermal contact with the sample.

Measurements were taken at 20°C and at every 10°C increment until 70°C. All measurements were within ±0.5°C of the target temperature and done in triplicates. Each measurement was spaced 1 h apart to allow the water bath and sample to equilibrate with the target temperature. For liquid samples, the water bath was turned off and left still for 30 s before measuring. This procedure prevents vibrations from the water bath that will cause convection in liquid samples and thus, measurement errors. For solid samples, the water bath continued to operate during measurement.

3.2.1.4Specific heat capacity measurement

The specific heat capacities of the samples were measured using the direct method of Differential Scanning Calorimetry (DSC822^{e}, Mettler-Toledo Inc., Columbus, OH). The instrument was baked out at 500 °C for 30 min before experiments to remove impurities in the measurement chamber. Sample weights for albumen, yolk, and shell were about 11 mg, 28 mg, and 32 mg, respectively. The samples were placed in 40 µL aluminum crucibles, hermetically sealed, and subjected to a temperature program that starts at 10 °C and ends at 80 °C. The actual measurement range is from 20°C to 70°C; the extra 10°C at both ends of the range is to accommodate for come-up time errors according to manufacturer's recommendations. Before measuring a sample, three runs of empty crucibles for both reference and sample were performed over the desired temperature program. The crucibles were then reused for real sample measurements. The

last reading from the empty crucibles was subtracted from thermographs of the measured sample. This procedure, known as blank curve correction, is necessary to reduce variability introduced by the crucibles. A heating rate of 10 °C/min was used in accordance to the manufacturer's recommendation (Mettler Toledo, 1998). All measurements were done in triplicates.

3.2.1.5 Curve fitting

All curve fitting operations were performed using the MATLAB 2012 Curve Fitting Toolbox™ (The MathWorks, Inc., Natick, MA). For certain curve fitting operations, the data was centered and scaled to reduce round-off errors introduced by computational operations on large numbers.

3.2.2 Simulations

3.2.2.1 Governing Equations

When it comes to determining the electric field in RF heating models, the quasi-static approximation is used by many researchers (Birla et al., 2008b; Choi and Konrad, 1991; Marra et al., 2007; Romano and Marra, 2008; Tiwari et al., 2011a, 2011b; Wang et al., 2012). In this approximation, the electric field intensity, $\boldsymbol{E}$ (V m^{-1}) at any point between the electrodes is calculated as the negative gradient of a constant voltage, V (V) ($\boldsymbol{E} = -\nabla V$), when only air is present between the two electrodes. Assuming isotropic material properties, $\boldsymbol{E}$ can then be determined in the egg anywhere between the electrodes (Konrad, 1982):

$$-(\sigma + j\omega\varepsilon_o\varepsilon_r)(\nabla \cdot \nabla V) = 0 \quad (1)$$

where σ is the electrical conductivity (S/m) of the domain, $j = \sqrt{-1}$ is the imaginary number, $\omega = 2\pi f$ is the angular frequency (s^{-1}), f is the frequency (Hz) of the RF waves, ε_0 is the permittivity of free space ($10^{-9}/(36\pi)$ F m^{-1}), and ε_r is the complex relative permittivity (dimensionless) of the domain. ε_r can be expanded to the sum $\varepsilon_r = \varepsilon_r' - i\varepsilon_r''$, where ε_r' is the dielectric constant and ε_r'' is the loss factor. For food products, σ is generally assumed to be negligible in comparison to the permittivity term.

The reasoning for this approximation is that the wavelengths at RF frequencies (about 11 m at 27.12 MHz) are significantly larger than the gap between the electrodes, making wave propagation calculations unnecessary (Choi and Konrad, 1991). Although the most accurate simulations can only be obtained by modeling the entire RF system (Chan et al., 2004), the solution time would be greatly increased. Therefore, the quasi-static approximation is used in this study to get a general idea of how RF heating works on an egg.

Using the calculated electric field, power density, Q (W m^{-3}) within a material between the two electrodes due to RF energy can then be determined:

$$Q = 2\pi f \varepsilon_0 \varepsilon'' |\boldsymbol{E}|^2 \quad (2)$$

where ε'' is the loss factor of the material, and $|\boldsymbol{E}|$ is the amplitude of the electric field (V m^{-1}).

The power density can then be used in Fourier's heat transfer equation to solve for temperature, T (K) in the material:

$$\frac{\partial T}{\partial t} = \frac{k}{\rho C_p}\nabla^2 T + \frac{Q}{\rho C_p} \quad (3)$$

Where t is the heating time (s), k is thermal conductivity (W m^{-1} K^{-1}), ρ is density (kg m^{-3}), and C_p is specific heat capacity (J kg^{-1} K^{-1}).

3.2.2.2 Finite Element Model

There can be an infinite number of ways to position the egg in the RF oven. In this situation, it is wise to first survey how the egg industry handles eggs, and then design accordingly. A visit to an egg processing plant revealed that the common method of handling eggs in a processing line is using suction cups on the pointed ends of the egg. Furthermore, eggs are normally transported in trays, with the pointed ends facing upwards or downwards. Therefore, placing the eggs in the RF oven in such a vertical position is a good starting point for this study. For this position, there are two possible variations:

- The blunter end (with air cell) at the top, nearer to the top electrode (orientation A), and
- The blunter end at the bottom, nearer to the bottom electrode (orientation B).

Besides the orientation of the egg, it is also necessary to consider contributions from the gap between the electrodes, G (cm) and the vertical position of the egg from the bottom

electrode to the bottom of the egg, P (cm). The latter can be expressed as a function of the former:

$$P = M \times (G - h) \tag{4}$$

where h is the height of the egg (cm). M is a multiplier of the empty vertical space between the electrodes and can be adjusted to change the vertical position of the egg. When M = 0, the egg sits at the bottom and when M = 1, the egg touches the top electrode. Therefore, the configuration of the RF oven can be easily varied by adjusting G and M.

The geometries for the aforementioned positions were investigated in COMSOL Multiphysics® 4.3a (COMSOL, Inc., Palo Alto, CA). The geometry of a 6 kW Radio Frequency Heater (Strayfield Limited, England) was reconstructed, ignoring minor geometric features such as screws (**Fig. 3.3**). The diameters at various locations along the major axis of 3 large eggs were measured using a pair of calipers, averaged, and interpolated to create the curved geometry of an egg. The eggs were then frozen and sliced in half to obtain measurements of their inner components. Expansion due to freezing was assumed to be negligible.

Three different model configurations with various simplifications were then evaluated (**Fig. 3.4**):

a. 3D model: The RF oven was modeled as a cuboid. The thin top electrode was simplified to a plane. Since the cuboid shape of the oven is inherently symmetric, only a quarter of it was modeled in 3D.
b. 2D axisymmetric model: The 3D model was simplified to a 2D cut plane, with the axisymmetric axis placed at the middle of the oven.
c. 2D simplified model: The 2D axisymmetric model was further simplified to just the space between the electrodes (hereon referred to as 2Ds).

By simplifying the 3D model to the axisymmetric 2D model and subsequently to the 2Ds model, the computation time can be reduced effectively. Although both the 2D and 2Ds models imply that the oven is being modeled as a cylinder, the maximum, average, and minimum temperatures of the egg at the end of the mesh convergence studies of both the 2D and 2Ds models only varied by less than 2% of the 3D model. This is expected because the dimensions of the top electrode are much larger than the egg; in the egg's perspective, the top electrode appears to be an infinite plane. Therefore, fringe effects from the edges of the top electrode do not significantly affect the egg. The 2Ds model was used for the optimization study in Section 3.2.2.6.

A constant voltage was assumed at the top electrode because studies have shown that the voltage does not vary by more than 7% between standby and full load (Metaxas, 1996). The value of this voltage is given by an equation determined in Section 3.3.2.1. Walls and the bottom electrode were grounded with $V = 0$. Specifically for 2Ds model, the additional boundary conditions were assigned as follows: The axis of symmetry (left edge) and the opposite edge (right edge) were given the electric insulation conditions.

This means that the fringing effect of electric field on the edge of the electrode is assumed to have negligible effect on the final outcome of the model. This assumption is reasonable as the size of the electrode is significantly larger than the size of the eggs. The initial temperature of the entire model was set to room temperature (24.5°C). A convection boundary condition was placed upon the egg shell with h = 20 W m^{-2} K^{-1}) and an ambient temperature of 24.5°C.

3.2.2.3Mesh Convergence

In order to ensure that the simulation results are independent of the number of mesh elements, mesh convergence studies were performed. The mesh convergence RF heating setup had a gap between electrodes of 10 cm, a vertical distance between the bottom of the egg and bottom electrode of 1.5 cm, and an arbitrary 8000 V applied to the top electrode. The simulation was then performed for 5 minutes. A very coarse mesh was first investigated, and then the number of elements was increased until the converged mesh was found. A mesh setup *n* is considered to be converged when the maximum, average, and minimum temperatures of the egg do not vary by more than 0.1% of the mesh setup *n-1*, and the same set of temperatures of the next five or more investigated mesh sizes do not vary by more than 0.1% of it. It should be noted that these convergence criteria require all three temperature statistics to be converged: if the average temperature converged at mesh setup *n* while the maximum temperature only converged at mesh setup *n+1*, then mesh setup *n*+1 is considered the converged mesh (see **Fig. 3.5** for example). This mesh convergence procedure was done for the 3D, 2D and 2Ds models.

For the 2Ds mesh convergence model (**Fig. 3.4(a)**), the mesh distribution within each domain is as follows:

- Yolk: 947 elements, minimum size set to 0.125 mm
- Albumen: 10447 elements, elements, minimum size set to 0.01 mm
- Shell: 3573 elements, elements, minimum size set to 0.01 mm
- Air cell: 365 elements, elements, minimum size set to 0.01 mm
- Surrounding air: 9464 elements, elements, minimum size set to 0.125 mm

Only triangular elements were used. It should be noted that the number of elements do vary between each model investigated during the optimization routine described in Section 3.2.2.6, but they remain in the same ballpark since the minimum sizes are still the same. The minimum sizes were set to a very small number to investigate the effect of the air cell since preliminary studies indicate that the air cell contributes to an interesting phenomenon described later in this paper.

3.2.2.4 Validation Studies

Whenever a physical phenomenon is modeled, it is always necessary to compare the results to experimental results to build confidence in the model. The validation studies in this paper were performed on the same type of eggs used in the property measurements. Depending on the setup being validated, the gap between the electrodes, *G* was adjusted using in-built electrode drive motors while the vertical position of the egg (related to *M*) was adjusted using polypropylene cups which are transparent to RF waves. These adjustments to *G* and *M* for the voltage study can be found in Section 3.2.2.5,

while the configuration used to validate the optimal setup study is given in Section 3.2.2.6. A permanent marker was used to mark three locations on the shell (**Fig. 3.6**). After the heating process was completed, a screwdriver (1 mm diameter) was used to puncture these locations and a thermocouple array was inserted to measure the temperature of the egg at specific locations. The setup consisted of three thermocouples (type T, OMEGA Engineering, Inc., Stamford, CT), a polyethylene block, and a data acquisition device (USB-TC, Measurement Computing Corporation, Norton, MA) (**Fig. 3.6**). The temperature measurement was performed after RF heating. Although other researchers have used fiber optic thermocouple successfully under an RF environment, it was unfeasible to measure the temperature during heating because the presence of these sensors in the egg will change the positions of the yolk and albumen.

It should be noted that there exists a delay of approximately 25 s from the end of the heating process to the measurement of temperature. This delay includes the time needed to shut down the RF oven, open the oven, take out the egg, puncture the shell of the eggs, and insert the thermocouples to collect temperature readings. Naturally, the temperature of the egg will change during that 25 second delay due to cooling by the surrounding air. Therefore, simulations were performed to view the significance of the temperature profile difference between the moment the RF process was stopped (t = 0 s) versus exposure to natural convection (h = 20 W m^{-2} K^{-1}) for 25 s. The initial temperature profile used in this study was exported from simulation of an RF configuration (G = 13 cm, M = 0.25) after 7 min of heating. The results of this study are visualized in **Fig. 3.7**. At points close to the air cell, there are large decreases in temperature because of high

temperature gradients versus the air around the egg and also because these points are in close proximity to the surface of the egg shell and thus more prone to being affected by convective cooling. On the other hand, the points located close to the center of the egg did not have much difference in terms of temperature before and after cooling. In fact, the temperatures at these points increased due to heat diffusion, albeit a little: the maximum increase was only 0.406°C. Therefore, the thermocouple array for validation experiments was designed to insert thermocouples at these non-volatile locations to avoid fluctuations between replications because the convective cooling may not be consistent between replications. For example, the egg might sometimes be moved faster through the air to create stronger convection. In addition, the egg was held by the author's hand during handling, which affected the temperature at locations close to the surface.

3.2.2.5 The Effect of Electrode Gap and Position of Egg

An investigation by Zhu et al. (2014) revealed that the gap between the electrodes of an RF applicator has an impact on the voltage of the top electrode. This is true in free-running oscillator RF systems, whereby the output of the machine increases as the amount of load between the electrodes increases, or the gap between the electrode decreases (Strayfield, 2007). Therefore, it is necessary to derive an equation that provides the voltage of the top electrode as the configuration of the RF oven changes. This equation can be used in the simulations during a search of the optimal configuration.

To derive the voltage equation, the effect of *G* and *M* were investigated across the following ranges:

- G: From 11 cm to 13 cm, in 1 cm increments
- M: From 0.25 to 0.75, in 0.25 increments

Thus, 9 configurations were investigated, with three replicates per configuration. The temperatures of the heated eggs at certain locations were measured following the procedures in Section 3.2.2.4. For each RF configuration, simulations with similar configurations were swept across a range of top electrode voltages (7000 V to 10,000 V) in increments of 100 V. The differences between simulation and validation results were expressed in terms of root-mean-square error (RMSE):

$$RMSE = \frac{\sum_i^n \left(T_{sim,i} - T_{val,i}\right)^2}{n} \quad (5)$$

where $T_{sim,i}$ is the temperature predicted by simulation at location i, $T_{val,i}$ is the thermocouple reading at location i in the validation studies, and n are the total number of locations measured. The results were then filtered by choosing the top electrode voltages that gave the lowest RMSE. Regression analysis was subsequently performed on the filtered data using SAS 9.4 (SAS Institute Inc., Cary, NC). The resulting regression equation was used for the simulations.

3.2.2.6Finding the Optimal Setup

The search for the optimal RF heating setup requires an examination of various configurations of the RF oven restricted within the domain of the voltage equation derived in Section 3.2.2.5. Therefore, simulations were performed by varying the following parameters:

- G: From 11 cm to 13 cm, in 0.5 cm increments
- M: From 0.25 to 0.75, in 0.125 increments

The aforementioned parameters were investigated for both orientation A and B, therefore a total of 50 configurations were simulated. Simulations were performed on a Dell workstation with two Intel E5-2630 processors and 88 GB RAM running a Windows 7 64 bit operating system.

The simulation results were filtered to obtain the temperature profile at the time just before any of the following conditions were violated:

Condition 1: The maximum temperature in the egg yolk exceeds 65 °C.

Condition 2: The maximum temperature of the albumen exceeds 56.7 °C.

Condition 3: RF heating has been performed for 20 min.

The temperature constraints were chosen to avoid coagulation in the respective domains, as stated in section 3.1. The time constraint is to ensure the simulations do not go on forever in cases when the heating rate is too slow. One of the setups (G = 13 cm, M =

0.25) was then chosen to be validated according to the procedures outlined in Section 3.2.2.4.

3.3 Results and Discussion

3.3.1 Material Properties

3.3.1.1 Dielectric Properties

The dielectric properties for all three egg components were found to fit the following power equation:

$$\varphi = af^b + c \tag{6}$$

Where φ is either the dielectric constant, ε' or loss factor, ε'' while *f* is frequency (Hz) and ranges from 10 MHz to 3 GHz. The remaining coefficients *a*, *b*, and *c* are given in **Table 3.2**. A plot of the equations can be found in **Fig. 3.8**. Using the values calculated from equation (6), regression equations for the frequency 27.12 MHz (**Table 3.3**) were derived for use in the simulations. The dielectric properties calculated from these equations at 24°C varied by less than 8% of the measurements made by Guo et al. (2007), with the exception of albumen loss factor which went up to 12%.

The dielectric properties for all the egg components appear to peak at the lower end of the investigated frequency spectrum, and then flatten out as frequency increases. At lower frequencies, an increase in temperature caused an increase in the ε' of albumen and yolk. At higher frequencies, an inverse relationship is observed. For the shell, ε'

increases with temperature at all frequencies. At a constant temperature, the ε' of all three components decreases as frequency increases.

At all the measured frequencies, the ε'' of all three egg components increases as temperature increases. On the other hand, the ε'' of all three components have an inverse relationship with frequency. This is especially apparent in the ε'' of albumen, whereby the ε'' at 20 MHz is almost a hundred times more than at 2450 MHz. Albumen has a higher ε'' than yolk at all frequencies, but the difference in ε'' decreases as frequency increases. Since the ε'' positively contributes to the ability of a material to generate heat in an electric field, the abilities of albumen and yolk to generate heat will be affected by frequency in the same way as the ε''. Therefore, the albumen and yolk should heat at similar rates at higher frequencies. In fact, Dev et al. (2008) reported that both the albumen and yolk heat at almost the same rate at microwave oven frequencies (2.45 GHz). They also noted that the egg shell was almost transparent to microwave frequencies, another feature exhibited by the measured properties in this paper.

3.3.1.2 Thermal Properties

The *k* of the egg components were fitted to the following regression equation:

$$k = a\left(\frac{T - 318.2}{18.71}\right)^2 + b\left(\frac{T - 318.2}{18.71}\right) + c \tag{7}$$

where *T* is temperature (°C) in the range of 20°C, inclusive, to 70°C, inclusive. The c_p of the egg components were fitted to a cubic function:

$$c_p = a\left(\frac{T-318.2}{18.71}\right)^3 + b\left(\frac{T-318.2}{18.71}\right)^2 + c\left(\frac{T-318.2}{18.71}\right) + d \quad (8)$$

where T is temperature (°C) in the range of 20°C, inclusive, to 70°C, inclusive. The coefficients for both k and c_p are listed in **Table 3.4** and **Table 3.5**, respectively. Note that the polynomial variables are not T alone; they are actually the result of a minus and division operation on T. This is the result of the centering and scaling operation described in Section 3.2.1.5., a necessary operation to avoid round-off errors.

The k of all measured samples increased with temperature while the c_p of the liquid components generally decreased with increasing temperature. It should be noted that the c_p of the shell increases with temperature. At 20°C, the k and c_p of albumen and yolk are not significantly different with reported results at 22°C (Coimbra et al., 2006). The slight differences may be due to different measurement methods and egg composition. Plots for equations (7) and (8) can be found in **Fig. 3.9**.

3.3.2 Simulation and Validation

3.3.2.1 Voltage Regression Equation

At $p < 0.1$, only the linear effect from G and the interaction effect from G and M were found to significantly contribute to the top electrode voltage. A regression equation was built from these parameters:

$$V = 10400 - 19155Gk + 1643.63MGk \quad (9)$$

where k = 1 V/cm is simply a unit conversion constant necessitated by the fact that equation (9) is a regression equation for quantities with different units.

This equation is visualized using a contour plot in **Fig. 3.10**. As the gap between the electrode increases, the voltage at the top electrode drops. This trend has also been observed in experiments with soybeans (Zhu et al., 2014). At the same time, an egg placed closer to the top electrode induces more output from the RF machine compared to one placed closer to the bottom electrode. This behavior is not modeled by the analytical expression for the top electrode voltage mentioned by Birla et al. (2008a). However, one should remember that the aforementioned equation assumes a slab of sample that is at least as large as the electrodes; this obviously does not apply to an egg.

3.3.2.2 The Search for the Optimal Setup

Before analyzing the simulation results, it is necessary to confirm if the model has satisfactory agreement with experimental results. The comparison between the simulation and validation results for Orientation A with G = 13 cm, M = 0.25 is shown in **Fig. 3.11**. Both results follow similar trends: the region close to the air cell almost always has the highest temperature. After 5 minutes, the disparity between simulation and validation results appear to grow, which can be explained by heat redistribution during the delay (about 25 s) between end of the RF process and thermocouples insertion. RMSE values for thermocouple locations (a), (b), and (c) are 0.36°C, 0.35°C, and 0.48°C, respectively.

One notable feature shared among all 50 investigated configurations is concentrated heating at the interface between the air cell, albumen, and shell. This

phenomenon predicted by the simulations was visible in validation experiments (**Fig. 3.12**). The concentrated heating around the air cell led to the formation of a 'coagulation ring' which turned out to be a useful visual indicator of how well the simulations and validation studies agreed with each other. During removal of the yolk and albumen from the shell, part of the 'coagulation ring' adhered strongly to the albumen, thus leaving some coagulation flecks in the albumen. These coagulation flecks should not be confused with coagulation at other parts of the egg because it is evident from **Fig. 3.12(c)** that these flecks were always located at the 'blunt' or broader end of the albumen. Therefore, the model gave a rather good prediction of focused heating in the eggs.

Closer examination of the simulations revealed that the formation of the 'coagulation ring' was due to a concentration of electric field in that region (**Fig. 3.13**). The electric field starts at the top electrode and moves downwards towards the bottom electrode. On the way, the field is attracted towards the egg (**Fig. 3.13(1)**). Upon entering the shell, the fields did not point straight downwards to the air cell; instead there was a net shift towards the nearest entry point directly into the albumen which turns out to be the interface between the shell, air cell and albumen (**Fig. 3.13(2)**). This created a chokepoint of electric energy at the albumen (**Fig. 3.13(4)**) resulting in a large concentration of heat in that region due to the relationship between **Equations 2** and **3**. Therefore, the albumen at that area will coagulate before any other regions resulting in the 'coagulation ring.' The redirection of electric field in the shell can be attributed to the differences in dielectric properties between air and albumen. This phenomenon has been observed in other heterogeneous foods such as lasagna containing meatballs (Wang et al.,

2012), whereby the sauce filling the space between closely-placed meatballs receive a higher power dissipation density, Q compared to the rest of the sauce domain. The sequence of events presented here provides a better understanding of how non-uniform heating occurs in RF heating.

Now that confidence in the model has been established, the simulation results can be analyzed. For all 50 configurations investigated, the maximum temperature condition for the albumen was violated before that of the yolk (Condition 2 in Section 3.2.2.6). Since *S.* Enteritidis survives better in the yolk than the albumen (Bradshaw et al., 1990), it is imperative to rank the 50 configurations based on the maximum temperature of the yolk. The influence of G and M on the maximum yolk temperature before violation of the optimization constraints is visually depicted in **Fig. 3.14**. Both plots appear to be mirrored at M = 0.5, which is when the egg is placed in the middle of the gap between both electrodes. Therefore, the temperature profile of a configuration investigated in Orientation A can be almost replicated in Orientation B as long as the position of the egg in the latter is mirrored to that of the former. In addition, the yolk reaches a higher temperature as the gap between the electrodes increases. This relationship holds true because a larger gap leads to an overall lower heating rate as suggested by equation (9). The lower heating rate allows natural convection to take away some heat from the surface of the egg, thus delaying the formation of the 'coagulation ring' while giving more time for the yolk to heat up. However, **Fig. 3.15** shows that a larger electrode gap comes with an unwanted side-effect too, namely, a longer process time. Therefore, optimization of the process for pasteurization is not just a simple matter of increasing the electrode gap. It

should be noted that none of the configurations achieved a yolk temperature that is sufficient for pasteurization. As mentioned in Section 3.1, the D-value for *Salmonella* in the yolk at 60°C ranges from 0.28 to 1.1 min (Doyle and Mazzotta, 2000; Jordan et al., 2011) whereas the highest yolk temperature achieved in this optimization study is a little below 52°C. If actions are taken to prevent or at least delay the formation of the 'coagulation ring,' it would be possible to achieve a much higher yolk temperature and subsequently pasteurize of the egg.

3.4 Conclusion

Eggs treated with RF heating in a vertical position without any additional aid is likely to form a 'coagulation ring' at the interface between the albumen, air cell, and shell before the yolk is sufficiently pasteurized. Increasing the electrode gap may alleviate this problem, but would introduce undesirable issues such as longer process time. Additional processing aids, such as cooling of the air cell, are recommended in order to ensure successful pasteurization of eggs using RF heating. The orientation of the egg was found to have insignificant effect on the temperature profile.

When ingredients of starkly different dielectric properties are in contact and treated with RF heating, non-uniform heating is likely to occur due to redirection and concentration of the electric field. With this knowledge, the heating uniformity of multicomponent food products treated with RF heating can be improved by reducing the differences in dielectric properties among the ingredients. For example, the salt content could be adjusted to increase or decrease the dielectric constant and loss factor. In

addition, air bubbles should also be removed from food products using methods such as ultrasonic treatment to achieve better RF heating uniformity.

3.5 Acknowledgements

This research was supported by the Agricultural Research Division of the University of Nebraska and the Mussehl Poultry Foundation. The authors would also like to extend their gratitude to Dr. Sheila Purdum and Leo Sweet of the Animal Science Department of the University of Nebraska-Lincoln for providing shell eggs and allowing usage of their egg grading equipment.

3.6 References

Agilent Technologies, 2012. Agilent 85070E Dielectric Probe Kit 200 MHz to 50 GHz Technical Overview.

Alfaifi, B., Tang, J., Jiao, Y., Wang, S., Rasco, B., Jiao, S., Sablani, S., 2014. Radio frequency disinfestation treatments for dried fruit: Model development and validation. J. Food Eng. 120, 268–276. doi:10.1016/j.jfoodeng.2013.07.015

Ben-lalli Ameziane, Bohuon, P., Collignan, A., Méot, J.-M., 2013. Modeling heat transfer for disinfestation and control of insects (larvae and eggs) in date fruits. J. Food Eng. 116, 505–514. doi:10.1016/j.jfoodeng.2012.11.031

Birla, S.L., Wang, S., Tang, J., 2008a. Computer simulation of radio frequency heating of model fruit immersed in water. J. Food Eng. 84, 270–280. doi:10.1016/j.jfoodeng.2007.05.020

Birla, S.L., Wang, S., Tang, J., Tiwari, G., 2008b. Characterization of radio frequency heating of fresh fruits influenced by dielectric properties. J. Food Eng. 89, 390–398. doi:10.1016/j.jfoodeng.2008.05.021

Bradshaw, J.G., Shah, D.B., Forney, E., Madden, J.M., 1990. Growth of Salmonella enteritidis in yolk of shell eggs from normal and seropositive hens. J. Food Prot. 53, 1033–1036.

Buffler, C.R., 1993. Microwave cooking and processing. Van Nostrand Reinhold, New York, NY.

Carson, J.K., Kemp, R.M., 2014. The influence of particle size on the accuracy of the thermal conductivity probe. J. Food Eng. 142, 46–48. doi:10.1016/j.jfoodeng.2014.06.011

Centers for Disease Control and Prevention, 2012a. What is Salmonellosis? [WWW Document]. URL http://www.cdc.gov/salmonella/general/ (accessed 10.16.13).

Centers for Disease Control and Prevention, 2012b. Multistate Outbreak of Human Salmonella Enteritidis Infections Associated with Shell Eggs (Final Update) [WWW Document]. URL http://www.cdc.gov/salmonella/enteritidis/index.html (accessed 10.16.13).

Centers for Disease Control and Prevention, 1988. Update: Salmonella enteritidis Infections and Grade A Shell Eggs -- United States [WWW Document]. URL http://www.cdc.gov/mmwr/preview/mmwrhtml/00001079.htm (accessed 10.16.13).

Chan, T.V.C.T., Tang, J., Younce, F., 2004. 3-dimensional numerical modeling of an industrial radio frequency heating system using finite elements. J. Microw. Power Electromagn. Energy 39, 87–106.

Chen, J., Pitchai, K., Birla, S., Gonzalez, R., Jones, D.D., Subbiah, J., 2013a. Temperature-dependent dielectric and thermal properties of microwaveable model foods.

Chen, J., Pitchai, K., Birla, S., Jones, D.D., Subbiah, J., 2013b. Development of a multi-temperature calibration method for the measurement of dielectric properties applied to microwaveable food.

Choi, C.T.M., Konrad, A., 1991. Finite element modeling of the RF heating process. IEEE Trans. Magn. 27, 4227–4230. doi:10.1109/20.105034

Coimbra, J.S.R., Gabas, A.L., Minim, L.A., Garcia Rojas, E.E., Telis, V.R.N., Telis-Romero, J., 2006. Density, heat capacity and thermal conductivity of liquid egg products. J. Food Eng. 74, 186–190. doi:10.1016/j.jfoodeng.2005.01.043

De Loor, G.P., 1968. Dielectric properties of heterogeneous mixtures containing water. J. Microw. Power 3, 67–73.

Dev, S.R.S., Raghavan, G.S.V., Gariepy, Y., 2008. Dielectric properties of egg components and microwave heating for in-shell pasteurization of eggs. J. Food Eng. 86, 207–214. doi:10.1016/j.jfoodeng.2007.09.027

Doyle, M.E., Mazzotta, A.S., 2000. Review of Studies on the Thermal Resistance of Salmonellae. J. Food Prot. 63, 779–795.

Gao, M., Tang, J., Villa-Rojas, R., Wang, Y., Wang, S., 2011. Pasteurization process development for controlling Salmonella in in-shell almonds using radio frequency energy. J. Food Eng. 104, 299–306. doi:10.1016/j.jfoodeng.2010.12.021

Guo, W., Trabelsi, S., Nelson, S. o., Jones, D. r., 2007. Storage Effects on Dielectric Properties of Eggs from 10 to 1800 MHz. J. Food Sci. 72, E335–E340. doi:10.1111/j.1750-3841.2007.00392.x

Hou, H., Singh, R.K., Muriana, P.M., Stadelman, W.J., 1996. Pasteurization of intact shell eggs. Food Microbiol. 13, 93–101. doi:10.1006/fmic.1996.0012

Hrivniaková, L., Schmid, D., Luckner-Hornischer, A., Lassnig, H., Kornschober, C., Angermayer, J., Allerberger, F., 2011. Salmonellosis outbreak due to Salmonella enteritidis phage type 14b resistant to nalidixic acid, Austria, September 2010. Euro Surveill. Bull. Eur. Sur Mal. Transm. Eur. Commun. Dis. Bull. 16.

Janmohamed, K., Zenner, D., Little, C., Lane, C., Wain, J., Charlett, A., Adak, B., Morgan, D., 2011. National outbreak of Salmonella Enteritidis phage type 14b in

England, September to December 2009: case-control study. Euro Surveill. Bull. Eur. Sur Mal. Transm. Eur. Commun. Dis. Bull. 16.

Jiao, S., Johnson, J.A., Tang, J., Wang, S., 2012. Industrial-scale radio frequency treatments for insect control in lentils. J. Stored Prod. Res. 48, 143–148. doi:10.1016/j.jspr.2011.12.001

Jordan, J.S., Gurtler, J.B., Marks, H.M., Jones, D.R., Shaw Jr., W.K., 2011. A mathematical model of inactivation kinetics for a four-strain composite of Salmonella Enteritidis and Oranienburg in commercial liquid egg yolk. Food Microbiol. 28, 67–75. doi:10.1016/j.fm.2010.08.008

Konrad, A., 1982. Three-dimensional finite element solution of anisotropic complex potential problems. J. Appl. Phys. 53, 8408–8410. doi:10.1063/1.330375

Liu, Y., Wang, S., Mao, Z., Tang, J., Tiwari, G., 2013. Heating patterns of white bread loaf in combined radio frequency and hot air treatment. J. Food Eng. 116, 472–477. doi:10.1016/j.jfoodeng.2012.11.029

Marra, F., Lyng, J., Romano, V., McKenna, B., 2007. Radio-frequency heating of foodstuff: Solution and validation of a mathematical model. J. Food Eng. 79, 998–1006. doi:10.1016/j.jfoodeng.2006.03.031

Metaxas, A.C., 1996. Foundations of electroheat: a unified approach. Wiley.

Mettler Toledo, 1998. User Com - Measuring specific heat capacity.

Mossong, J., Ragimbeau, C., Schuh, J., Weicherding, P., Peetso, R., Wildemauwe, C., Imberechts, H., Rabsch, W., Bertrand, S., 2012. Investigation of an excess of Salmonella enteritidis phage type 14b and MLVA type 4-7-3-13-10-2-2 in Luxembourg, Belgium and Germany during 2010. Bull. Société Sci. Médicales Grand-duché Luxemb. 49–62.

Nakamura, R., Fukano, T., Taniguchi, M., 1982. Heat-Induced Gelation of Hen's Egg Yolk Low Density Lipoprotein (LDL) Dispersion. J. Food Sci. 47, 1449–1453. doi:10.1111/j.1365-2621.1982.tb04958.x

Nelson, S.O., 1984. Density dependence of the dielectric properties of wheat and whole-wheat flour, in: Journal of Microwave Power. Presented at the Annual International Microwave Power Symposium. 18, International Microwave Power Institute, pp. 55–64.

Nyfors, E., Vainikainen, P., 1989. Industrial microwave sensors. Artech House.

Ramachandran, R., Malhotra, D., Anishaparvin, A., Anandharamakrishnan, C., 2011. Computational fluid dynamics simulation studies on pasteurization of egg in stationary and rotation modes. Innov. Food Sci. Emerg. Technol. 12, 38–44. doi:10.1016/j.ifset.2010.11.008

Romano, V., Marra, F., 2008. A numerical analysis of radio frequency heating of regular shaped foodstuff. J. Food Eng. 84, 449–457. doi:10.1016/j.jfoodeng.2007.06.006

Schuman, J. d., Sheldon, B. w., Vandepopuliere, J. m., Ball Jr, H. r., 1997. Immersion heat treatments for inactivation of Salmonella enteritidis with intact eggs. J. Appl. Microbiol. 83, 438–444. doi:10.1046/j.1365-2672.1997.00253.x

Serrano, L.E., Murano, E.A., Shenoy, K., Olson, D.G., 1997. D values of Salmonella enteritidis isolates and quality attributes of shell eggs and liquid whole eggs treated with irradiation. Poult. Sci. 76, 202–206.

Shinde, A., Das, S., Datta, A.K., 2013. Quality improvement of orthodox and CTC tea and performance enhancement by hybrid hot air–radio frequency (RF) dryer. J. Food Eng. 116, 444–449. doi:10.1016/j.jfoodeng.2012.12.001

Stadelman, W.J., Newkirk, D., Newby, L., 1995. Egg Science and Technology, Fourth Edition. Psychology Press.

Strayfield, 2007. 6 KW RADIO FREQUENCY HEATER. Strayfield.

Tiwari, G., Wang, S., Tang, J., Birla, S.L., 2011a. Analysis of radio frequency (RF) power distribution in dry food materials. J. Food Eng. 104, 548–556. doi:10.1016/j.jfoodeng.2011.01.015

Tiwari, G., Wang, S., Tang, J., Birla, S.L., 2011b. Computer simulation model development and validation for radio frequency (RF) heating of dry food materials. J. Food Eng. 105, 48–55. doi:10.1016/j.jfoodeng.2011.01.016

Wang, J., Luechapattanaporn, K., Wang, Y., Tang, J., 2012. Radio-frequency heating of heterogeneous food – Meat lasagna. J. Food Eng. 108, 183–193. doi:10.1016/j.jfoodeng.2011.05.031

Wang, S., Tiwari, G., Jiao, S., Johnson, J.A., Tang, J., 2010. Developing postharvest disinfestation treatments for legumes using radio frequency energy. Biosyst. Eng. 105, 341–349. doi:10.1016/j.biosystemseng.2009.12.003

Zhang, L., Lyng, J.G., Brunton, N.P., 2004. Effect of radio frequency cooking on the texture, colour and sensory properties of a large diameter comminuted meat product. Meat Sci. 68, 257–268. doi:10.1016/j.meatsci.2004.03.011

Zhu, H., Huang, Z., Wang, S., 2014. Experimental and simulated top electrode voltage in free-running oscillator radio frequency systems. J. Electromagn. Waves Appl. 28, 606–617. doi:10.1080/09205071.2014.881724

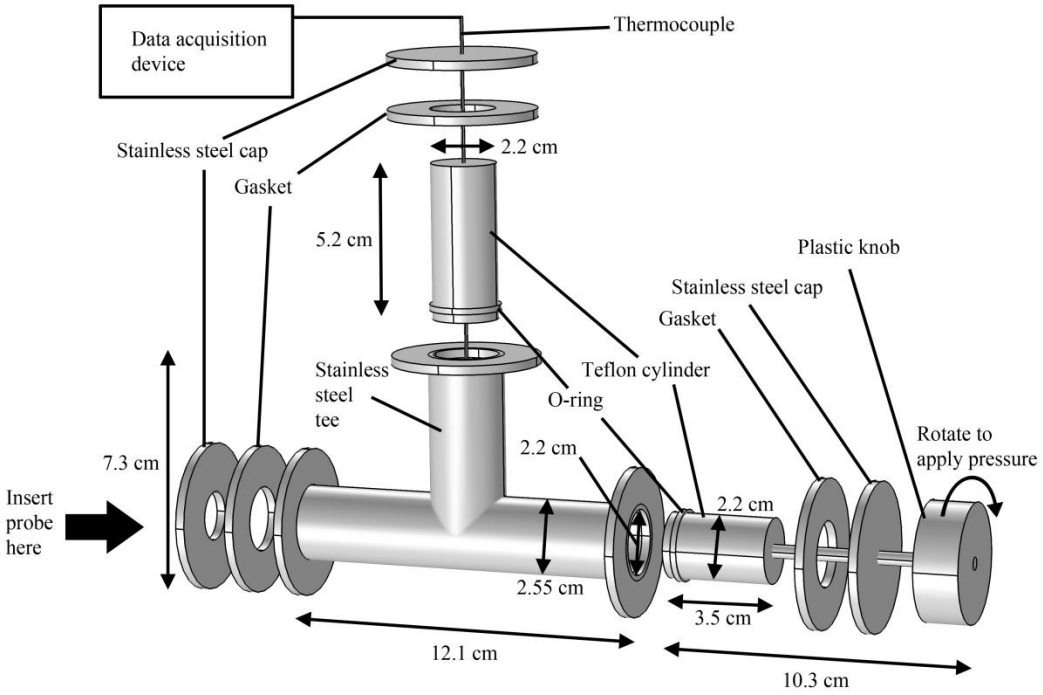

Fig. 3.1 Test cell for dielectric properties measurement of granular materials with a built-in piston to adjust the volume (and thus, density) of the sample. For liquid materials, the Teflon cylinders and plastic knob are unnecessary and thus omitted.

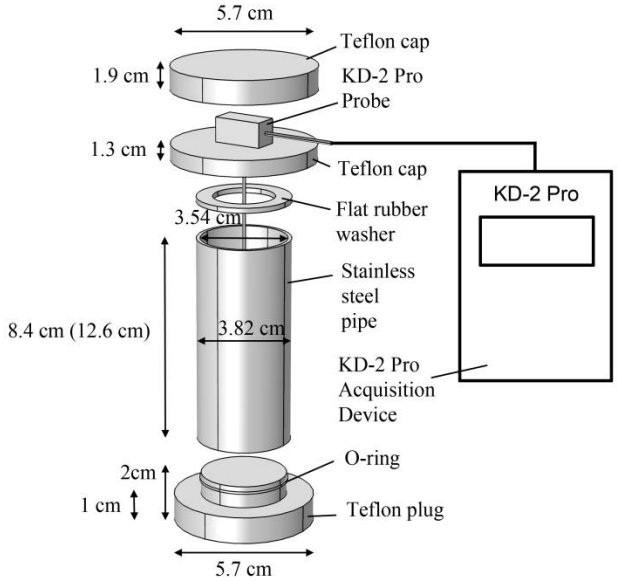

Fig. 3.2 Test cell for thermal conductivity measurement using the KD-2 Pro KS-1 probe. For granular materials, a longer pipe was used (length given in brackets) to accommodate the longer TR-1 probe.

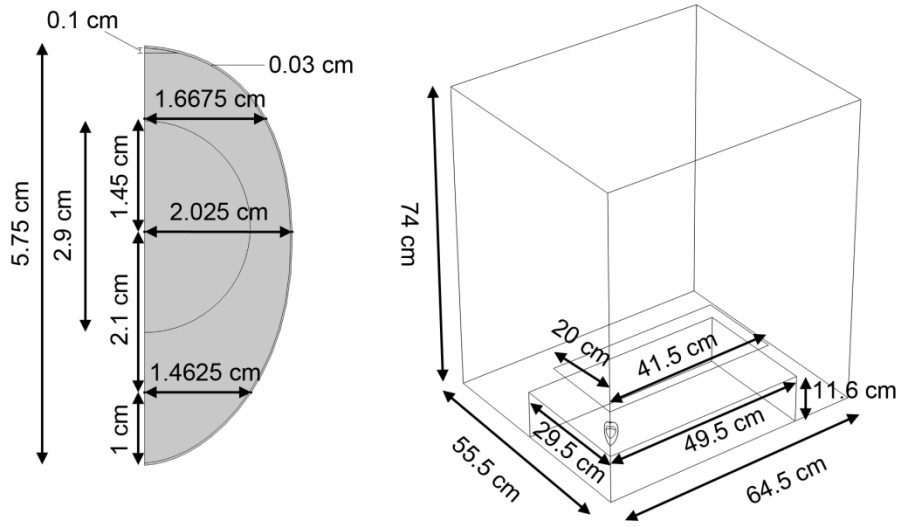

Fig. 3.3 Geometry of the model and its dimensions.

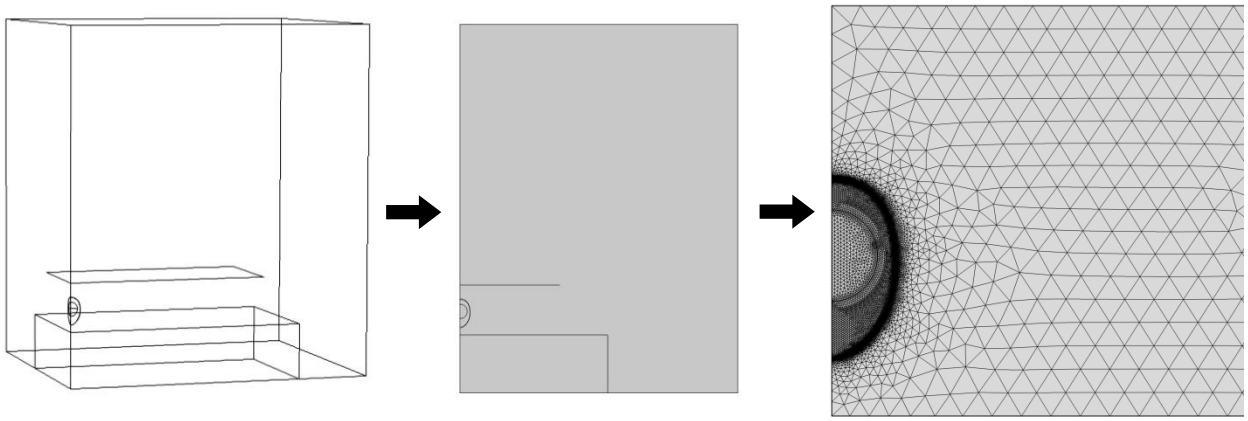

(a) (b) (c)

Fig. 3.4 Simplification of the model geometry for Orientation A, from (a) 3D to (b) 2D axisymmetric and finally to (c) a 2D axisymmetric model focused only on the space between the electrodes. Diagram is not to scale.

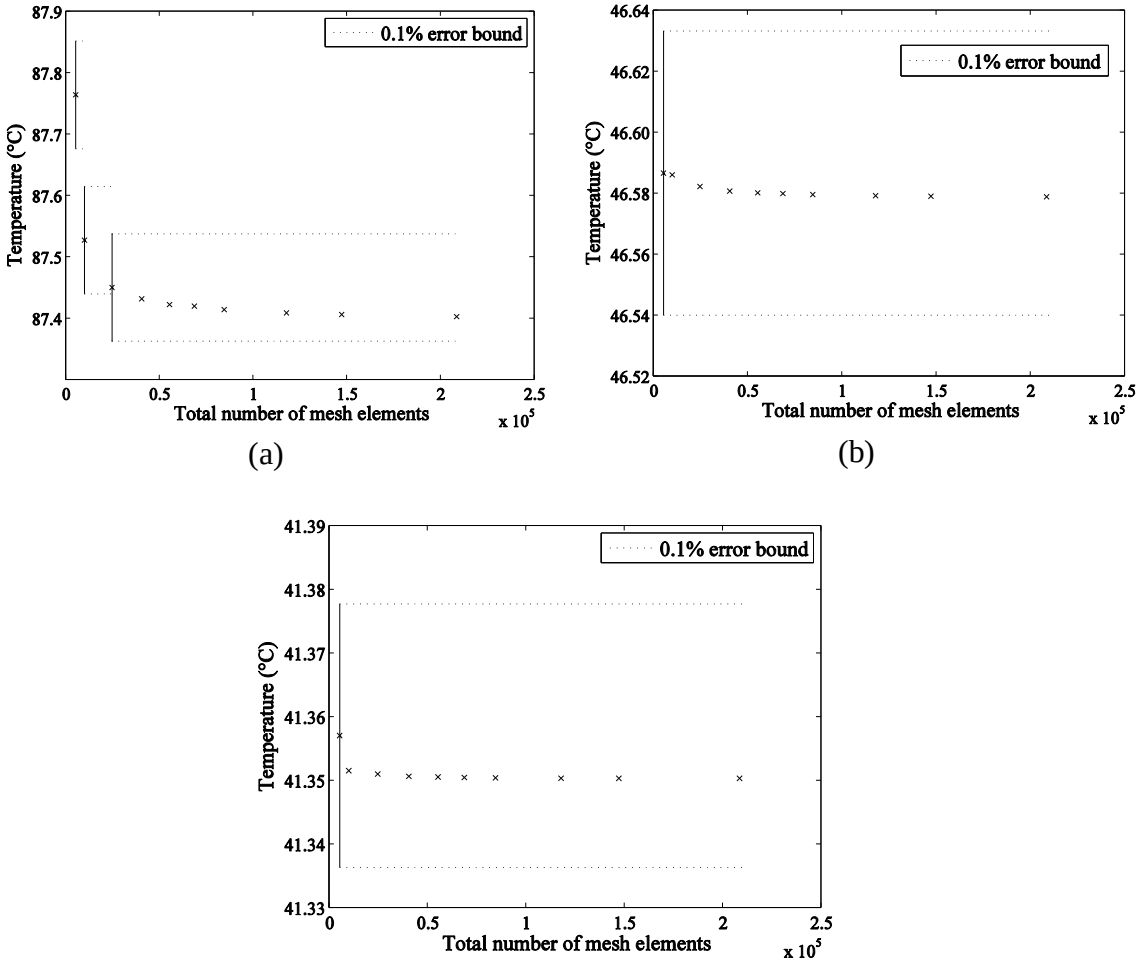

Fig. 3.5 Mesh Convergence plots for the 2Ds model: (a) maximum temperature, (b) average temperature, and (c) minimum temperature. Dashed lines represent a 0.1% error bound. Notice that the mesh converged first at (b), then at (a) and (c). In this case, the converged mesh from (a) and (c) takes priority over (b).

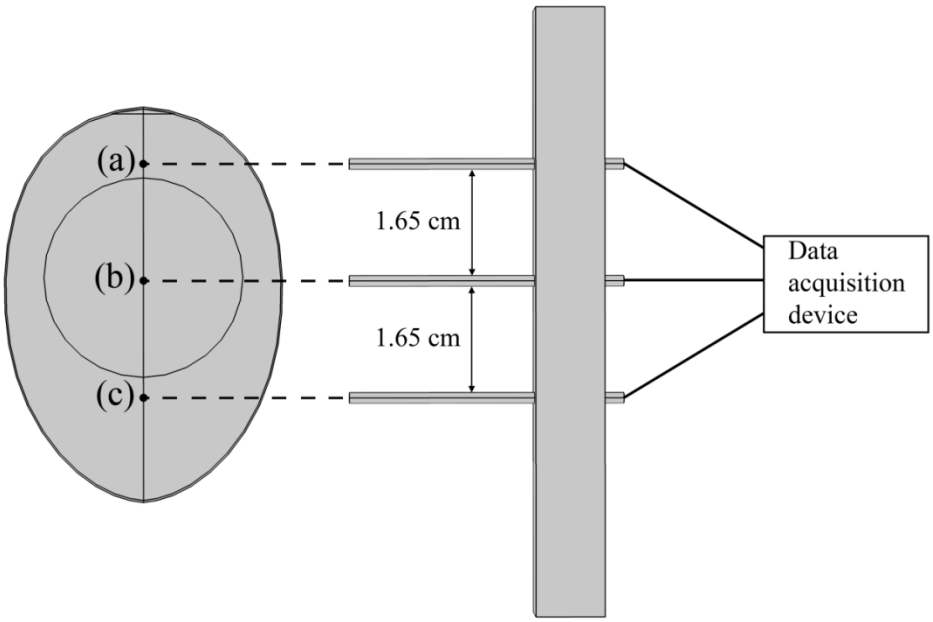

Fig. 3.6 Thermocouple array used for the validation studies. The locations measured by the thermocouples are labelled (a), (b), and (c).

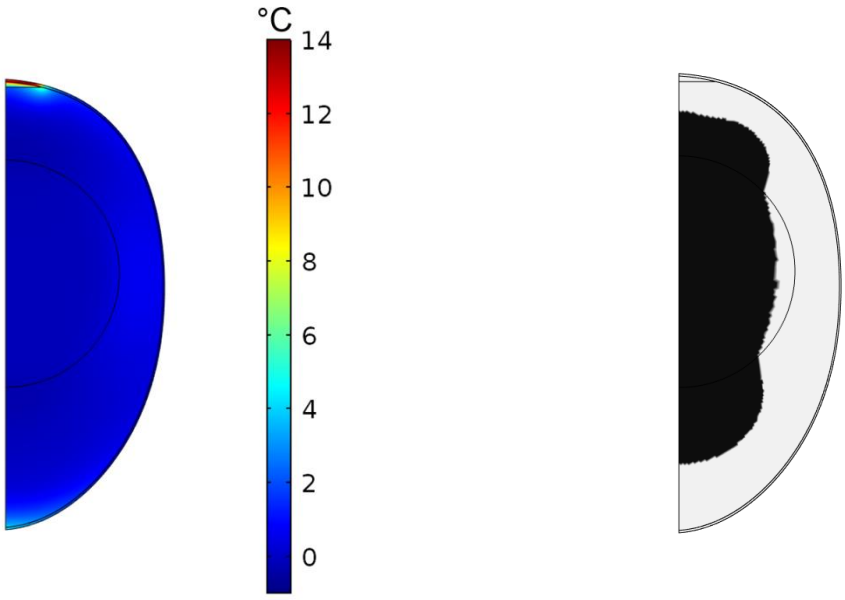

(a) Decrease in temperature (b) Regions with increased temperature

Fig. 3.7 Contour plots showing the significance of convective cooling (h = 20 W/(m^2 K^1)) for 20 s after RF heating using Orientation A with G = 13 cm and M = 0.25: (a) Decrease in T after 25 s of cooling at the end of RF heating for 420 s and (b) Boolean plot showing regions that actually increased in temperature (maximum increase of 0.406°C) during the cooling (black means increased temperature).

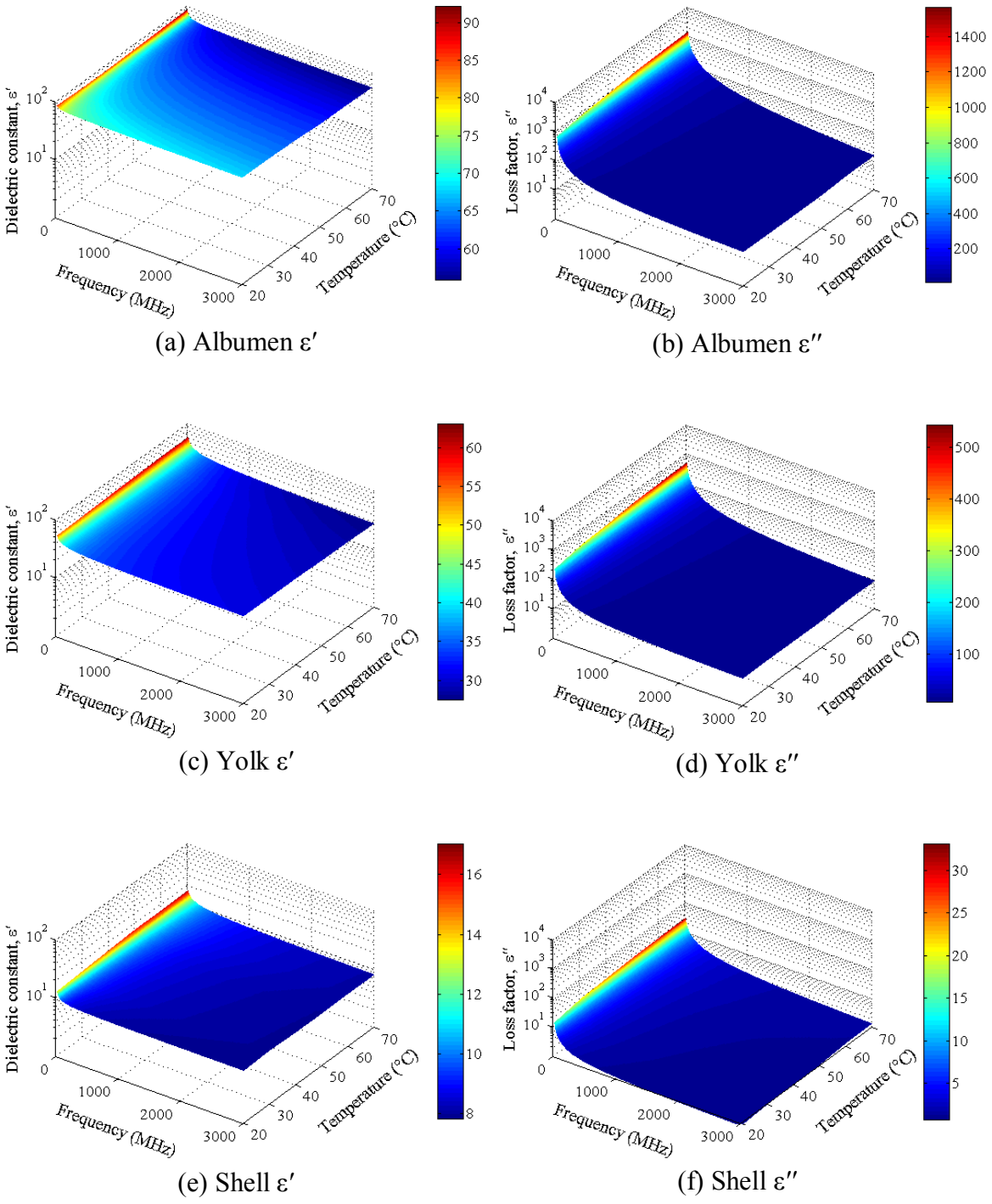

Fig. 3.8 Surface plots of the regression equations for albumen (a) ε′ and (b) ε″, yolk (c) ε′ and (d) ε″, and shell (e) ε′ and (f) ε″. Linear interpolation was performed between each temperature.

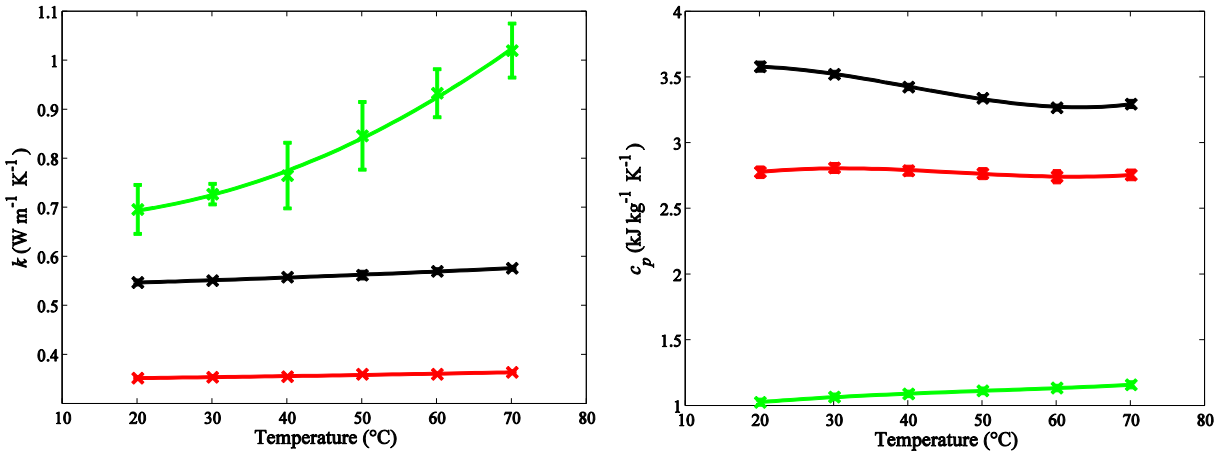

(a) Thermal conductivity, k (b) Specific heat capacity, c_p

Fig. 3.9 Graphs for k and c_p of (×) yolk, (×) albumen, and (×) shell as functions of T. One half of each error bar represents one standard deviation.

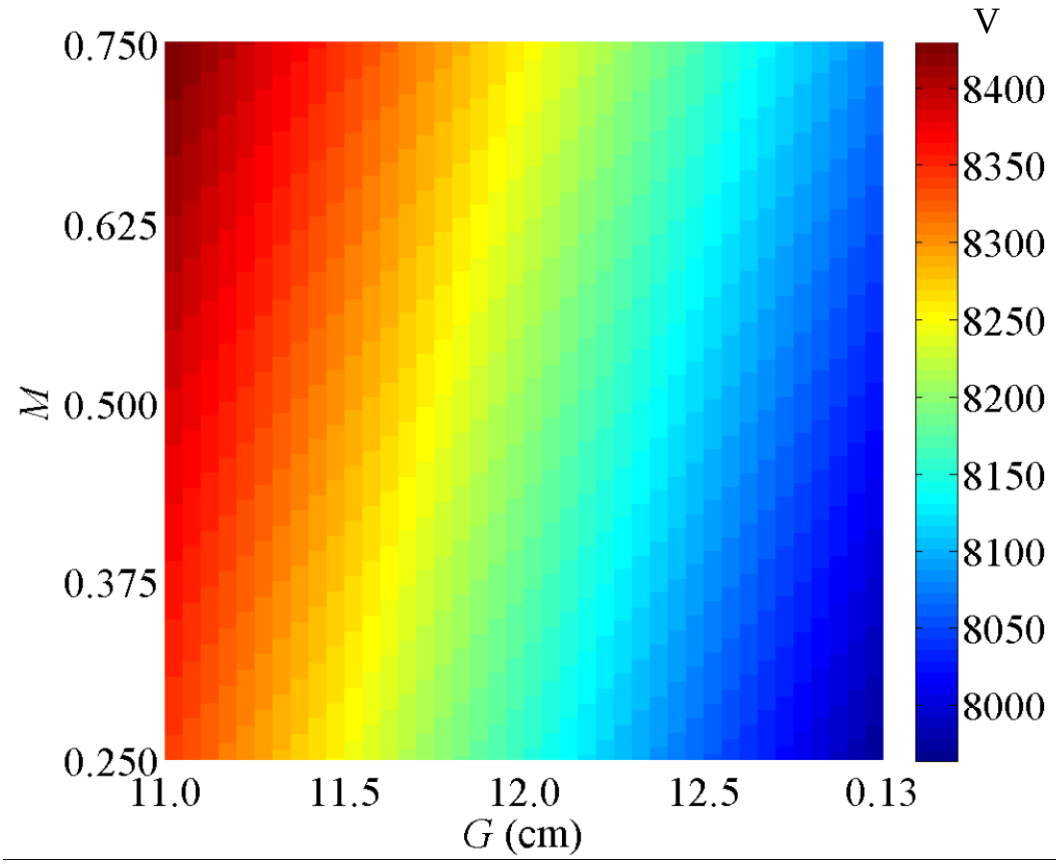

Fig. 3.10 Contour plot of voltage (V) as a function of *G* and *M*.

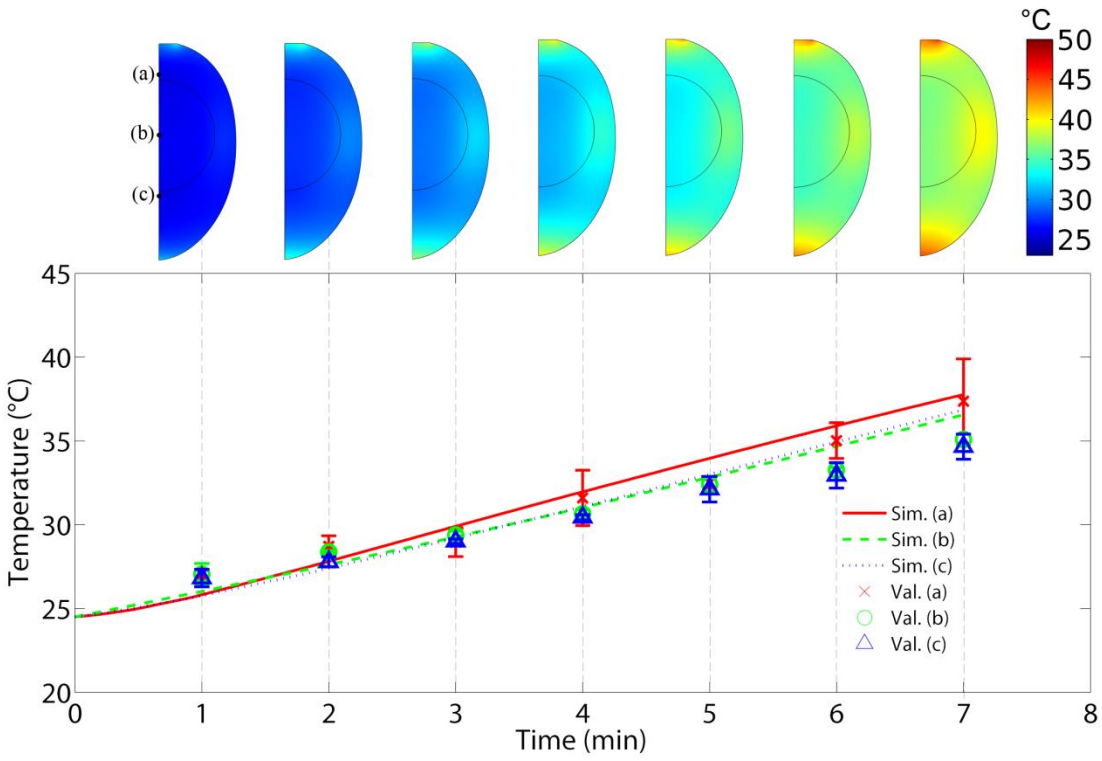

Fig. 3.11 Temperature profile evolution over time for Orientation A with G = 13 cm and M = 0.25, along with temperature contour plots at corresponding time points (shell and air cell not shown for clarity purposes). The lines represent simulation results while discrete points are for validation results. The alphabets correspond to thermocouple locations labelled in **Fig. 7**. One half of each error bar represents one standard deviation.

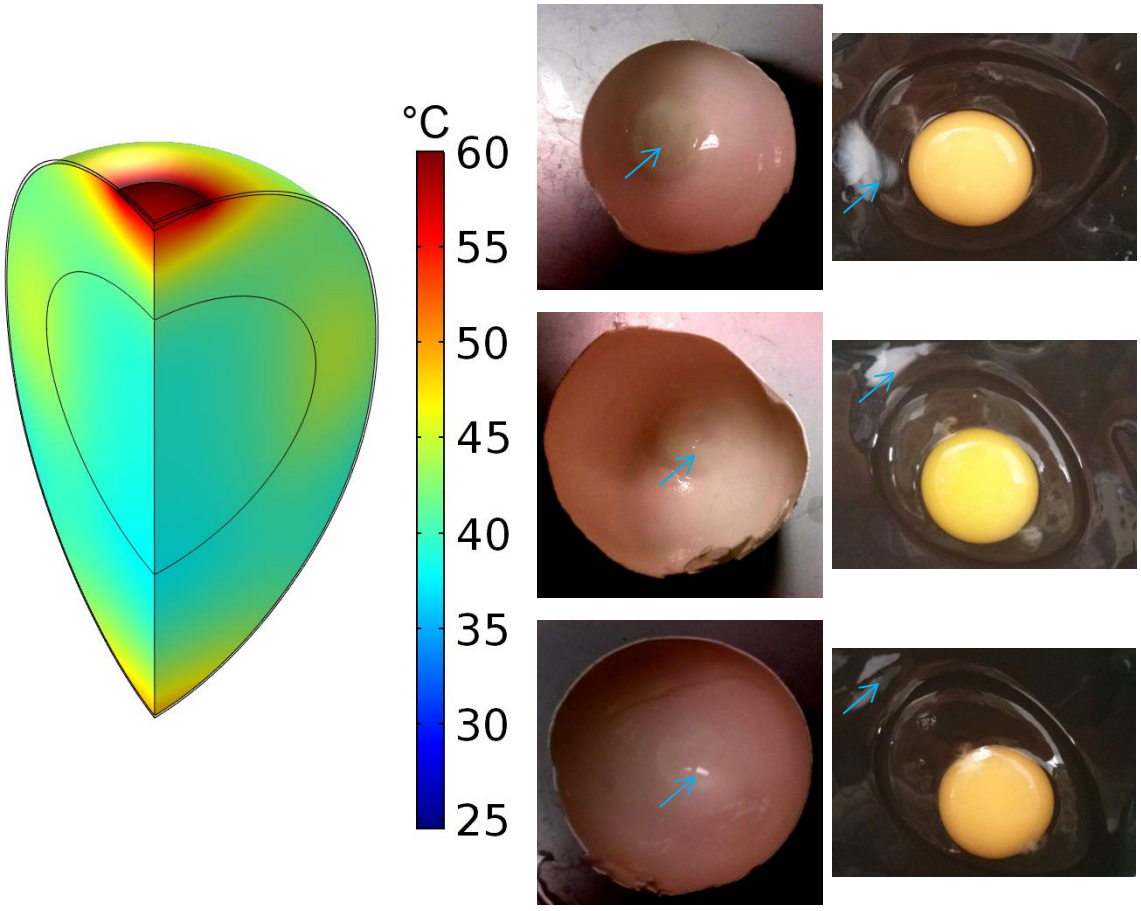

(a) Simulation result (b) Ring on the shell (c) Coagulation flecks

Fig. 3.12 The appearance of a 'coagulation ring' in simulation as well as validation results. (a)The temperature profile snapshot at t = 300 s for Orientation A with G = 11 cm and M = 0.75 shows the formation of a 'coagulation ring' around the air cell (only the yolk and albumen are shown). During the validation studies, (b) this feature was also spotted on the shells (color balance adjusted to emphasize rings), although (c) some of it adhered to the egg contents.

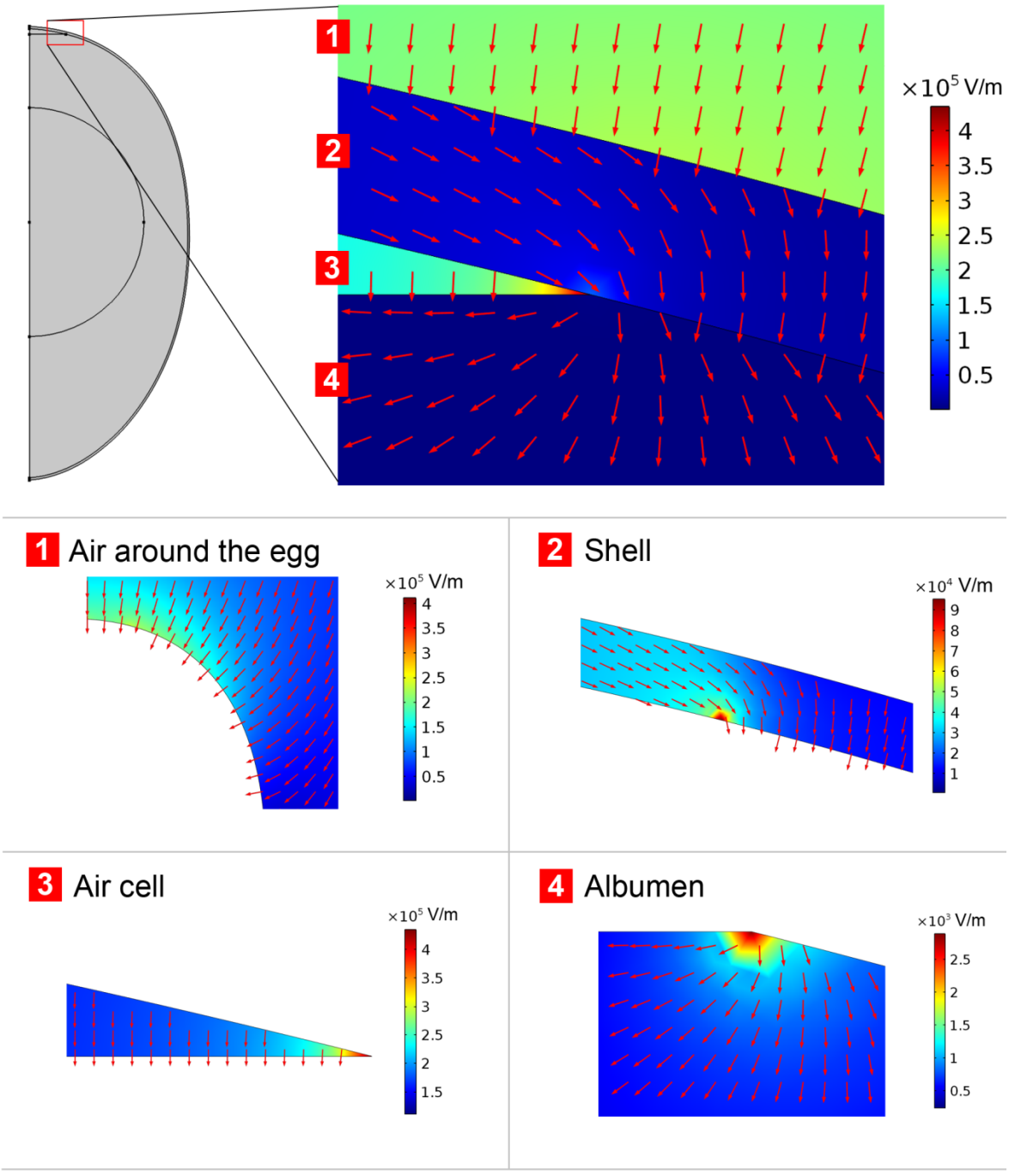

Fig. 3.13 Electric field contour and arrow plots near the air cell along with zoomed-in plots at four different locations for orientation A with G = 13 cm and M = 0.25: (1) the air around the egg, (2) the portion of the shell close to the 'coagulation ring', (3) the edge of the air cell close to the 'coagulation ring', and (4) the top portion of the albumen close to the 'coagulation ring'. Arrows only represent direction, not magnitude.

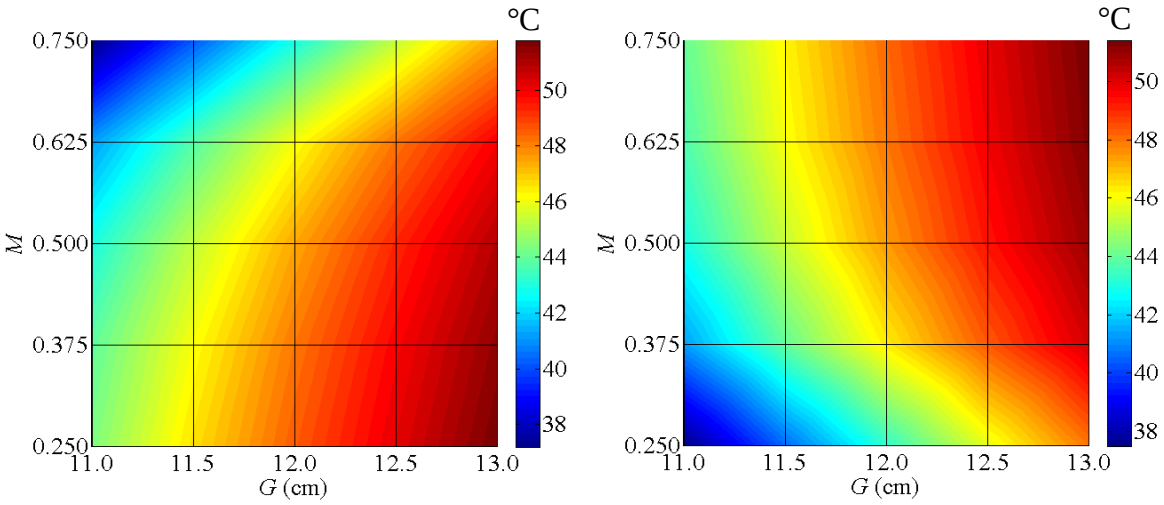

(a) Air cell closer to top electrode (b) Air cell closer to bottom electrode

Fig. 3.14 Contour plots of the maximum yolk temperature (°C) versus *M* and *G* at the time just before the optimization constraints were violated for (a) Orientation A and (b) Orientation B. Linear interpolation was performed between each data point for the contours.

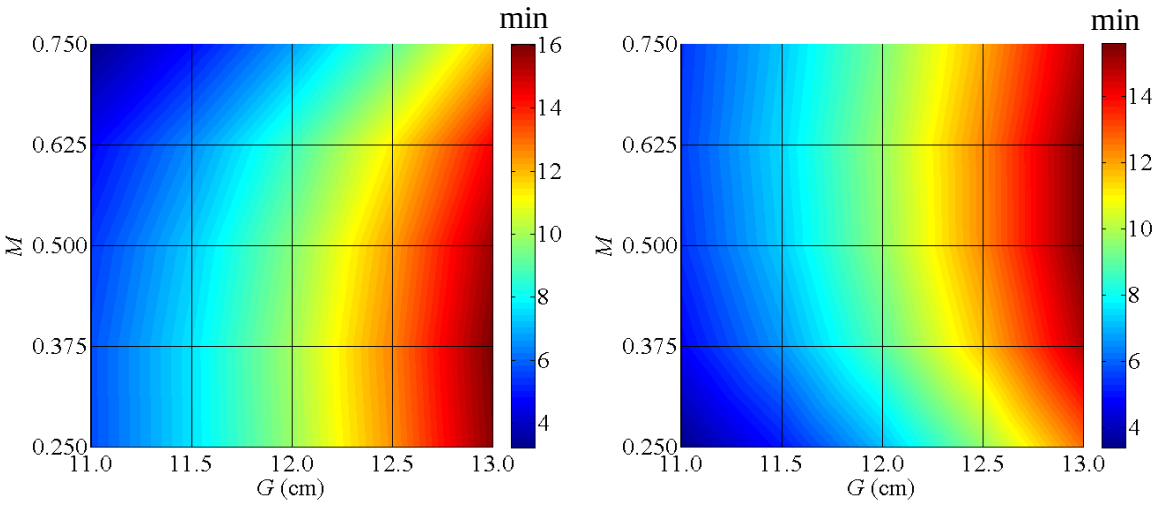

(a) Air cell closer to top electrode (b) Air cell closer to bottom electrode

Fig. 3.15 Contour plots of the time (min) when the maximum yolk temperature in **Fig. 14** were recorded for (a) Orientation A and (b) Orientation B. Linear interpolation was performed between each data point for the contours.

Table 3.1 Material properties of the domains in the finite element model.

Property	Albumen	Yolk	Shell	Air[c]
ρ (kg m^{-3})	$1045 - 0.0559T$ [a]	$1148 - 0.0559T$ [a]	2300[b]	$353T^{-1}$
ε'	Table 3	Table 3	Table 3	1
ε''	Table 3	Table 3	Table 3	0
k (W m^{-1} K^{-1})	Table 4	Table 4	Table 4	$-2.28 \times 10^{-3} + 1.15 \times 10^{-4}T - 7.90 \times 10^{-8}T^2 + 4.12 \times 10^{-11}T^3 - 7.44 \times 10^{-15}T^4$
c_p (J kg^{-1} K^{-1})	Table 5	Table 5	Table 5	$1.05 \times 10^3 - 3.73 \times 10^{-1}T + 9.45 \times 10^{-4}T^2 - 6.02 \times 10^{-7}T^3 + 1.29 \times 10^{-10}T^4$

[a]Coimbra et al. (2006), [b]Ramachandran et al. (2011), [c]COMSOL Multiphysics

Table 3.2 Coefficients for the regression equations (Eq. 6) for dielectric properties of egg components as functions of *f* (Hz) at various temperatures with adjusted R^2 values.

Component	Dielectric Property	T (°C)	a	c	d	Adj. R^2
Albumen	ε'	20	3.863×10^{3}	-0.3060	63.12	0.954
		30	6.694×10^{4}	-0.4776	63.28	0.968
		40	2.638×10^{5}	-0.5555	61.79	0.967
		50	7.763×10^{5}	-0.6152	60.11	0.963
		60	2.749×10^{6}	-0.6779	57.81	0.977
		70	4.352×10^{7}	-0.6937	54.73	0.983
	ε''	20	1.924×10^{10}	-1.0220	10.07	0.999
		30	2.035×10^{10}	-1.0060	7.431	0.999
		40	2.227×10^{10}	-1.0010	6.335	0.999
		50	2.453×10^{10}	-0.9984	5.616	0.999
		60	2.569×10^{10}	-0.9942	5.027	0.999
		70	2.678×10^{10}	-0.9908	4.685	0.999
Yolk	ε'	20	1.542×10^{4}	-0.3759	26.52	0.989
		30	3.553×10^{4}	-0.4192	26.44	0.998
		40	3.947×10^{4}	-0.4217	25.81	0.999
		50	3.874×10^{4}	-0.4167	24.92	0.998
		60	3.871×10^{4}	-0.4131	23.91	0.996
		70	4.612×10^{4}	-0.4188	22.58	0.995
	ε''	20	4.493×10^{9}	-0.9995	6.490	0.958
		30	4.706×10^{9}	-0.9809	5.498	0.999
		40	5.302×10^{9}	-0.9781	5.250	0.999
		50	6.103×10^{9}	-0.9775	5.164	0.999
		60	6.912×10^{9}	-0.9774	5.148	0.999
		70	6.986×10^{9}	-0.9742	5.105	0.999
Shell	ε'	20	5.355×10^{5}	-0.6829	7.664	0.990
		30	9.687×10^{4}	-0.5692	7.570	0.998
		40	5.347×10^{4}	-0.5258	7.410	0.996
		50	2.752×10^{4}	-0.4799	7.197	0.992
		60	1.523×10^{4}	-0.4396	7.044	0.993
		70	9.428×10^{3}	-0.4058	6.761	0.989
	ε''	20	2.390×10^{3}	-0.8536	0.591	0.993
		30	1.914×10^{3}	-0.8181	0.562	0.999
		40	1.816×10^{3}	-0.8055	0.560	0.999
		50	1.874×10^{3}	-0.7997	0.587	0.999
		60	1.992×10^{3}	-0.7979	0.707	0.998
		70	1.997×10^{3}	-0.7932	0.758	0.998

Table 3.3 Regression equations for dielectric properties of egg components at 27.12 MHz as functions of T (°C) with adjusted R^2 values.

Component	ε'	Adj. R^2	ε''	Adj. R^2
Albumen	$0.0053T^2 - 0.45T + 90.67$	0.937	$205.6T^{0.465} - 326.7$	0.999
Yolk	$12.82T^{0.1975} + 28.24$	0.993	$278.4T^{0.2599} - 431.9$	0.997
Shell	$3.081T^{0.3072} + 4.45$	0.999	$216.9T^{0.04521} - 236.8$	0.998

Table 3.4 Coefficients for the regression equation for thermal conductivity, *k* of egg components (Eq. 7), as functions of *T* (°C) with adjusted R^2 values.

Component	a	b	c	Adj. R^2
Albumen	0.0009	0.0110	0.5609	0.992
Yolk	0.0004	0.0044	0.3582	0.925
Shell	0.0298	0.1240	0.8074	0.995

Table 3.5 Coefficients for the regression equation for specific heat capacity, c_p of egg components (Eq. 8), as functions of T (°C) with adjusted R^2 values.

Component	a	b	c	d	Adj. R^2
Albumen	0.0428	0.0331	-0.1830	3.381	0.996
Yolk	0.0270	-0.0064	-0.0563	2.782	0.964
Shell	0.0056	-0.0053	0.0394	1.106	0.998

Chapter IV. Radio Frequency Heating of Shell Eggs Immersed in Deionized Water

Abstract

A total of 90 different configurations of a radio frequency (RF) oven were simulated for heating of a shell egg immersed in deionized water using a finite element model. One of the setups was chosen for validation. The model incorporated the assumptions of an infinite water domain and no liquid movement within the egg. A regression equation that relates the top electrode voltage to the gap between the electrodes and vertical position of the egg was also developed. The RMSE between the simulation and validation results ranged from 0.76°C to 2.86°C. Concentrated heating occurred in the yolk in all the investigated setups and a few of the setups had a maximum temperature above 60°C in the yolk after 20 min of RF heating. The cooling effect of the water along with lower electric field intensity in the egg caused the focused heating in the yolk. Power dissipation density in the egg was inversely related with the radius of the water cylinder, suggesting that the RF heating process could be made shorter and more efficient if the water cylinder was reduced in size.

4.1 Introduction

The chicken egg is a major agricultural commodity originating from the poultry industry. During the year 2012, an estimated 7,753 million dozen chicken eggs were produced in US, which, at 117.4 cents per dozen, is valued at about 9.1 billion dollars (United States Department of Agriculture, 2013). Its high nutritional value and versatile

functionality has led to its usage in many food products, be it cooked or uncooked. The latter is a concern because eggs are prone to contamination by *Salmonella* Enteritidis. The most recent outbreak of *S.* Enteritidis in eggs in the US occured during the year 2010, resulting in approximately 1,939 illnesses (Centers for Disease Control and Prevention, 2012).

The necessity for an effective pasteurization method led to the development of a radio frequency (RF) heating setup in Chapter III. However, it was discovered that the air cell in an egg focuses the electromagnetic waves to the interface between the air cell, albumen, and shell, thus causing a 'coagulation ring' that may not meet consumer expectations. While RF heating is excellent for homogenous food products, its heating uniformity is not guaranteed in heterogeneous foods that consist of multiple components with different dielectric properties such as lasagna (Wang et al., 2012), fruits (Birla et al., 2004), and eggs. To overcome this problem, researchers have come up with a few solutions such as enclosing the food in a medium with similar dielectric properties, mixing the food, or attaching an external heating or cooling device (Birla et al., 2004; Jiao et al., 2014a; Wang et al., 2007). In the case of shell eggs, it is desirable to focus heating at the yolk since the albumen coagulates at a lower temperature (56.7°C) than the yolk (65°C) (Nakamura et al., 1982; Stadelman et al., 1995), and also to prevent concentrated heating near the air cell, as seen in Chapter III. Therefore, a combination of surface cooling and electric field modification is required; this can be achieved via enclosure in another medium. It is desirable that the medium does not convert a significant proportion of RF energy into heat, and that it should also be food-grade since it will be in contact

with the eggs. One possible solution that satisfies all these constraints is immersing the egg in deionized water during RF heating.

The objective of this study is to determine if water-assisted RF heating could focus heating to the yolk of shell eggs. The specific objectives are to: (1) determine if liquid movement within an egg due to temperature gradients is negligible; (2) find the minimum radius of the water cylinder that results in an "infinite water" domain; (3) measure the convective heat transfer coefficient at the surface of the egg; (4) derive an equation for the top electrode voltage; and (5) validate simulation results of deionized water-assisted RF heating of shell eggs with experimental results.

4.2 Materials and Methods

4.2.1 Materials

The eggs were obtained in the similar procedure described in Chapter III. The properties of all materials used in the simulations are summarized in **Table 4.1**. The container for deionized water used in the validation studies was carved out of a bucket made of polyethylene. The vertical positions of the egg and the water container were adjusted with polypropylene cups.

4.2.2 Simulations

4.2.2.1 Overview

The software, governing equations, geometry, geometry simplification procedure (3D, 2D, and 2Ds in **Fig. 4.1**), mesh convergence procedure (**Fig. 4.2**), and validation methods used for the simulations have been described in Chapter III. There is a slight

change in the geometry: a cylindrical body of deionized water was added to the model (**Fig. 4.3**).

The addition of the deionized water domain raises some questions on how it fits into the electromagnetic and heat transfer equations. Preliminary studies show that the temperature of the water does not change much (< 1°C) during RF heating for 240 s. Therefore, heat transfer within the water was ignored in the simulations. As for the surface of the egg shell, a convective heat transfer boundary condition was applied:

$$Q = h(T_s - T_a) \tag{1}$$

where Q is the heat flux pointing out of the egg, h is the convective heat transfer coefficient (W m^{-2} K^{-1}), T_s is the temperature (K) at the surface of the egg, and T_a is the temperature of the surrounding fluid (K). The value of h is dependent on various parameters such as geometry of the object and properties of the fluid, therefore it was measured in Section 4.2.2.4.

As seen in Chapter III, the RF oven configuration is affected by multiple spatial variables such as the orientation of the egg, its vertical position, and the gap between the electrodes. The addition of the body of water introduces a slightly different array of variables:

- The vertical orientation of egg: orientation A is when the air cell is facing upwards towards the top electrode while orientation B is when the air cell is facing the opposite direction

- The vertical position of the egg within the water, z_e
- The height of the water, h_w
- The vertical position of the water from the bottom electrode, z_w
- The gap between the electrodes, G

In this study, h was fixed at a constant value (7 cm), while z_e was assumed to be negligible because the position of the egg inside the water does not change the composition of the heated objects as a whole. However, a value for z_e is still required, therefore the egg was always placed in the vertical center of the body of water. Therefore, we are now left with three variables. It should be noted that z_e can be expressed as a function of G:

$$z_e = M \times (G - h_w) \tag{2}$$

where h_w is the height of the water (cm). M is a multiplier of the empty vertical space between the electrodes and can be adjusted to change the vertical position of the water. The water is touching the bottom electrode when M = 0 and touches the top when M = 1. Therefore, M will be used as the variable for adjusting the position of the water instead of z_e because it is not dependent on G or h_w.

4.2.2.2Significance of Liquid Movement in Egg

Considering that the egg is being strongly heated by RF energy at certain locations while its surface is being cooled by the surrounding water, large temperature gradients can be expected to occur within the egg. Temperature gradients may induce liquid movement and necessitate the incorporation of fluid dynamics into the model.

However, to reduce computational effort, it is desirable to assume that the aforementioned phenomenon is negligible. Therefore, the prevalence of liquid movement within the albumen of shell eggs was investigated.

Movement of the albumen can be observed visually with the aid of a dye. To prepare the dye, 12.5 µL of albumen from an egg was first drawn into a syringe (NS601806, National Scientific Company, Rockwood, TN), followed by green food coloring (McCormick & Co., Inc., Hunt Valley, MD), and finally another 12.5 µL of albumen. This procedure was necessary to ensure that the dye does not escape out of the syringe needle when it is being inserted into or removed from the egg. A hole on the shell of an egg was made 2.7 cm away from the end without the air cell along the long axis of the shell using a screwdriver. The dye mixture was injected 0.7 cm deep into the hole, which was then sealed with electrical tape (Scotch® Super 33+™ Vinyl Electrical Tape, 3M, St. Paul, MN). The egg was candled to confirm the position of the dye (**Fig. 4.4(a)**) before being subjected to one of three treatments (**Fig. 4.4(b)**): immersion up to 2 cm from the broad end (air cell) of the egg in 50°C water for 10 min (treatment A), RF treatment for 10 min (treatment B), or left at room temperature for 10 minutes (control – treatment C). Treatment A aims to emulate the worst-case-scenario whereby an extreme temperature gradient exists between the ends of the egg. The RF oven configuration for treatment B was from a preliminary study to investigate the effectiveness of using deionized water as a processing aid. Its configuration is shown in **Fig. 4.5**. After being subjected to a treatment, the egg was cooked in a 90°C water bath for 10 min, peeled, and

divided into several slices using an egg slicer. Each treatment was performed in triplicates, for a total of 9 eggs.

4.2.2.3Infinite Water Assumption

It is desirable to find a minimum radius of the water cylinder such that the heating pattern of the egg is not affected by variability introduced by the edges of the water domain. Nonuniform heating due to edges is a known problem in RF heating of foods. For example, the edges and corners of a cuboid sample is prone to over-heating (Alfaifi et al., 2014) or cooling (Wang et al., 2014), depending on what is being heated. Cylindrical samples are no exception to this because the power dissipation density at its edges are high compared to other regions in the sample (Tiwari et al., 2011). Therefore, an infinitely large (radius-wise) water cylinder would negate the effects from the edges, but the large amount of water required makes this an unattractive solution. It is thus necessary to find a minimum radius of the water cylinder such that the egg is isolated from fringe effects from the top electrode and the walls of the water container without using a huge amount of deionized water. This investigation was carried out with a set of preliminary simulations whereby the radius of the water cylinder was gradually increased until no significant difference (less than 5%) is seen in the maximum, average, and minimum temperature power dissipation density in the albumen and yolk. Only the albumen and yolk were investigated because these components are important for pasteurization purposes and the air cell is likely to have negligible power dissipation which could distort the minimum power dissipation density readings. The preliminary simulations used an

electrode gap of 13 cm, an arbitrary top electrode voltage of 7500 V, and the egg and water were placed in the vertical center of the gap between the electrodes.

4.2.2.4Determination of Convective Heat Transfer Coefficient

During RF heating, the temperature inside the egg would be rising while the deionized water surrounding it remains close to room temperature, thus creating temperature gradients in the water close to the surface of the egg. This leads to natural convection cooling of the egg. Therefore, it was necessary to measure the convective heat transfer coefficient, h (W m^{-2} K^{-1}) at the surface of an egg when placed in deionized water during RF heating. This coefficient will then be used in heat transfer equations of the model.

The lumped system analysis was used to measure h. This approach assumes that internal conductive resistance is negligible compared to external convective resistance. In other words, heat absorbed at the surface of an object is assumed to be instantly distributed uniformly throughout the object. With this assumption, the following heat balance equation across the boundary of the egg can be written (Singh and Heldman, 2008):

$$mc_p \frac{dT}{dt} = hA(T_a - T) \tag{3}$$

where m is the mass of the object (kg), c_p is the specific heat capacity of the object (J kg^{-1} K^{-1}), T is the temperature (K) at every location throughout the egg at a given time t (s), and A is the surface area of the object.

By performing separation of variables and integrating, we get:

$$-\ln\left(\frac{T_a - T}{T_a - T_i}\right) = \frac{hA}{mc_p}t \tag{4}$$

Assuming h and the material properties remain constant, the above equation appears to follow the form of a linear equation $y = kt$. Therefore, h is part of the slope, k and can be easily derived from a plot of equation (4).

Since the lumped system analysis requires that the object has a very low internal conductive resistance, an egg-shaped object made of a material with high thermal conductivity is required for this analysis. Thus, a block of 6061-T6 aluminum alloy (k = 167 W m^{-1} K^{-1}, c_p = 896 J kg^{-1} K^{-1}, ρ = 2700 kg m^{-3}) was shaped into an egg using Computer Numerical Control (CNC) machining with a final mass of 0.1358 kg (MatWeb, n.d.). Since a computer-aided design (CAD) model was used as the input for the CNC machine, A was determined to be 0.00672 m^3 by numerically integrating the surface area of the CAD model. Expansion of the egg and its surface area due to heating was assumed to be negligible. A hole was drilled to the center of the aluminum egg which was then filled with thermal paste (Arctic Silver® 5, Arctic Silver, Visalia, CA) to improve thermal contact with a thermocouple (type T, OMEGA Engineering, Inc., Stamford, CT) inserted into that hole. The aluminum egg was equilibrated to 40°C via immersion in a circulating water bath (RTE-100, Neslab Instruments, Inc., Portsmouth, NH), and then transferred to the container of deionized water used in RF heating. Data from the thermocouple was recorded using a data acquisition device (USB-TC, Measurement Computing Corporation, Norton, MA). The experiment was repeated to obtain four

replicates. The acquired data was transformed into the form of equation (4), and h was determined from the slope, k:

$$h = \frac{kmc_p}{A} \tag{5}$$

A simple rearrangement of equation (4) could be performed to calculate T from the newly determined value of h:

$$T = T_a - (T_a - T_i)e^{-\frac{hA}{mc_p}t} \tag{6}$$

Equation (6) can be used to plot a time-temperature curve that can be compared to the experimental results to see how well both curves agree with each other.

One important question to ask is whether the temperature of the water surrounding the egg, T_a remains constant throughout RF heating because it is assumed to be constant in the lumped system analysis. To test its variability, the deionized water was stirred with a glass rod before each experiment and thermocouples were inserted into the water to obtain its average temperature. This was repeated immediately after the lumped system analysis experiment was completed. The average temperature before and after were then compared to answer this question.

4.2.2.5 The Effect of Electrode Gap and Position of Water

In Chapter III, it was seen that the voltage of the top electrode depends on the gap between the electrodes and the vertical position of the heated sample. Therefore, this relationship needs to be established to be used as an input in the model.

During preliminary studies, electrode gaps smaller than 13 cm regularly caused arcing. Therefore, a minimum value of 13 cm was used for G in this study. Following the procedure used in Chapter III, the effect of G and M were investigated across the following ranges:

- G: From 13 cm to 17 cm, in 2 cm increments
- M: From 0.25 to 0.75, in 0.25 increments

Thus, 9 configurations were investigated, with three replicates per configuration. Eggs were then heated according to these configurations and analysis were performed as in Chapter III, Section 3.2.2.5. The only difference is that the voltage sweep was performed from 6000 V to 8000 V. The derived regression equation was used as an input in the simulations.

4.2.2.6Finding the Optimal Setup

Using the prepared model, a sweep could be performed across the three variables discussed in Section 4.2.2.1 to identify an optimal RF configuration. At the same time, it is necessary to adhere to the domain of G and M used in the voltage regression equation; therefore both variables were investigated accordingly:

- G: From 13 cm to 17 cm, in 0.5 cm increments
- M: From 0.25 to 0.75, in 0.125 increments

Keeping in mind that there are two possible vertical orientation of the egg, a total of 90 configurations were simulated using a Dell workstation with two Intel E5-2630 processors and 88 GB RAM running a Windows 7 64bit operating system.

The simulation results were filtered to obtain the temperature profile at the time just before any of the following conditions were violated:

Condition 1: The maximum temperature in the egg yolk exceeds 65 °C.

Condition 2: The maximum temperature of the albumen exceeds 56.7 °C.

Condition 3: RF heating has been performed for 20 min.

Condition 1 and 2 are for filtering out results that have coagulation in either the albumen or yolk. One of the setups (G = 13 cm, M = 0.75) was validated experimentally.

4.2.3 Model Extrapolation

4.2.3.1RF oven scale-up

Results from Section 4.2.2 confirmed that RF heating assisted with deionized water is able to heat the yolk without coagulating the albumen. However, the process time was rather unsatisfactory. One of the limitations of the results is the low power of the pilot scale RF oven modeled in this study. It would be of practical interest to investigate if the results could be improved with a more powerful RF oven.

An RF oven with a higher power output would be doing more work per unit time. Since the top electrode voltage is related to the amount of work done, there exists a

positive correlation between power and top electrode voltage. Therefore, the RF oven in this extrapolation study is scaled-up by increasing the voltage of the top electrode. The RF setup used for this purpose is the one validated in Section 4.2.2.6 (G = 13 cm, M = 0.75). Top electrode voltage was increased to 8500 V, 9500 V, and 10,500 V from the original 7583.5 V. Once again, the results were filtered using the three conditions stated in Section 4.2.2.6 to obtain the temperature profile in the egg before any coagulation occurs.

Preliminary results indicate that the yolk managed to reach a reasonably high temperature for pasteurization. However, the albumen always remained close to the temperature of the surrounding deionized water. Therefore, the simulations were further extended by adding a hot water bath immersion process for 40 min because the RF heating only serves as a way to bring up the temperature in the yolk; the albumen close to the surface of the egg can be easily heated up at the end of the RF process using conventional thermal treatments. The spatial temperature data extracted from the end of the RF heating simulations were used as input to the water bath simulations, assuming that the egg was instantly transferred from the RF process into a water bath. The convective heat transfer at the surface of the egg was modeled using equation (1) with the h (W m^{-2} K^{-1}) values 100, 1000, and 10,000. These values are arbitrarily chosen; food processors can modify their water bath equipment to obtain a h value of their choosing. The ambient temperature was set to 55°C, which is slightly below the coagulation temperature of albumen (56.7°C). The time-temperature data were then used as input into a *Salmonella* thermal death time model described in Section 4.2.3.3.

4.2.3.2 Contamination in Water

The simulations so far assume an ideal situation whereby the egg is constantly immersed in deionized water. However, in a real world setting, the purity of the water may not be guaranteed during the entire process. It could be contaminated by residue on the surface of the egg and equipment or if the water filtration system is not working properly. Therefore, the validated model was extrapolated to model the effect of water contamination on the temperature profile in the egg.

Contamination of the water was modeled using dielectric properties of various salt solutions measured by Ikediala et al. (2002) at 27 MHz (**Table 4.5**). It was assumed that the thermal conductivity, specific heat capacity, and density of the water remained unchanged. The "contamination" of the water was adjusted by using the dielectric properties of tap water from Pullman, WA and salt solutions with concentrations 0.05%, 0.10%, 0.15%, and 0.20%.

Considering that the loss factor of the contaminated water is high enough to cause significant heat generation which may not be uniform, there will be temperature gradients in the water domain which will cause convection. Since the purpose of the model extrapolation is to only gain an insight of what might happen, the convection in the water and its effects on h are ignored. Instead, the water domain was modeled as a solid and a convective cooling condition (h = 20 W m^{-2} K^{-1}) was applied on its surface while its other surfaces were assumed to be insulated due to the low thermal conductivity of the plastic container. Its average temperature which increased over time was then used as T_a in

equation (1). The heat gained by the water from the egg was assumed to be negligible due to the relative sizes of the both domains.

4.2.3.3Integration with **Salmonella** *thermal death time model*

The scale-up of RF oven power in Section 4.2.3.1 allows the egg to reach a reasonably high temperature for pasteurization. The model can be integrated with a *Salmonella* thermal death time model to predict the lethality of RF heating combined with hot water immersion. The D-values for various *Salmonella* serovars in yolk (**Table 4.2**) and albumen (**Table 4.3**) were adapted from the work of Doyle and Mazzotta (2000), excluding the Senftenberg 775W serovar due to its abnormally high thermal resistance. The logarithm to base 10 of these values were then plotted against temperature and a linear equation for both yolk and albumen were fitted (**Table 4.4**). The Z-values were derived directly as inverse of the gradients of the linear equations. With these linear equations, the D-value of the *Salmonella* mixture can be determined at any temperature:

$$D = D_{ref} \times 10^{\frac{T_{ref}-T}{Z}}$$

where D is the D-value of the *Salmonella* mixture (min) at the temperature T (°C), D_{ref} is the D-value of the *Salmonella* mixture (min) at the reference temperature T_{ref} (°C), and Z is the Z-value determined from the linear equations derived earlier. The D_{ref} and T_{ref} were simply calculated from an arbitrary temperature using the equations in **Table 4.4**: 3.79 min at 55°C for albumen and 11 min at 55°C for yolk.

The question now arises on how one could calculate the log reduction of *Salmonella*. One thing to note here is the discrete nature of the results of the simulations: temperature values are given at discrete time points, not as a function of time. Therefore, when it comes to calculating the log reduction between time point t_i and t_{i-1}, it will become necessary to decide what D-value to use. One could use the D-value calculated using the temperature at t_i, t_{i-1}, or an average of both. Since temperature is always expected to increase in a heating process, the D-value at t_{i-1} would be a conservative estimate since we are assuming that the D-value doesn't increase during the time interval $t_i - t_{i-1}$ even though the temperature is increasing. On the other hand, by using the D-value at t_i, one would be overestimating the lethality of the process. The average of D-values would be a balance between both extremes. To ensure food safety, it is always better to be safe than sorry, therefore the conservative estimate will be used to calculate the log reduction of *Salmonella*:

$$N_r = \frac{t_i - t_{i-1}}{D_{i-1}}$$

where N_r is the amount of log reduction of *Salmonella*, and D_{i-1} is the D-value calculated using the temperature at time point t_{i-1}.

4.3 Results and Discussion

4.3.1 Liquid movement in Eggs

For all three treatments, no significant movement of the dye was observed. **Fig. 4.6** shows the slices of the eggs after being boiled. Although there is some spreading of

the dye around the initial injection point, there is no clear movement of the dye towards the top or bottom of the eggs. This indicates that the dye only moved via diffusion, and liquid movement due to temperature-induced density differences is negligible. Computational fluid dynamics studies performed by Denys et al. (2004) and Ramachandran et al. (2011) suggest that egg white movement due to temperature-induced density differences is in the order of 10^{-4} to 10^{-5} m/s. Such low velocities might not generate sufficient propelling force for the dyes to move. Besides that, both studies assumed that the egg white is a free flowing liquid within the egg; in reality, the egg white consists of a thick and thin part, the former of which behaves like a gel and adheres to the yolk. Therefore, the actual magnitude of the velocities may actually be less than the ones predicted in both studies. In addition, measurements by Kumbár et al. (2015) demonstrated that the viscosity of egg white is inversely proportional to storage time. Considering that the eggs in this study were used on the same day on which they were laid, the viscosities of the egg whites were at their highest. Since liquid movement can be safely neglected, its physics were not incorporated in the simulations.

4.3.2 Infinite Water Assumption

The radius of the water cylinder at which the infinite water assumption is satisfied was found to be 13.5 cm. Any further increase in radius does not change the maximum, average, or minimum power dissipation density by more than 5% (**Fig. 4.7**). At this radius, it is assumed that the egg is no longer affected by fringe effects from the edges of the water domain and the top electrode. In other words, from the submerged egg's perspective, it appears as if the electric field is coming down from the surface of the

water in a uniform fashion. In contrast, if the water cylinder is too small, the walls of the container would modify the electric field such that the electric field at the surface of the water is anisotropic. A picture speaks a thousand words (or arrows), therefore the reader is referred to **Fig. 4.8** for a visual representation of how the fringe effects are removed as the radius of the water cylinder increases. The electric field around the egg when the radius of the water cylinder was at 7.5 cm had a higher magnitude compared to that of 17.5 cm radius. At the same time, there exists a region between the egg and the edge of the 17.5 cm radius water cylinder where the electric field just points downwards. From the perspective of the egg, it seems as if the water is infinite. A suitable metaphor for this situation is a person stuck in the middle under rain clouds versus a person near the edge of the rain clouds. To the former person, it seem as if rain is falling everywhere, but to the latter, he or she can see that outside of the rain clouds is a sunny and dry weather. The radius of 13.5 cm is a fine balance between these two extremes: reducing the size of the rain cloud while still "tricking" the person that he or she is completely surrounded by rain. The 13.5 cm radius was used in simulations and for the water container in validation studies.

It is interesting to note that all three statistics for the power dissipation density have an inverse relation with the radius of the water cylinder. This implies that the power transfer from the RF oven to the egg is more efficient when the water cylinder is narrower. The higher power dissipation density is probably due to the higher electric field magnitude around the egg when the radius of the water cylinder is smaller. Therefore, this parameter could be tweaked to increase the heating rate.

4.3.3 Convective Heat Transfer Coefficient

Analysis of the curves plotted using equation (4) and (5) produced an average *h* of 362.5 W m^{-2} K^{-1} with a standard deviation of 14.1 W m^{-2} K^{-1}. Along with the properties described in Section 4.2.2.4, this produces a Biot number less than 0.1, thus validating the lumped system analysis. A comparison between the theoretical temperatures at the center of an aluminum egg calculated using equation (6) and the value of *h* versus the experimental temperatures is given in **Fig. 4.9**. One half of each error bar represents the standard deviation of the measurements. The trend of the theoretical temperature slightly deviates from the experimental temperature. Since the disparities between both temperatures are not contained within the standard deviation of the experimental measurements, the difference in trend is not caused by experimental errors. It is more likely that *h* has some form of dependence on temperature: the experimental temperature dips faster at the beginning when the aluminum egg is close to 40°C but its cooling rate slowed down when its core temperature was closer to the ambient temperature. Therefore, the calculated value of *h* overpredicts cooling when the temperature is close to 40°C but slightly underpredicts cooling at the other end of the temperature spectrum. However, this disparity is only 2.7°C at most (at 35°C) and the RMSE between both measurements is 1.2°C. In addition, simulations show that the temperature of the egg near its surface is at most 30°C even after 20 min of heating. Therefore, simulations were performed with this value of *h*, keeping in mind of the slight error introduced by it.

4.3.4 Voltage Equation

Linear effects from both G and M significantly affected the top electrode voltage at p = 0.05. On the other hand, quadratic and interaction effects were deemed insignificant. Therefore, the resulting regression equation incorporated only G and M:

$$V = 11714 - 29722Gk_1 - 533.33Mk_2 \quad (7)$$

where k_1 = 1 V/cm and k_2 = 1 V. Both constants serve to ensure consistency of the units of the regression equation.

A plot of this equation can be found in **Fig. 4.10**. The top electrode voltage has an inverse relationship with both G and M. This relationship with G has been observed by Zhu et al. (2014) too. It should be noted that the effect from M pales in comparison to G (533.33 versus 29722).

4.3.5 Simulation and Validation

The comparison between the simulation and validation for the RF heating configuration with G = 13 cm and M = 0.75 for Orientation A is given in **Fig. 4.11**. The RMSE for thermocouple location (a), (b), and (c) are 0.76°C, 0.86°C, and 2.86°C, respectively. Throughout the duration of the process, both sets of data exhibited similar trends, with the yolk center always having a higher temperature compared to the locations on the albumen. However, there exists some disparity in the measurements made at (a) and (c). First of all, there is a noticeable difference between the experimental and simulation results. Secondly, the simulations predict (c) to have a slightly higher temperature than (a); the reverse was seen in the validation experiments. These errors do not seem to be caused by random errors because the standard deviations of the

measurements are rather small (less than 1.4°C). One possible explanation for the differences is the assumptions made for *h* in Section 4.3.3. It was observed that *h* had a slight dependence on temperature but this was not included in the final model. A comparison in terms of RMSE between the current validated model and models with different constant values of *h* is shown in **Fig. 4.12**. It is clear that as *h* increases, the RMSE decreases for all time points. This is especially true after 8 min. Since the temperature of the egg increases with time and the RMSE for the higher values of *h* improves significantly with time, there is now reason to suspect that there is a positive correlation between *h* and temperature. Another possibility that could have caused the disparity between the simulations and validations is the delay between the end of RF heating and temperature measurement. There exists a delay of approximately 25 s to shut down the RF oven, open the door, transfer the egg to the measurement station, drill holes on the shell, and insert the thermocouples. During this period, there is some movement and handling of the egg which could promote more heat transfer thus causing the consistent errors seen in the results. Regardless of these possibilities, it should be noted that the yolk is the main interest in this study instead of the albumen. The albumen is always the easiest component to pasteurize due to its proximity to the surface of the egg which allows usage of conventional thermal treatments. Besides that, it contains natural antimicrobials such as lysozyme, ovotransferrin, ovomucoid, and avidin (Howard et al., 2012).

All of the 90 simulated RF configurations reached 20 min of heating without violating any of the coagulation conditions. An overview of the temperature profile of the

eggs in Orientation A after 20 min of heating is given in **Fig. 4.13**. There is a clear trend that a smaller electrode gap induces more heating, particularly more so in the yolk. In addition, when the egg is closer to either of the electrodes (M = 0.25 or M = 0.75), a higher temperature in the yolk was achieved. In all cases, the center of the egg has a higher temperature than the regions close to the surface of the egg. This temperature distribution highlights a uniqueness of dielectric heating when combined with a cooling medium: the food is heated "inside-out."

It is imperative to understand how the addition of deionized water caused such a drastic change in the heating pattern in the egg. A comparison between egg in air versus submerged in water for Orientation A, G = 13 cm, and M = 0.5 is given in **Fig. 4.14**. The first thing to notice is that the electric field is uniformly pointing downwards when entering and exiting the water cylinder. On the other hand, there exists some attraction towards the egg when it is only surrounded by air. Even more interesting is how the electric field tends to point downward rather than to the egg inside the water (highlighted with the green dashed rectangle). The opposite happens in air: there is a strong attraction towards the egg. This difference could be explained by the difference in dielectric properties between air and deionized water: the latter has a dielectric constant which is more similar to the egg components compared to the former. Therefore, the elimination of the "coagulation ring" and focused heating in the yolk can be attributed to the cooling of the surface of the egg by the deionized water and a less intense electric field distribution within the egg.

As mentioned earlier, *Salmonella* contamination is more of an issue in the yolk than in the albumen. Therefore, the pasteurization capability of RF heating should be measured at the yolk. At 60°C, the D-value for *Salmonella* ranges from 0.28 to 1.1 min (Doyle and Mazzotta, 2000; Jordan et al., 2011). While the maximum temperature in the yolk managed to 60°C in some of the setups after 20 min of heating, the long process time makes the process rather unfeasible. In addition, the maximum temperature is located at the center of the yolk. For sufficient pasteurization, it is desirable that the entire yolk is at least 60°C to ensure that the entire yolk is pasteurized instead of just the center. Of course, a longer process time would eventually ensure that this condition is satisfied, but the process time in itself is already a problem.

The slow heating rate could be solved in multiple ways. First of all, the RF oven used in this study is a pilot-scale model that has an output of 6 kW. If a machine with higher power output was used, the heating rate would surely be increased. This possibility was investigated in the model extrapolation studies. Besides that, the results discussed in Section 4.3.2 on the radius of water suggest that a smaller radius of the water cylinder would produce a higher heating rate. It should be noted that a decrease in the radius of the water cylinder would break down the assumption that the temperature of the water remains constant. In this scenario, a constant *h* and ambient temperature in the convective heat transfer equations may no longer be applicable. It will become necessary to model fluid flow within the water domain to model the heat transfer from the egg to the water accurately.

4.3.6 Model Extrapolation

Upon increasing the voltage of the top electrode, the egg was able to achieve high temperatures sufficient for pasteurization. Besides that, the high temperatures were achieved faster as the voltage was increased: the RF heating for the voltages 7583.5 V, 8500 V, 9500 V, and 10500 V ended after 20 min, 16 min 34 s, 10 min 38 s, and 7 min 56 s, respectively. Since the water bath immersion was always performed for 40 min, the total process time simulated for all the voltages are 60 min, 56 min 34 s, 50 min 38 s, and 47 min 56 s, respectively. The temperature profiles of the eggs at the end of these RF heating simulations were used as input for the water bath simulations. The contour plots in **Fig. 4.15** shows the simulated log reduction of *Salmonella* in eggs processed with RF heating with water bath or water bath alone after total process time of 40 min. Hot water immersion by itself appears to be better than the RF heating and hot water combination at a voltage of 7583.5 V, but as the voltage was further increased, the RF heating and hot water combination had higher log reductions. It is apparent that as *h* increases, the log reduction in the albumen increases too, although this effect is not pronounced in the center of the yolk. This could be easily explained by the proximity of the yolk and albumen to the surface of the egg. Since the albumen is closer to the shell, it benefits more from a higher *h* and its temperature would increase faster. On the other hand, the yolk is relatively unaffected by a higher *h* because it only receives heat from the external environment via diffusion through the albumen. However, through detailed observation, one would notice that the log reduction near the surface of the yolk is affected by the increase in *h*. Again, this could be explained by the proximity to the surface of the egg.

In the context of food safety, one should always be concerned with the worst-case-scenario of a pasteurization process. In the worst-case-scenario of shell eggs, one should be interested in the minimum log reductions in the yolk because the albumen has natural defenses against bacterial infection (Howard et al., 2012). The plots in **Fig. 4.16** tells how the minimum log reductions in the yolk increases over time for various voltages and *h* values. Here, we see that the effect of *h* on the log reduction is quite pronounced (at least 1 log reduction) from h = 100 W m^{-2} K^{-1} to h = 1000 W m^{-2} K^{-1}. This observation confirms what we saw from **Fig. 4.15**: the surface of the yolk always has the minimum log reduction, but at the same time it is affected by changes in *h* too. However, further increase in h to 1000 W m^{-2} K^{-1} does not seem to do much, therefore one could simply stick with 100 W m^{-2} K^{-1} for a nice balance between *Salmonella* lethality and equipment efficiency. **Fig. 4.17** depicts the amount of time it takes for two RF heating setups with hot water immersion versus hot water immersion alone to achieve at least 3 log reductions. This threshold was chosen because a risk analysis performed by USDA/FSIS (2005) predicts that a 3 log reduction of *Salmonella* in shell eggs could reduce illnesses caused by *Salmonella* by around 70%. Clearly, the proposed RF heating and water bath immersion could reduce foodborne illnesses caused by *Salmonella* by a significant amount 30% faster than hot water immersion alone when the voltage of the top electrode is sufficiently high. For a voltage of 10500 V and h of 1000 W m^{-2} K^{-1}, one could expect to achieve a minimum of 3 log reductions within 37 min.

A study done by Schuman et al. (1997) revealed that hot water immersion at 57°C and 58°C for 65 min and 50 min, respectively, would produce at least 6 log reduction of

their *Salmonella* cocktail. However, they reported that the visual characteristics of the albumen were significantly changed at the end of the immersions. As mentioned in Section 4.1, the albumen begins coagulating at 56.7°C, thus giving rise to the quality degradation observed. A hot water immersion (57°C) and hot air (55°C) combination for pasteurizing eggs investigated by Hou et al. (1996) managed to achieve about 7 log reductions after 83 min of heating, but with significant changes in the visual characteristics of the albumen. In both of these studies, the process times are roughly double the time taken by the RF heating with water immersion setup mentioned earlier (~37 min). Besides that, the log reductions mainly reported in this study are the minimum amounts expected due to the capabilities of the finite element model; it would be difficult to measure the minimum log reductions in experiments. Therefore, for a better comparison with the aforementioned studies, one should look at the average log reductions in **Fig. 4.15** which are above 8 in some cases. Therefore, RF heating followed by hot water immersion has the potential to be a reliable pasteurization method for shell eggs.

The model was also extrapolated by modeling contamination of the deionized water surrounding the egg. A summary of the results is given in **Fig. 4.18**. When the salt concentration was akin to that of tap water, the temperature profile actually improved because the yolk as a whole was heated more uniformly and the albumen achieved a higher temperature. However, when the salt concentration was further increased, the differential heating effect between the yolk and albumen was lost. The concentrated heating in the yolk was lost, thus nullifying the benefits of RF heating achieved

beforehand. Besides that, an increase in salt content also decreased the amount of power absorbed by the egg, thus decreasing the efficiency of the process. This trend was not as straightforward for the water domain which absorbed more power up until 0.05% salt, but subsequently absorbed less power for higher contamination. This strange behavior can be explained using an analysis on how dielectric properties affect heating rate by Jiao et al. (2014b). They proposed that the heating rate for a slab of material with constant dielectric constant, ε' will continuously increase with its loss factor, ε'' as long as the following inequality is satisfied:

$$\varepsilon'' < \varepsilon' + \frac{d_m}{d_0} \tag{8}$$

where d_m is the thickness of the slab of material and d_0 is the thickness of the air gap between the electrodes. On the other hand, if the left hand side in the inequality (8) is larger than the right hand side, then the heating rate will decrease if the loss factor is continuously increased. The maximum heating rate would be achieved when the inequality becomes an equation. Therefore, the salt solutions were tested with this analysis with the following assumptions and conditions:

- The ε' of the salt solutions are assumed to be constant because they increased at a negligible rate compared to ε'' (see **Table 4.5**)
- The water cylinder is assumed as an infinite slab
- For the validated RF heating setup used in the water contamination studies,

$$\frac{d_m}{d_0} = \frac{7}{6}$$

Therefore, the line at which maximum heating rate should be achieved is:

$$\varepsilon'' = \varepsilon' + \frac{7}{6} \tag{9}$$

Equation (9) was plotted along with the ε'' and ε' values of the various salt solutions in **Fig. 4.19**. It is apparent that the tap water and 0.05% NaCl solution are in the thermal runaway region while the higher salt concentrations lie in the thermal "depression" region whereby any increase in loss factor would only lead to a decrease in heating rate. Comparing these results to the power dissipated by the water in **Fig. 4.18**, we see a clear agreement that the power dissipated by the water always increases with loss factor when the salt solution is in the thermal runaway region while the converse occurs in the thermal "depression" region. In any case, the contamination of the deionized water surrounding the egg should be controlled such that its dielectric properties are close to that of deionized water to achieve a satisfactory temperature profile and efficient power transfer.

It would be imperative to understand how drastic are the implications introduced by contamination of the water. **Fig. 4.20** provides an overview of how changes in the contamination level affect certain temperature values. To avoid coagulation in any of the egg components, it is necessary to enforce two conditions:

- The red dots (max yolk T) remains below the red dashed line (yolk coagulation T)
- The green asterisks (max albumen T) remains below the green dotted line (albumen coagulation T)

At the same time, for pasteurization purposes, the magenta dot (min yolk T) should be as close to 60°C as possible. The plot shows that 0.05% NaCl concentration causes the albumen to coagulate. Further increase in the NaCl concentration prevents coagulation in any of the egg components, but the pasteurization effectiveness worsens. On the other hand, if the contamination is controlled to be within the range of deionized and tap water, coagulation will be avoided. It is interesting to note that a slight amount of contamination actually increases the minimum temperature of the yolk, thus increasing the pasteurization efficiency. Thus, it will be a matter of finding a fine balance between coagulation and food safety to determine the acceptable contamination level of the water. Determination of contamination level could prove to be as simple as measuring the average temperature of the water because it appears to increase with contamination level up until 0.05% NaCl concentration. Therefore, food processors could simply monitor the temperature of the water on-line and add either deionized water or salt to adjust the contamination level of the water to achieve their needs instead of measuring the dielectric properties of the water.

4.4 Conclusion

By immersing an egg in deionized water, the “coagulation ring” encountered in Chapter III was eliminated and concentrated heating occurred in the yolk without coagulating the albumen. The vertical orientation of the egg was found to have insignificant effect on the temperature profile. The radius of the water surrounding the egg was found to have an inverse relationship with the heat generated in the egg.

Unfortunately, all of the investigated RF heating setups took 20 min but were unable to pasteurize the egg.

When the model was extrapolated to use a higher voltage at the top electrode, sufficient *Salmonella* lethality was achieved when the RF heating was followed by a hot water bath immersion. At a voltage of 10500 V and water bath convective heat transfer coefficient of 1000 W m^{-2} K^{-1}, a *Salmonella* thermal death time model predicted a minimum of 3.69 log reductions of *Salmonella* in the yolk after 40 min of process time.

The model was also extrapolated to predict what would happen if the deionized water surrounding the egg was contaminated. When the water was more contaminated than tap water, the power transfer to the egg suffered greatly and the focused heating in the yolk was lost. However, it was also discovered that a little contamination in the water could increase the pasteurization efficiency without coagulation of the egg. The contamination level was also found to have a positive relationship with the average temperature of the water which is more easily measured than dielectric properties. Therefore, food processors can measure the temperature of the water and adjust the process efficiency by ensuring the contamination level lies between deionized water and tap water.

Future studies should validate the extrapolations of the model in this study for both the top electrode voltage and water contamination. The latter is of particular importance due to the assumptions made for the temperature of the water and heat

transfer coefficient at the surface of the egg. The *Salmonella* thermal death time model should also be validated with microbiological experiments.

The process time of RF heating could be further reduced by decreasing the gap between the electrodes, although arcing may occur if the gap is too small. Alternatively, future work could aim to decrease the radius of the water to improve the heating rate, keeping in mind that at one point it will be necessary to model fluid flow within the water domain and derive an appropriate equation for *h* that will incorporate some form of dependence on temperature.

4.5 Acknowledgements

This research was supported by the Agricultural Research Division of the University of Nebraska and the Mussehl Poultry Foundation. The authors would also like to extend their gratitude to Dr. Sheila Purdum and Leo Sweet of the Animal Science Department of the University of Nebraska-Lincoln for providing shell eggs and allowing usage of their egg grading equipment.

4.6 References

Alfaifi, B., Tang, J., Jiao, Y., Wang, S., Rasco, B., Jiao, S., Sablani, S., 2014. Radio frequency disinfestation treatments for dried fruit: Model development and validation. J. Food Eng. 120, 268–276. doi:10.1016/j.jfoodeng.2013.07.015

Birla, S.., Wang, S., Tang, J., Hallman, G., 2004. Improving heating uniformity of fresh fruit in radio frequency treatments for pest control. Postharvest Biol. Technol. 33, 205–217. doi:10.1016/j.postharvbio.2004.02.010

Centers for Disease Control and Prevention, 2012. Multistate Outbreak of Human Salmonella Enteritidis Infections Associated with Shell Eggs (Final Update)

[WWW Document]. URL http://www.cdc.gov/salmonella/enteritidis/index.html (accessed 10.16.13).

Coimbra, J.S.R., Gabas, A.L., Minim, L.A., Garcia Rojas, E.E., Telis, V.R.N., Telis-Romero, J., 2006. Density, heat capacity and thermal conductivity of liquid egg products. J. Food Eng. 74, 186–190. doi:10.1016/j.jfoodeng.2005.01.043

Denys, S., Pieters, J.G., Dewettinck, K., 2004. Computational fluid dynamics analysis of combined conductive and convective heat transfer in model eggs. J. Food Eng. 63, 281–290. doi:10.1016/j.jfoodeng.2003.06.002

Doyle, M.E., Mazzotta, A.S., 2000. Review of Studies on the Thermal Resistance of Salmonellae. J. Food Prot. 63, 779–795.

Hou, H., Singh, R.K., Muriana, P.M., Stadelman, W.J., 1996. Pasteurization of intact shell eggs. Food Microbiol. 13, 93–101. doi:10.1006/fmic.1996.0012

Howard, Z.R., O'Bryan, C.A., Crandall, P.G., Ricke, S.C., 2012. Salmonella Enteritidis in shell eggs: Current issues and prospects for control. Food Res. Int. 45, 755–764. doi:10.1016/j.foodres.2011.04.030

Ikediala, J.N., Hansen, J.D., Tang, J., Drake, S.R., Wang, S., 2002. Development of a saline water immersion technique with RF energy as a postharvest treatment against codling moth in cherries. Postharvest Biol. Technol. 24, 209–221. doi:10.1016/S0925-5214(02)00018-2

Jiao, Y., Tang, J., Wang, S., 2014a. A new strategy to improve heating uniformity of low moisture foods in radio frequency treatment for pathogen control. J. Food Eng. 141, 128–138. doi:10.1016/j.jfoodeng.2014.05.022

Jiao, Y., Tang, J., Wang, S., Koral, T., 2014b. Influence of dielectric properties on the heating rate in free-running oscillator radio frequency systems. J. Food Eng. 120, 197–203. doi:10.1016/j.jfoodeng.2013.07.032

Jordan, J.S., Gurtler, J.B., Marks, H.M., Jones, D.R., Shaw Jr., W.K., 2011. A mathematical model of inactivation kinetics for a four-strain composite of Salmonella Enteritidis and Oranienburg in commercial liquid egg yolk. Food Microbiol. 28, 67–75. doi:10.1016/j.fm.2010.08.008

Kumbár, V., Nedomová, Š., Strnková, J., Buchar, J., 2015. Effect of egg storage duration on the rheology of liquid egg products. J. Food Eng. 156, 45–54. doi:10.1016/j.jfoodeng.2015.02.011

MatWeb, n.d. Aluminum 6061-T6 [WWW Document]. URL http://www.matweb.com/search/datasheet_print.aspx?matguid=1b8c06d0ca7c456694c7777d9e10be5b (accessed 9.3.14).

Nakamura, R., Fukano, T., Taniguchi, M., 1982. Heat-Induced Gelation of Hen's Egg Yolk Low Density Lipoprotein (LDL) Dispersion. J. Food Sci. 47, 1449–1453. doi:10.1111/j.1365-2621.1982.tb04958.x

Ramachandran, R., Malhotra, D., Anishaparvin, A., Anandharamakrishnan, C., 2011. Computational fluid dynamics simulation studies on pasteurization of egg in stationary and rotation modes. Innov. Food Sci. Emerg. Technol. 12, 38–44. doi:10.1016/j.ifset.2010.11.008

Schuman, J. d., Sheldon, B. w., Vandepopuliere, J. m., Ball Jr, H. r., 1997. Immersion heat treatments for inactivation of Salmonella enteritidis with intact eggs. J. Appl. Microbiol. 83, 438–444. doi:10.1046/j.1365-2672.1997.00253.x

Singh, R.P., Heldman, D.R., 2008. Introduction to Food Engineering, Fourth Edition, 4th ed. Academic Press, Amsterdam ; Boston.

Stadelman, W.J., Newkirk, D., Newby, L., 1995. Egg Science and Technology, Fourth Edition. Psychology Press.

Tiwari, G., Wang, S., Tang, J., Birla, S.L., 2011. Analysis of radio frequency (RF) power distribution in dry food materials. J. Food Eng. 104, 548–556. doi:10.1016/j.jfoodeng.2011.01.015

United States Department of Agriculture, 2013. World Agricultural Supply and Demand Estimates.

USDA/FSIS, 2005. Risk assessment for Salmonella Enteritidis in shell eggs and Salmonella spp. in egg products.

Wang, J., Luechapattanaporn, K., Wang, Y., Tang, J., 2012. Radio-frequency heating of heterogeneous food – Meat lasagna. J. Food Eng. 108, 183–193. doi:10.1016/j.jfoodeng.2011.05.031

Wang, S., Monzon, M., Johnson, J.A., Mitcham, E.J., Tang, J., 2007. Industrial-scale radio frequency treatments for insect control in walnuts: I: Heating uniformity and energy efficiency. Postharvest Biol. Technol. 45, 240–246. doi:10.1016/j.postharvbio.2006.12.023

Wang, Y., Zhang, L., Gao, M., Tang, J., Wang, S., 2014. Evaluating radio frequency heating uniformity using polyurethane foams. J. Food Eng. 136, 28–33. doi:10.1016/j.jfoodeng.2014.03.018

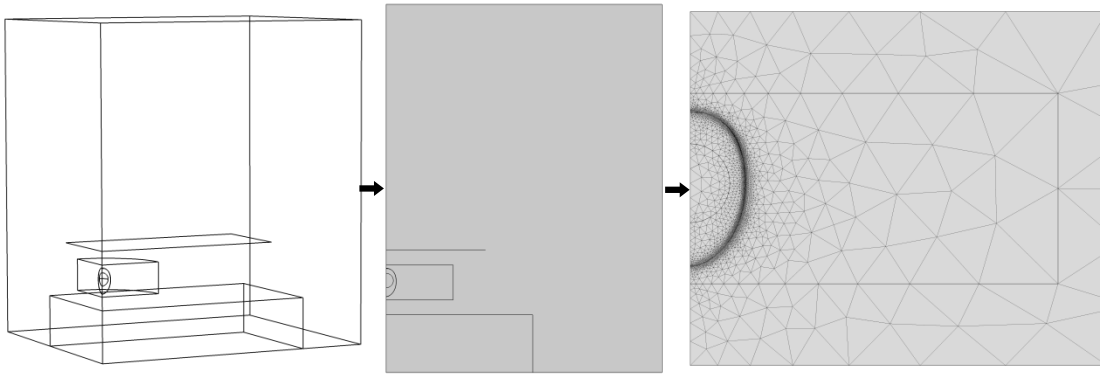

(a) 3D (b) 2D (c) 2Ds

Fig. 4.1. Simplification of the model geometry for Setup A, from (a) 3D to (b) 2D axisymmetric and finally to (c) a 2D axisymmetric model focused only on the space between the electrodes. Diagram is not to scale.

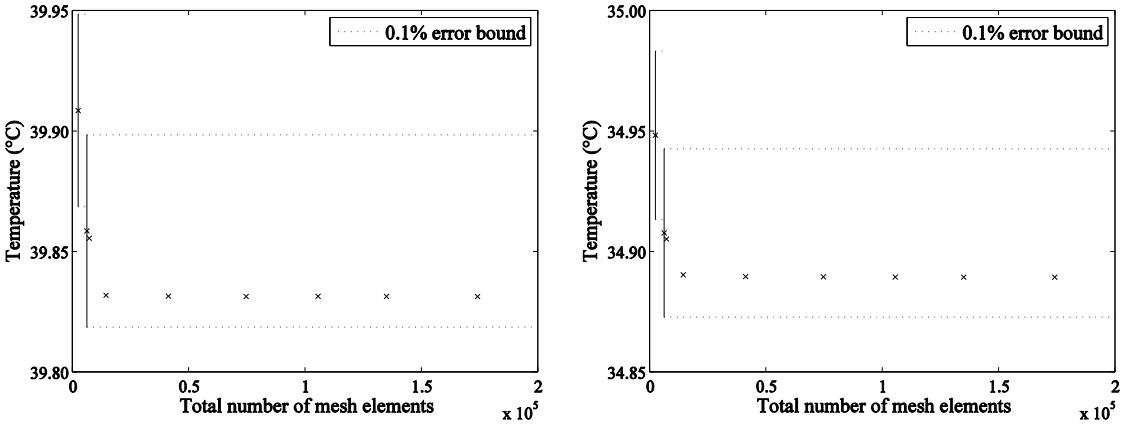

(a) Maximum temperature (b) Average temperature

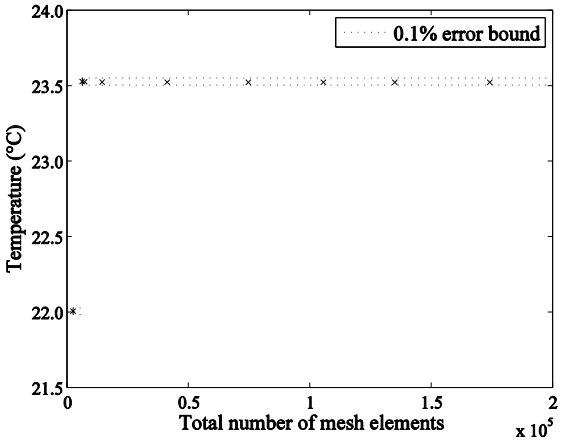

(c) Minimum temperature

Fig. 4.2. Mesh Convergence plots for the 2Ds model: (a) maximum temperature, (b) average temperature, and (c) minimum temperature. Dashed lines represent a 0.1% error bound. Notice that the mesh converged first at (c), then at (a) and (b) simultaneously. In this case, the converged mesh from (a) and (b) takes priority over (c).

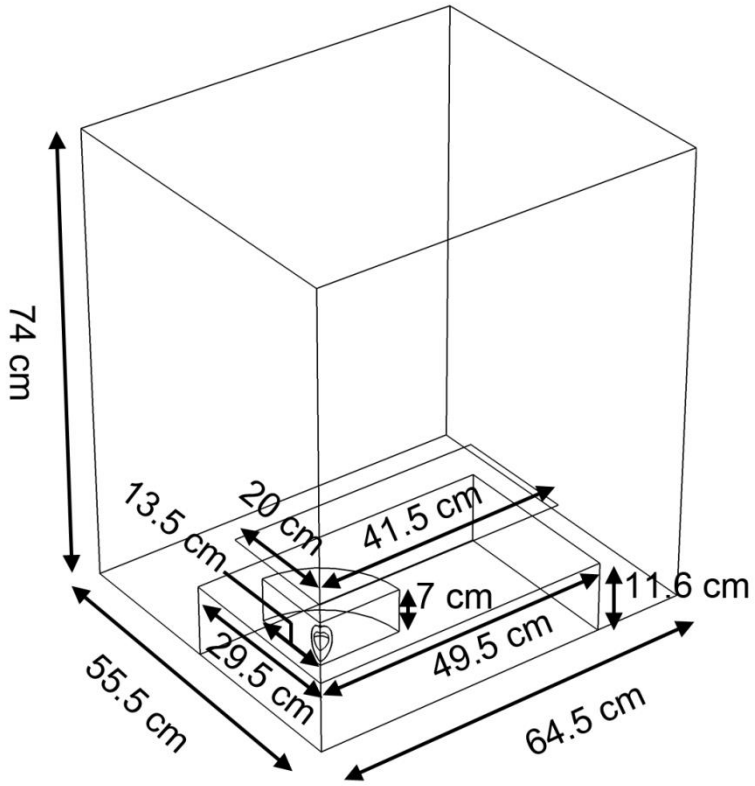

Fig. 4.3. Geometry of the model and its dimensions.

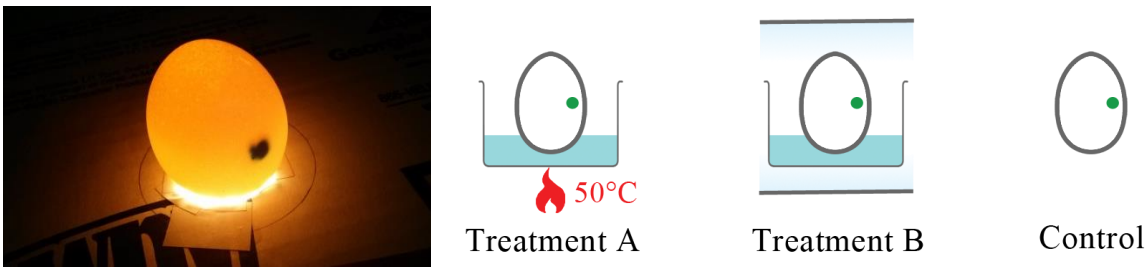

(a) Candling (b) Treatments

Fig. 4.4 Overview of the liquid movement experiments. The egg was (a) candled before being subjected to one of (b) three different treatments.

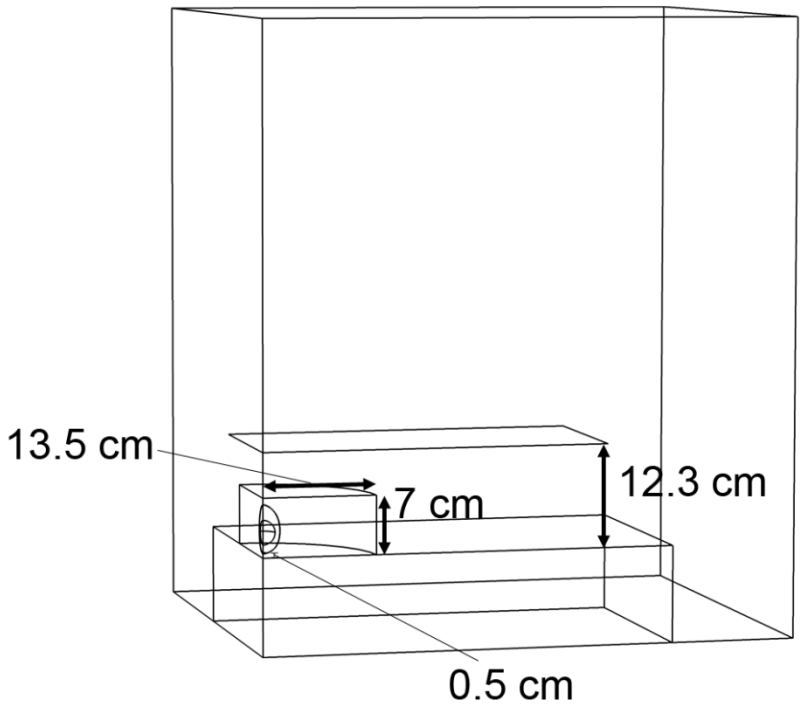

Fig. 4.5. The configuration of the RF oven used in treatment B of the liquid movement experiments.

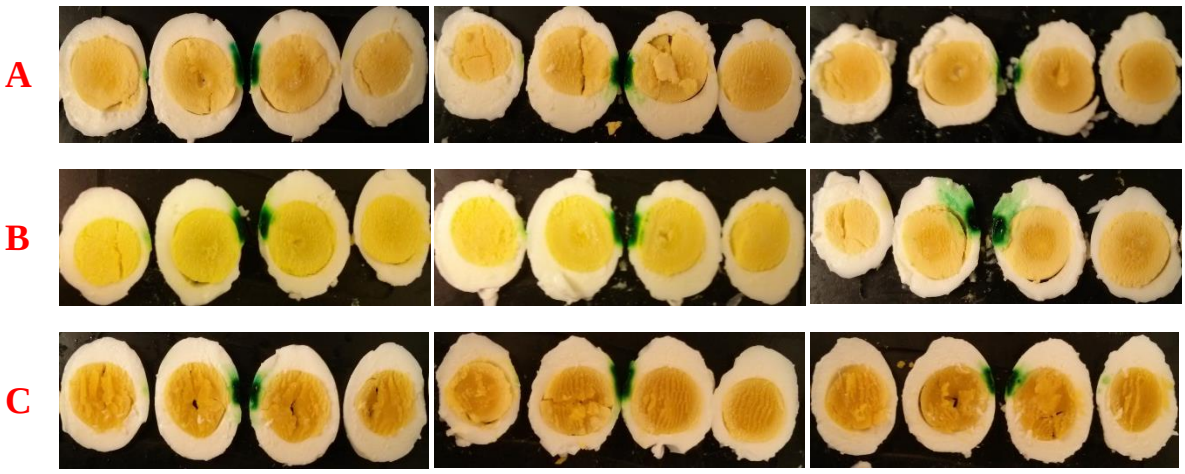

Fig. 4.6. Slices of eggs from the liquid movement experiment. Rows indicate treatment (A for water immersion; B for RF; C for control) while columns represent replications. The third replication in B was smeared by the cutting device during slicing.

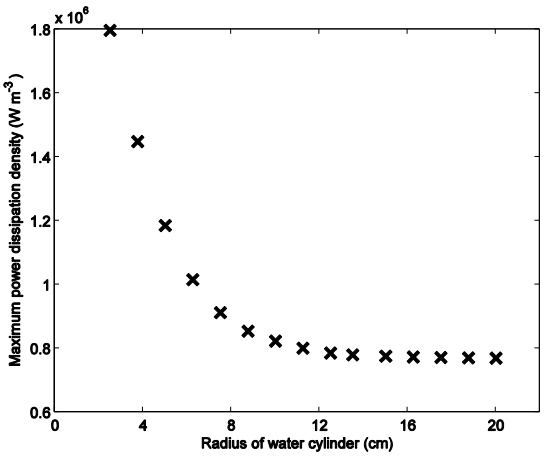

(a) Maximum power dissipation

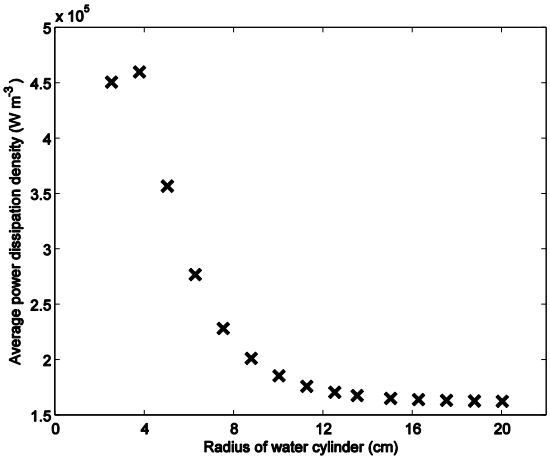

(b) Average power dissipation

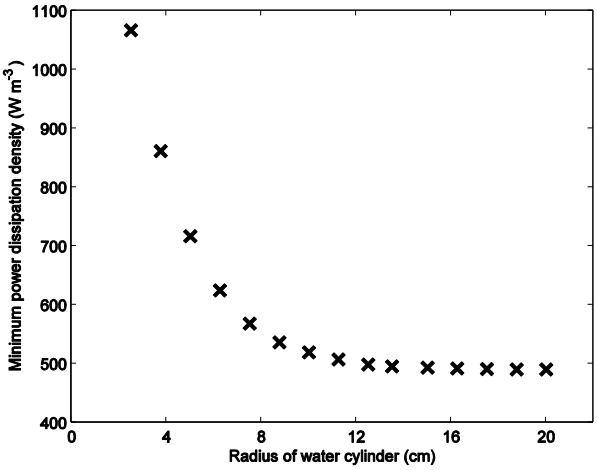

(c) Minimum power dissipation

Fig. 4.7. (a) Maximum, (b) average, and (c) minimum power dissipation density as a function of the radius of the water cylinder in the infinite water assumption test. A radius of 13.5 cm was found to have less than 5% difference than subsequently larger radiuses.

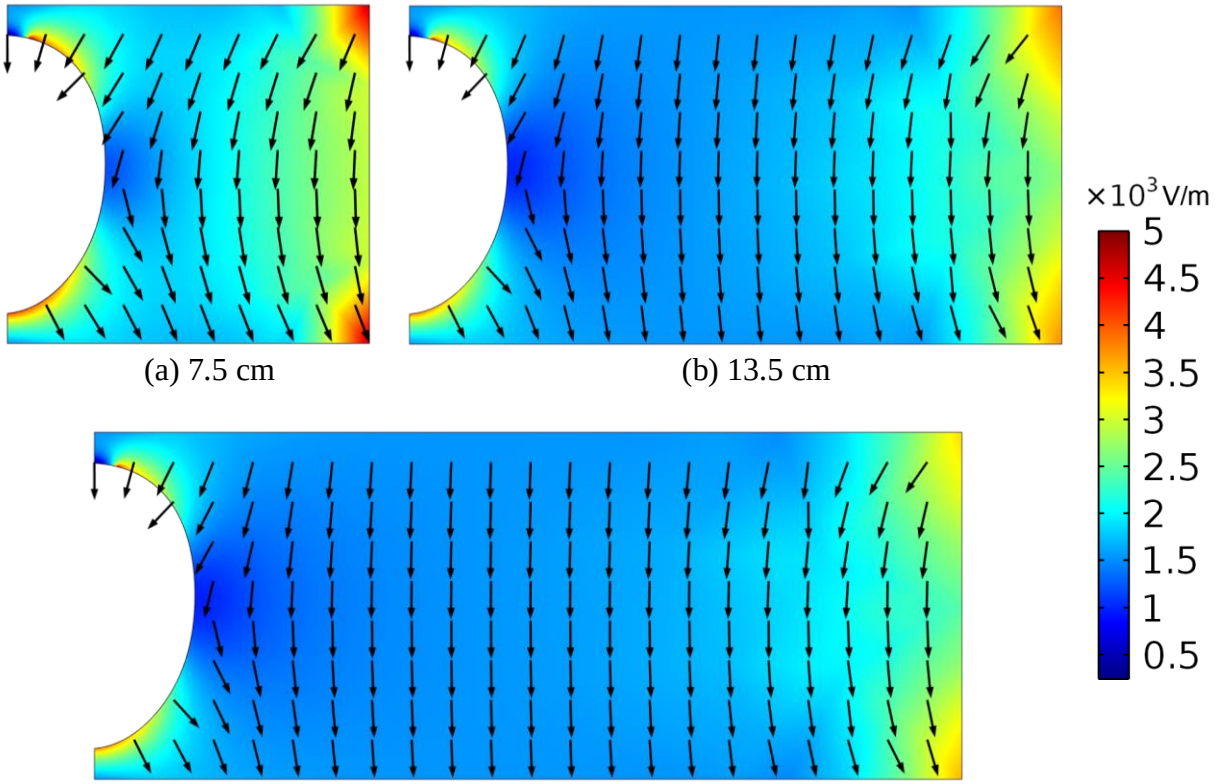

(a) 7.5 cm (b) 13.5 cm

(c) 17.5 cm

Fig. 4.8. Normalized electric field contour plot and electric field arrow plot in water cylinders with radius (a) 7.5 cm, (b) 13.5 cm, and (c) 17.5 cm. The size of the arrows does not represent the magnitude of the electric field.

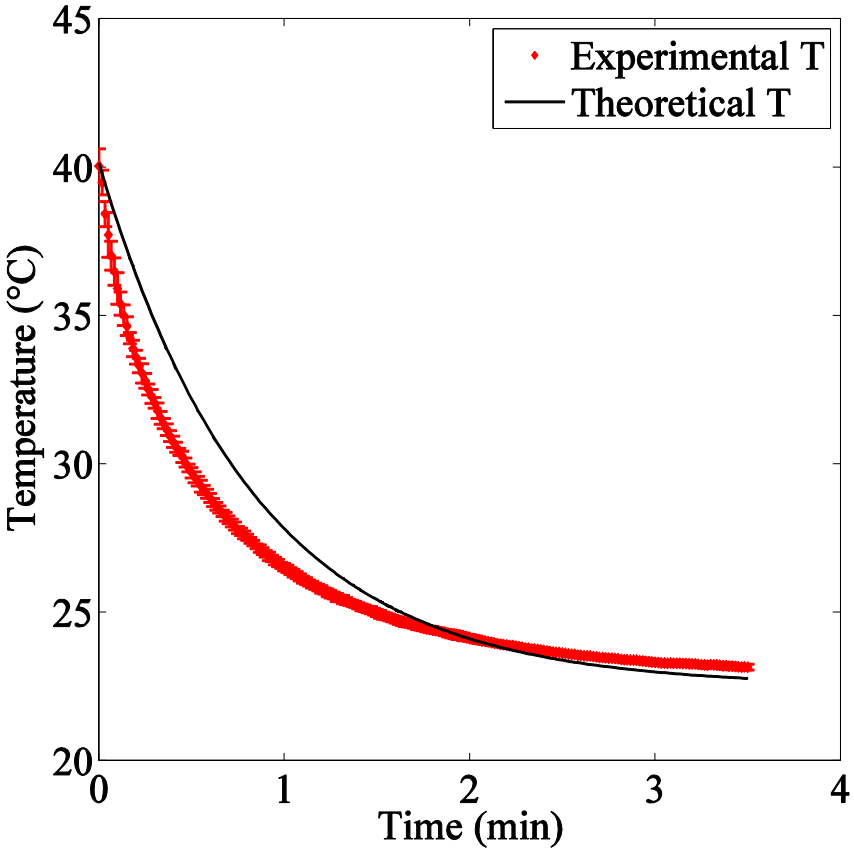

Fig. 4.9. Theoretical versus experimental temperature at the center of a 40°C aluminum egg immersed in 22.5°C deionized water over a period of 3.5 min. Theoretical values were calculated using Equation 6 and the value of *h* determined experimentally.

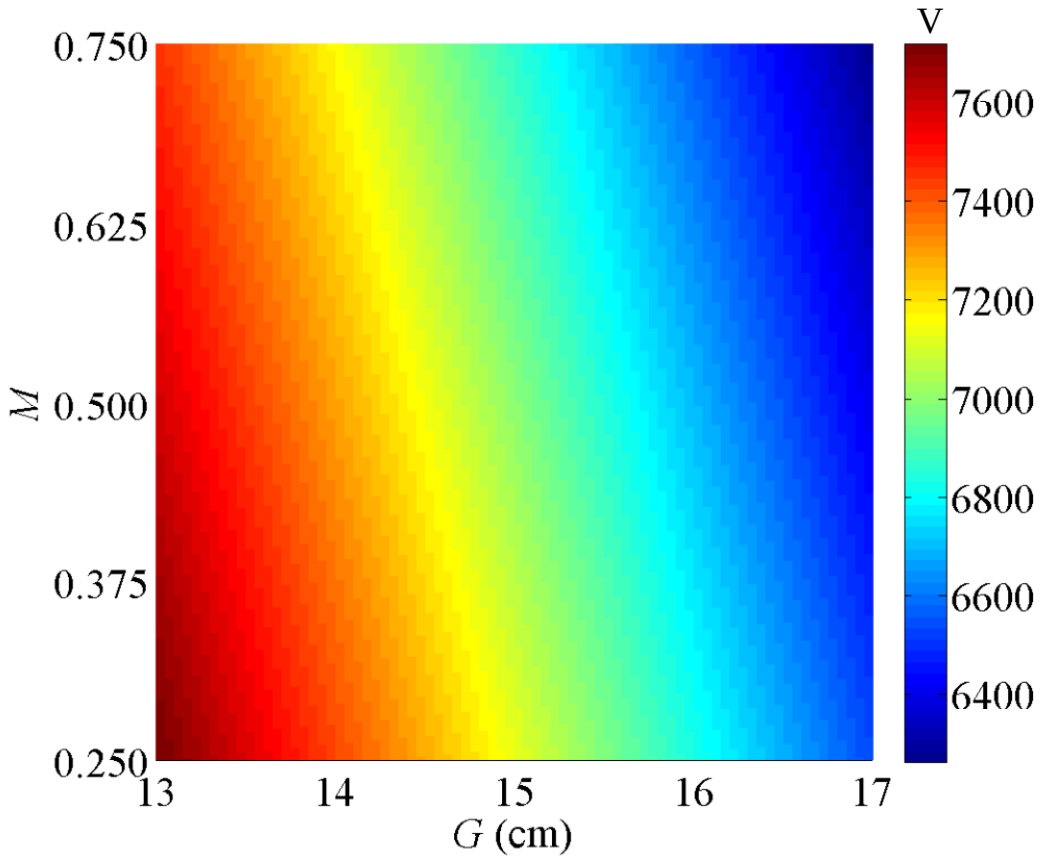

Fig. 4.10. Contour plot of voltage (V) as a function of *G* and *M*.

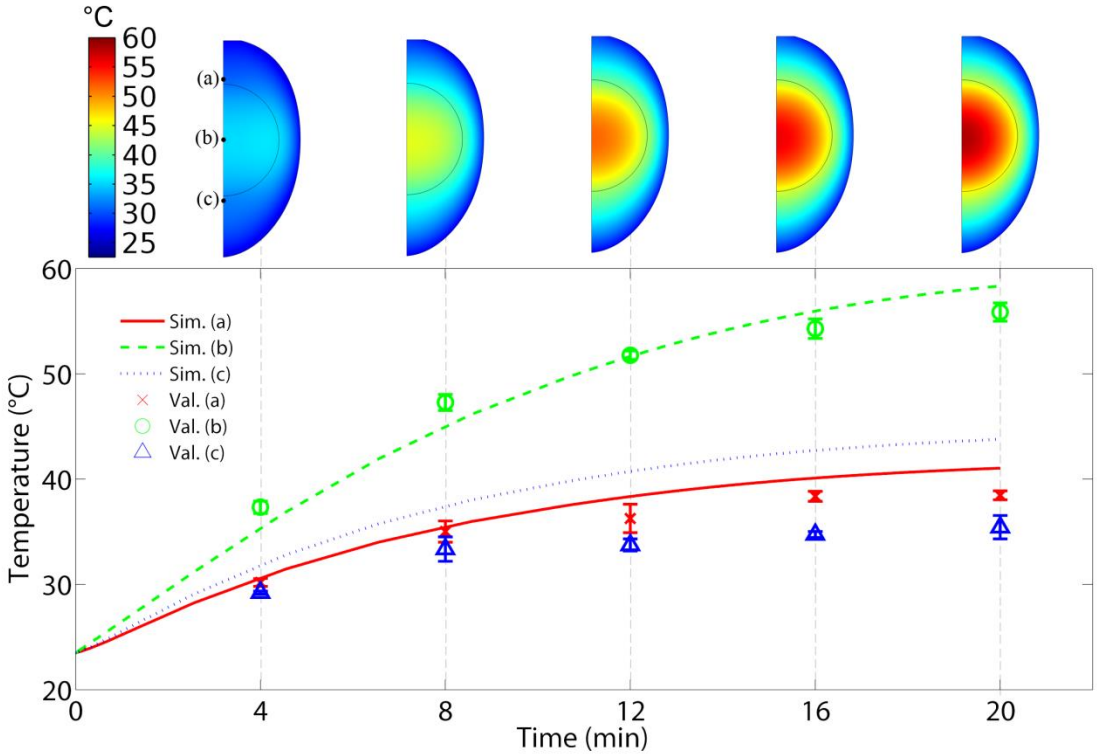

Fig. 4.11. Temperature profile evolution over time for Orientation A with G = 13 cm and M = 0.75, along with temperature contour plots at corresponding time points (shell and air cell not shown for clarity purposes). The lines represent simulation results while discrete points are for validation results. The alphabets correspond to thermocouple locations denoted on the first contour plot. One half of each error bar represents one standard deviation.

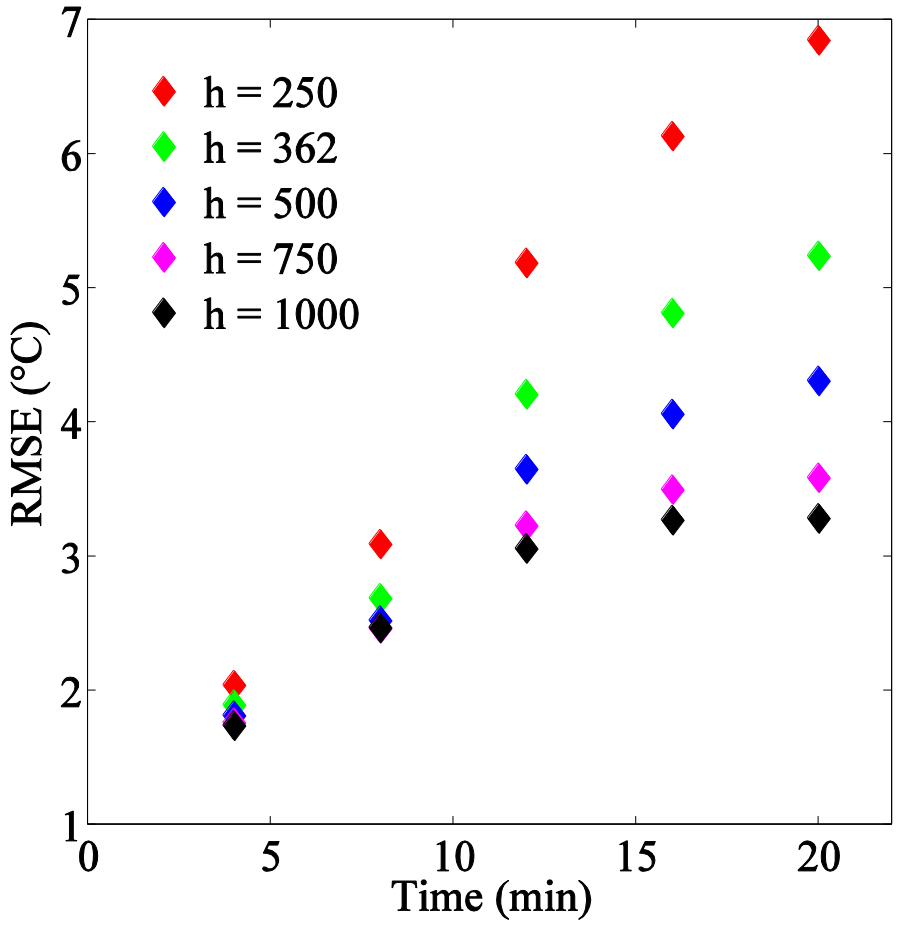

Fig. 4.12. The effect of *h* on the RMSE between the simulated and validation data for Orientation A with *G* = 13 cm and *M* = 0.75. The unit of *h* is W m^{-2} K^{-1}.The results in **Fig. 4.11** used a *h* value of 362 W m^{-2} K^{-1}.

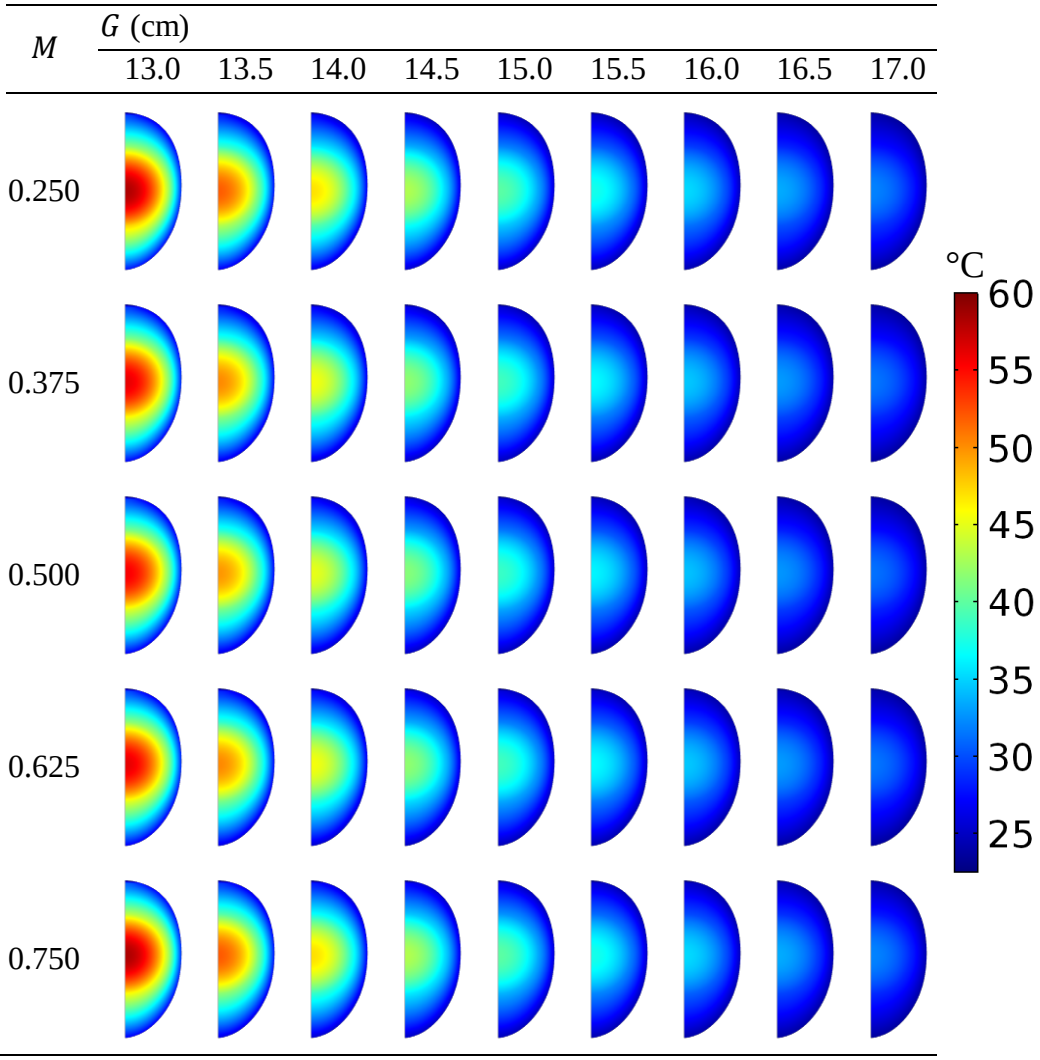

Fig. 4.13. Temperature contour plots of the eggs after 20 min of RF heating for Orientation A. Columns represent the gap between the electrodes while the rows are a measure of the vertical position of the egg.

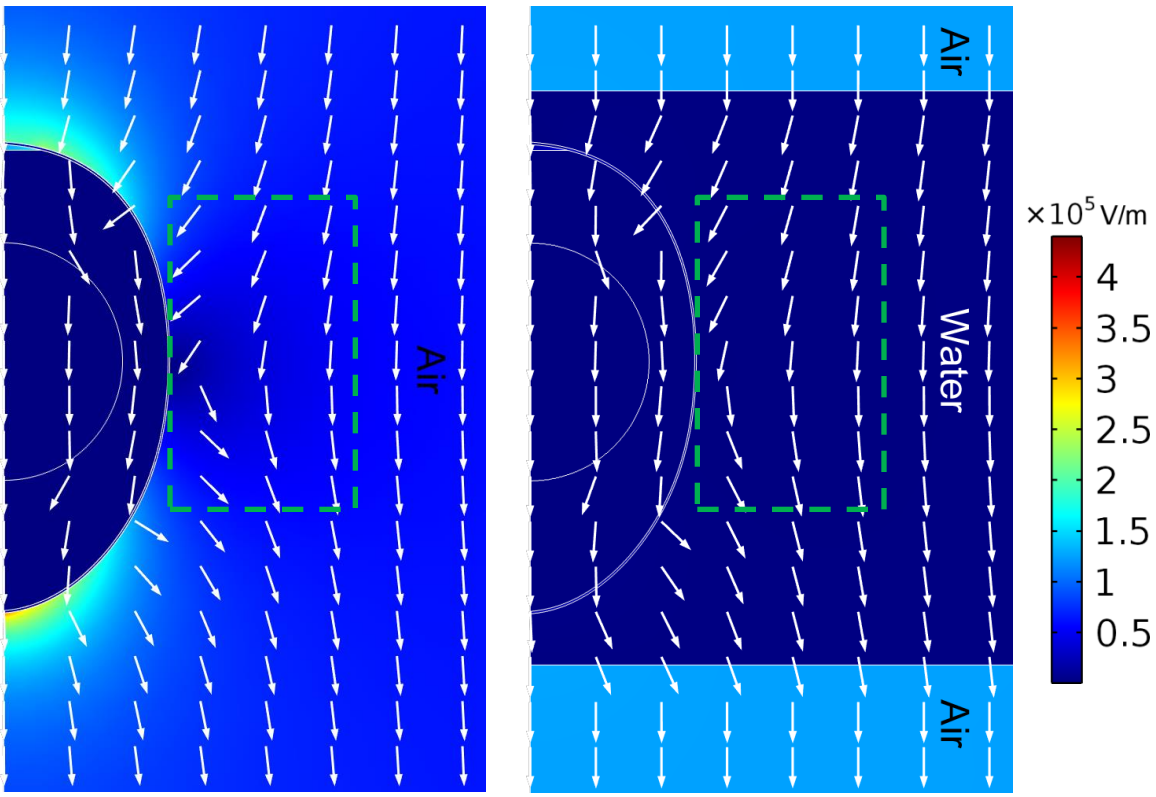

(a) Egg in air (b) Egg in deionized water

Fig. 4.14. Comparison of normalized electric field contour plot and electric field arrow plot for (a) egg in air versus (b) egg immersed in water. Both use Orientation A, G = 13 cm, and M = 0.5. The simulation results for (a) are from Chapter III of this thesis. The green dashed rectangle highlights a stark difference in electric field direction between both figures.

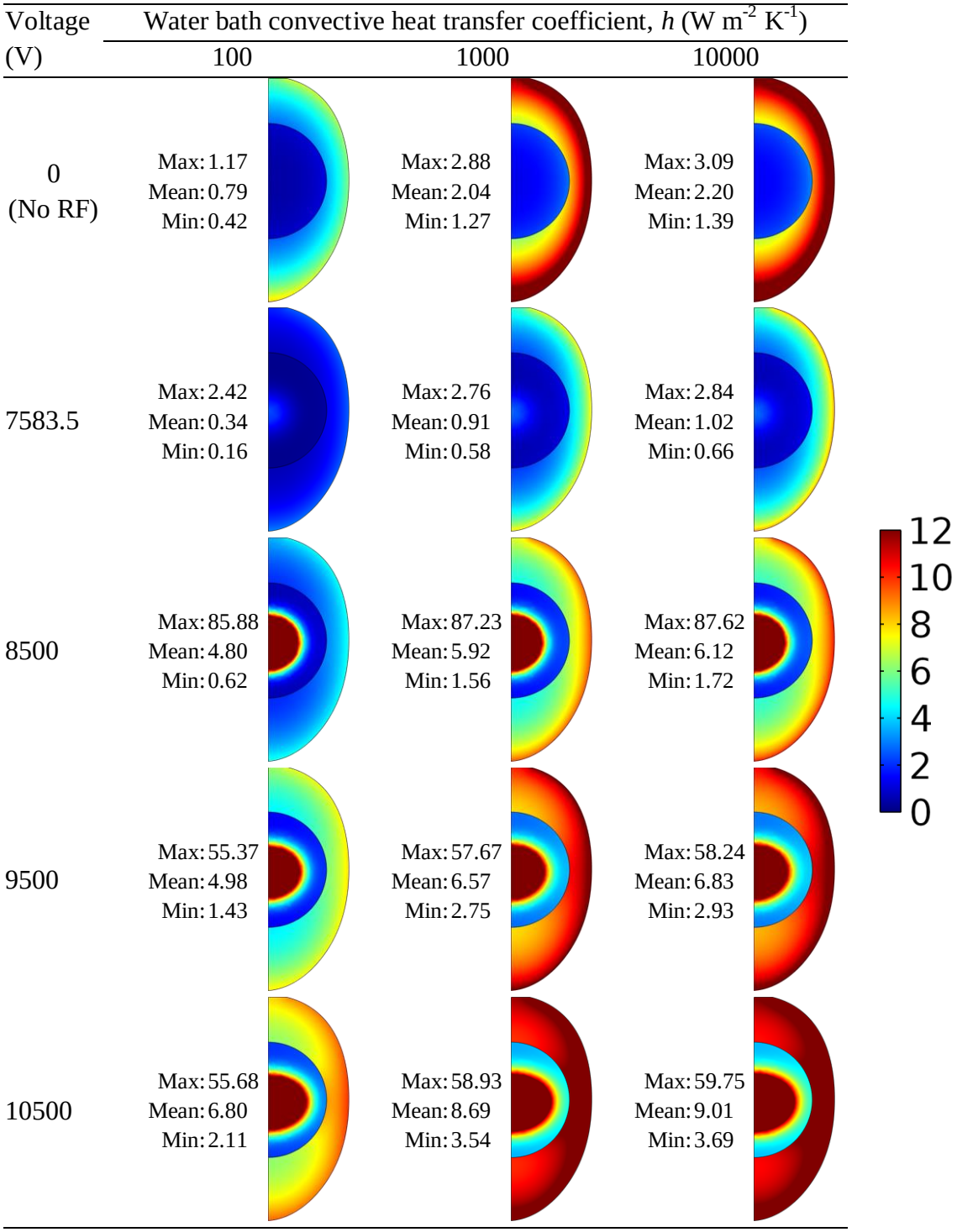

Fig. 4.15. Contour plots for simulated log reduction of *Salmonella* in the albumen and yolk, along with the maximum, mean, and minimum log reductions in the yolk after a total process time of 40 min of either hot water bath alone or RF heating + hot water bath. The colorbar is scaled down to a maximum of 12 for clear visualization of log reductions.

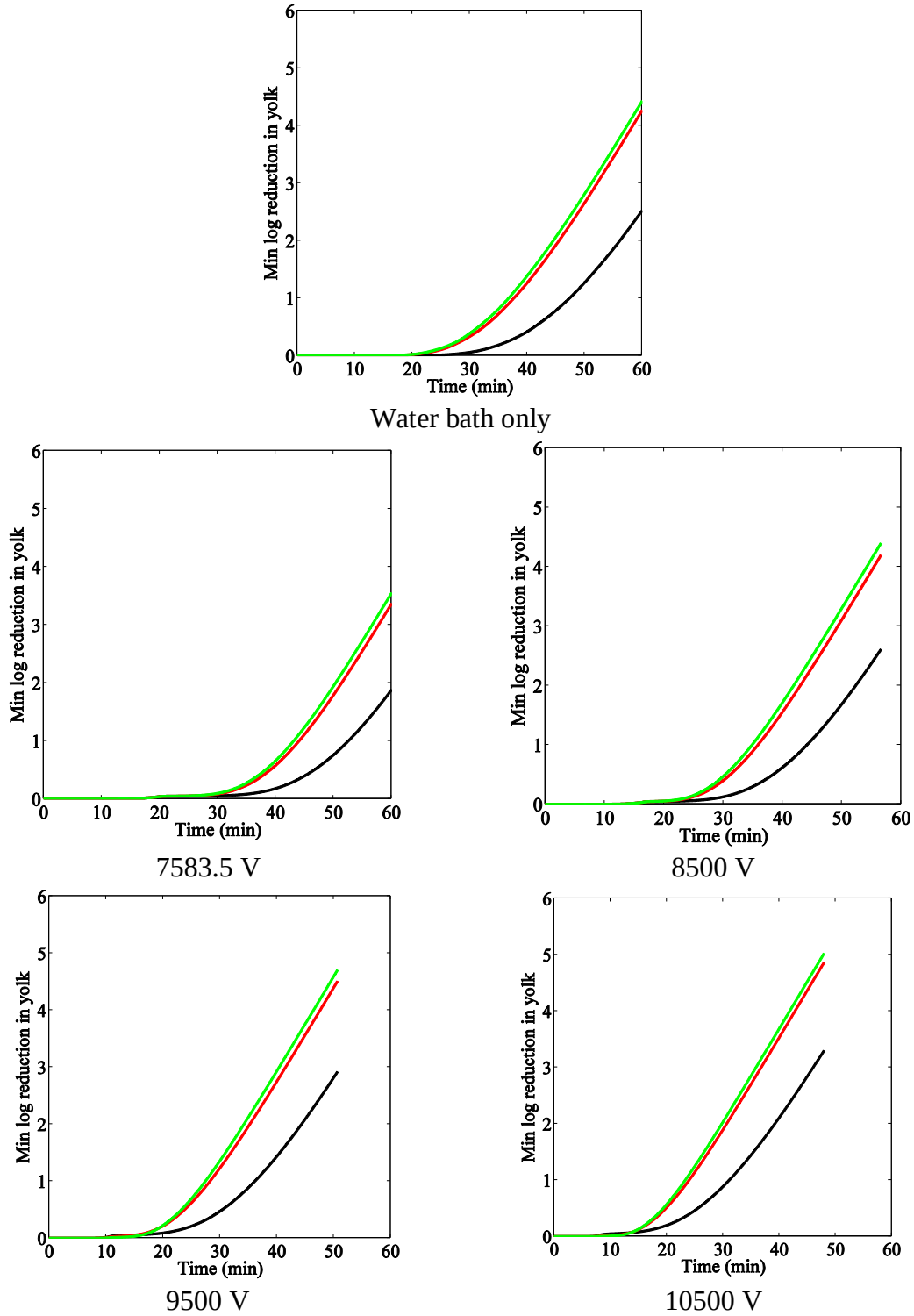

Fig. 4.16. Minimum simulated log reduction in the yolk as a function of time for various *h* values and top electrode voltages for either hot water bath alone or RF heating + hot water bath. Values of *h* (W m^{-2} K^{-1}): (–) 100, (–) 1000, and (–) 10000.

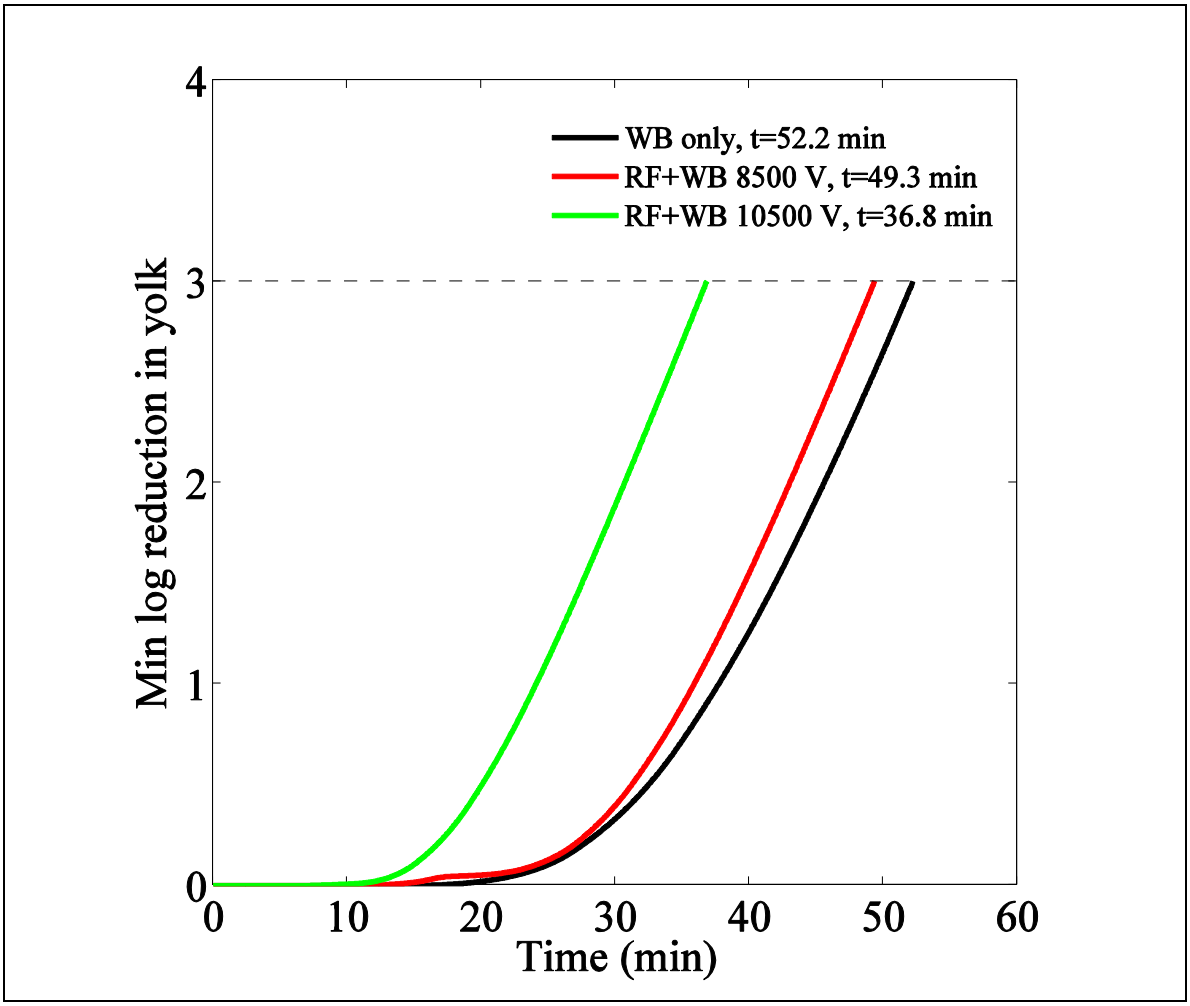

Fig. 4.17. Time taken for either hot water bath (WB) alone or RF heating at various voltages followed by hot water bath to achieve a minimum of 3 log reduction in the yolk.

Salt (NaCl) content	Temperature (°C)	Power dissipation density (W m^{-3})	Total power dissipated (W/m)		% of total power dissipated	
			Egg	Water	Egg	Water
Deionized	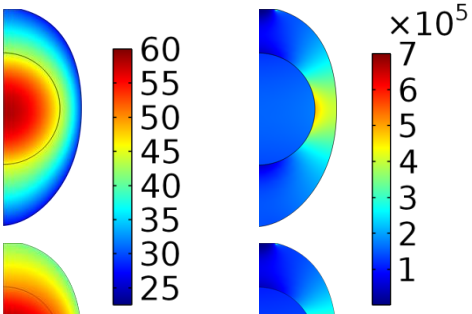		193.11	0.84	99.57	0.43
Tap water			167.42	450.05	27.11	72.89
0.05%			112.68	996.53	10.16	89.84
0.10%			81.87	911.81	8.24	91.76
0.15%			61.43	757.76	7.50	92.50
0.20%			48.49	641.42	7.03	92.97

Fig. 4.18. The effects of salt content of the water surrounding the egg on the temperature profile and power dissipation in the egg.

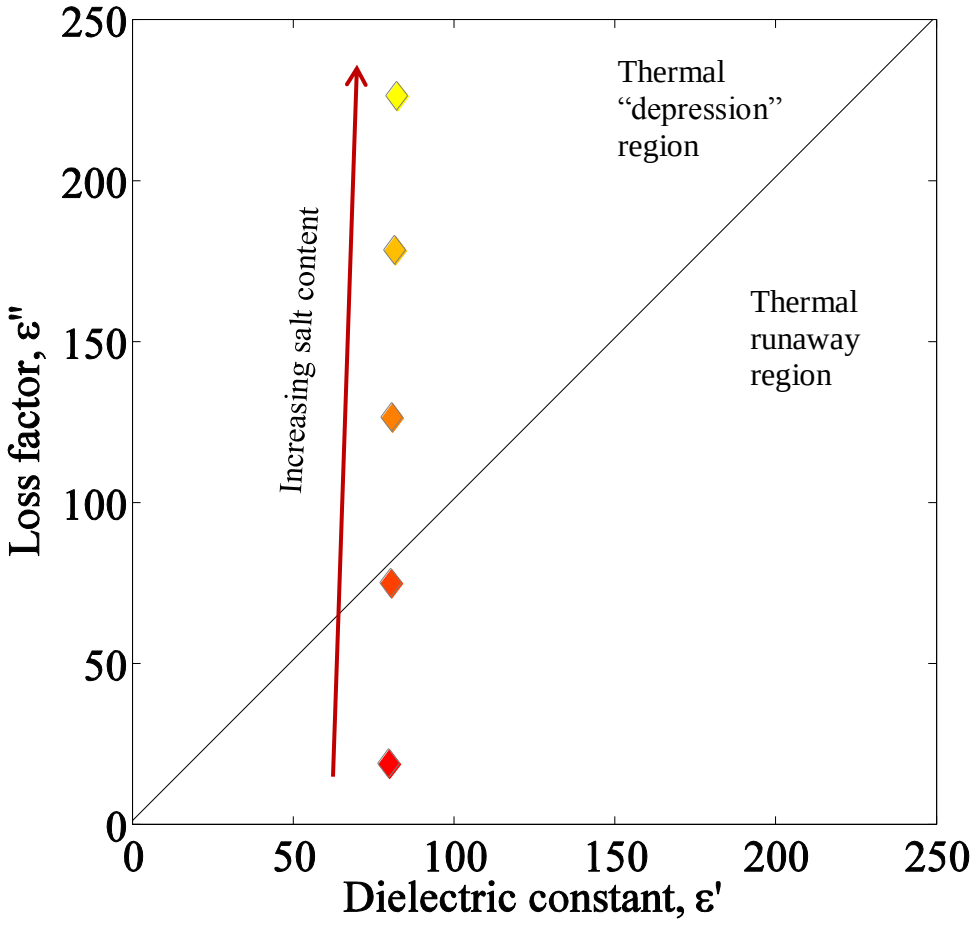

Fig. 4.19. Loss factor, ε'' versus dielectric constant, ε' for various salt solutions as compared to a reference material with maximum heating rate (black diagonal line). Salt concentration increases from tap water to 0.05%, 0.10%, 0.15% and 0.20% NaCl as red goes to yellow.

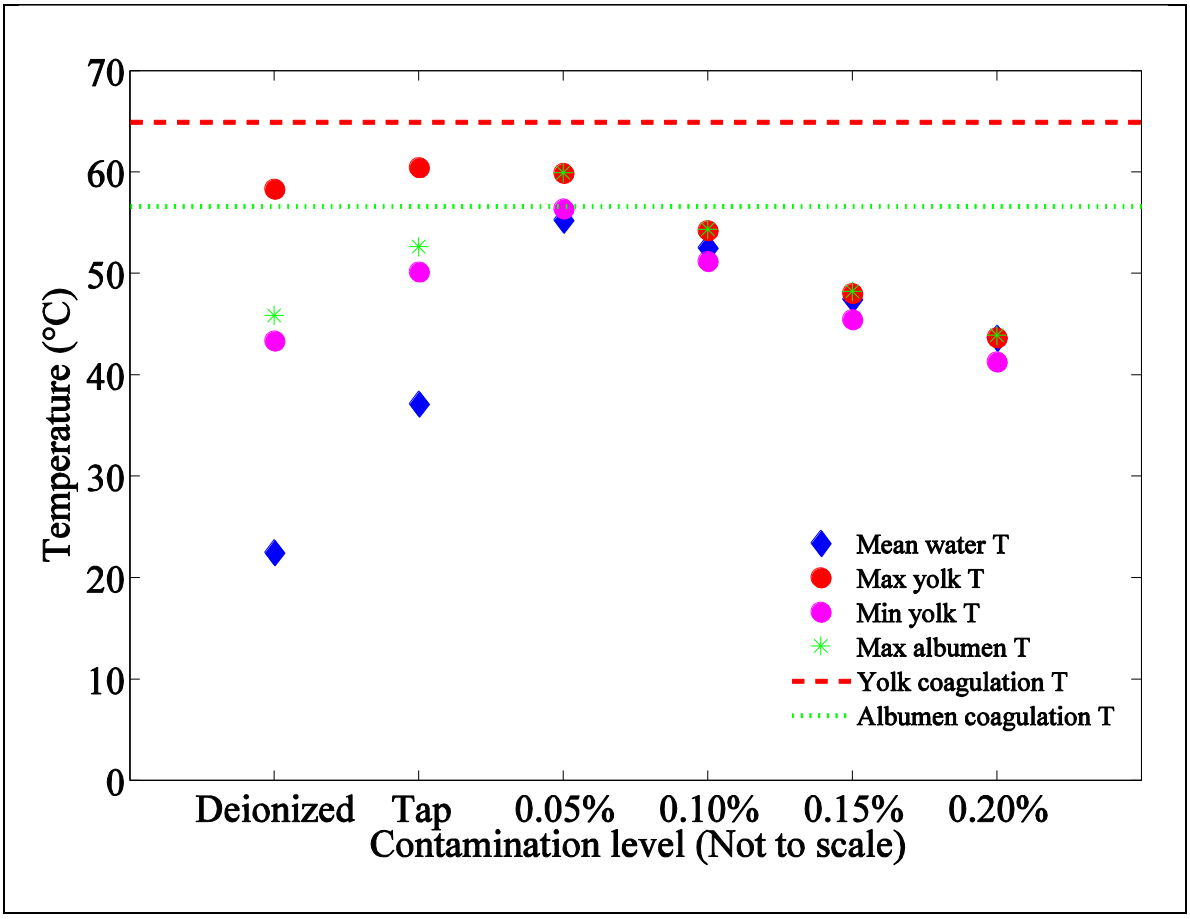

Fig. 4.20. Comparison of the mean water temperature, maximum yolk temperature, minimum yolk temperature, and maximum albumen temperature across the various levels of water contamination at t = 20 min. The percentages represent NaCl concentration. The coagulation temperature of yolk (65°) and albumen (56.7°C) are plotted as dashed and dotted lines, respectively.

Table 4.1. Material properties used in the model.

Property	Albumen	Yolk	Shell	Deionized water	Air
ρ (kg m^{-3})	1045 $-0.0559T$ [a]	1148 $-0.0559T$ [a]	2300[b]	8.38×10^{2} $+1.40T$ $-3.01 \times 10^{-3}T^{2}$ $+3.72 \times 10^{-7}T^{3}$ [c]	$353T^{-1}$ [c]
ε'	$5.3 \times 10^{-3}T^{2}$ $-4.5 \times 10^{-1}T$ $+9.1 \times 10^{1}$ [d]	$1.3 \times 10^{1}T^{0.1975}$ $+2.8 \times 10^{1}$ [d]	$3.1T^{0.3072}$ $+4.5$ [d]	80.1 [e]	1 [c]
ε''	$2.1 \times 10^{2}T^{0.465}$ -3.3×10^{2} [d]	$2.8 \times 10^{2}T^{0.2599}$ -4.3×10^{2} [d]	$2.2 \times 10^{2}T^{0.04521}$ -2.4×10^{2} [d]	0.03 [e]	0 [c]
k (W m^{-1} K^{-1})	$9.0 \times 10^{-4}\theta^{2}$ $+1.1 \times 10^{-2}\theta$ $+5.6 \times 10^{-1}$ [d]	$4.0 \times 10^{-4}\theta^{2}$ $+4.4 \times 10^{-3}\theta$ $+3.6 \times 10^{-1}$ [d]	$3.0 \times 10^{-2}\theta^{2}$ $+1.2 \times 10^{-1}\theta$ $+8.1 \times 10^{-1}$ [d]	-8.69×10^{-1} $+8.94 \times 10^{-3}T$ $-1.58 \times 10^{-5}T^{2}$ $+7.98 \times 10^{-9}T^{3}$ [c]	-2.28×10^{-3} $+1.15 \times 10^{-4}T$ $-7.90 \times 10^{-8}T^{2}$ $+4.12 \times 10^{-11}T^{3}$ $-7.44 \times 10^{-15}T^{4}$ [c]
c_p (J kg^{-1} K^{-1})	$4.3 \times 10^{-2}\theta^{3}$ $+3.3 \times 10^{-2}\theta^{2}$ $-1.8 \times 10^{-1}\theta$ $+3.4$ [d]	$2.7 \times 10^{-2}\theta^{3}$ $-6.4 \times 10^{-3}\theta^{2}$ $-5.6 \times 10^{-2}\theta$ $+2.8$ [d]	$5.6 \times 10^{-3}\theta^{3}$ $-5.3 \times 10^{-3}\theta^{2}$ $-3.9 \times 10^{-2}\theta$ $+1.1$ [d]	120×10^{4} $-8.04 \times 10^{1}T$ $+3.10 \times 10^{-1}T^{2}$ $-5.38 \times 10^{-4}T^{3}$ $+3.63 \times 10^{-7}T^{4}$ [c]	1.05×10^{3} $-3.73 \times 10^{-1}T$ $+9.45 \times 10^{-4}T^{2}$ $-6.02 \times 10^{-7}T^{3}$ $+1.29 \times 10^{-10}T^{4}$ [c]

$\theta = \left(\frac{T-318.2}{18.71}\right)$, [a]Coimbra et al. (2006), [b]Ramachandran et al. (2011), [c]COMSOL Multiphysics, [d]Chapter III of this thesis, [e]Ikediala et al. (2002)

Table 4.2. D-values of various *Salmonella* serovars at various conditions in egg albumen (adapted from Doyle and Mazzotta (2000)).

Serovar and condition	Temperature (°C)						Z-value
	55	55.5	56.7	57.6	58.3	60	
T, pH 7.3					0.54	0.2	4.2
T, no additions						0.3	
E, no additions	1.5					0.2	
E+T, pH 8.2	7.99		2.96				3.54
E+T+S(not 775W), pH 8.8		2.74	1.44	0.78			4.03

Serovars: T = Typhimurium, E = Enteritidis, S = Senftenberg

Table 4.3. D-values of various *Salmonella* serovars in egg yolk (adapted from Doyle and Mazzotta (2000)).

Serovar	Temperature (°C)					Z-value
	55	58.8	60	61.1	62.2	
T			0.67	0.2	0.14	3.24
T		0.7	0.4			4.4
T	8		0.8			4.6
E			0.65	0.31	0.255	5.6
E	21		1.1			
T+E, BHI			0.28	0.16	0.087	4.33
S(not 775W), TPB			0.73	0.28	0.21	4.07

Serovars: T = Typhimurium, E = Enteritidis, S = Senftenberg

Table 4.4. Linear regression equations for the logarithm to base 10 of D-value for *Salmonella* as a function of temperature.

Egg Component	Log_{10}D-value equation	R^2	Z-value
Albumen	$\log_{10} D = -0.2452\mathrm{T} + 14.065$	0.9726	4.08
Yolk	$\log_{10} D = -0.2673\mathrm{T} + 15.743$	0.976	3.74

Table 4.5. Dielectric properties of various solutions used to model contamination of water adapted from Ikediala et al. (2002).

Solution	Dielectric constant, ε'	Loss factor, ε''
Tap water	79.6	19.0
0.05% NaCl	80.3	75.1
0.10% NaCl	80.6	126.6
0.15% NaCl	81.5	178.5
0.20% NaCl	82.1	226.4

Chapter V: Conclusions and Future Research

5.1 Conclusions

When eggs are processed with RF heating without any processing aids, a 'coagulation ring' would form near the air cell before the yolk is sufficiently pasteurized. The vertical orientation of the egg was found to have insignificant effect on the final temperature profile. The 'coagulation ring' was explained by a difference in dielectric properties between the various components in the egg. As a result, the electric field was redirected and concentrated at undesirable locations thus causing non-uniform heating. Therefore, the egg was immersed in deionized water during RF heating which eliminated the "coagulation ring" was eliminated while resulting in concentrated heating in the yolk.

The radius of the water cylinder surrounding the egg was found to have an inverse relationship with the power dissipation in the egg. Therefore, it might be possible to speed up the RF heating process by decreasing the size of the water domain. Extrapolation of the model revealed that increase in the top electrode voltage allowed pasteurization conditions to be achieved 30% faster than a simulated hot water immersion method: 3 log reductions of *Salmonella* were achieved within 37 min for an RF heating setup with a top electrode voltage of 10500 V and a hot water bath convective heat transfer coefficient of 1000 W m^{-2} K^{-1}. When the water surrounding the egg was slightly contaminated, the heating rate was further increased, although there is a threshold at which further increase in contamination decreases the efficiency of the process and heats up the water more than the egg. However, this turned out to be a bonus because it would

be possible to measure the contamination level of the water simply by measuring its temperature instead of its dielectric properties. Therefore, food processors can adjust their process parameters by just measuring the temperature of the water.

5.2 Future Research

Although the results in Chapter IV proposed that a decrease in the radius of the deionized water could increase the heating rate of RF heating of eggs, this conclusion was reached using a model that assumed no fluid flow within the water domain. In reality, temperature gradients caused by nonuniform heating would create pressure differences and cause movement in the water domain, thus changing the convective heat transfer coefficient at the surface of the egg. Therefore, one should model this physics appropriately before adjusting the radius of the water to optimize the heating rate.

This research focused on only a single egg; in reality, there should be multiple eggs being heated at once because the industry usually processes eggs in trays. It would be interesting to see if multiple eggs placed beside each other would increase the power dissipation density as seen when the radius of the water domain was decreased.

The extrapolations made using the model developed in this study need to be validated. One could design an RF oven with a higher power output to achieve the top electrode voltages proposed in this study. Besides that, one should model the fluid flow in contaminated water for accurate simulation of the convective heat transfer. With this information, it would be possible to determine optimum thermocouple placement for determination of the contamination level of the water surrounding the egg.